

**A THERMAL MODEL TO EVALUATE SUB-FREEZING  
STARTUP FOR A DIRECT HYDROGEN HYBRID FUEL  
CELL VEHICLE POLYMER ELECTROLYTE FUEL CELL  
STACK AND SYSTEM**

**UCD-ITS-RR-04-05**

March 2004

by

Meena Sundaresan  
Institute of Transportation Studies  
University of California, Davis 95616, USA  
Fax (530) 752-6572  
msundaresan@ucdavis.edu

Institute of Transportation Studies  
One Shields Avenue  
University of California  
Davis, California 95616  
Tel: 530-752-0247 Fax: 530-752-6572  
<http://www.its.ucdavis.edu/>  
email: [itspublications@ucdavis.edu](mailto:itspublications@ucdavis.edu)

**A Thermal Model to Evaluate Sub-freezing Startup for a  
Direct Hydrogen Hybrid Fuel Cell Vehicle  
Polymer Electrolyte Fuel Cell Stack and System**

By

MEENAKSHI SUNDARESAN

B.S.M.E. (University of Texas at Austin) 1995

M.S.M.E. (University of California, Davis) 2002

DISSERTATION

Submitted in partial satisfaction of the requirements for the degree of

DOCTOR OF PHILOSOPHY

in

Transportation Technology and Policy

in the

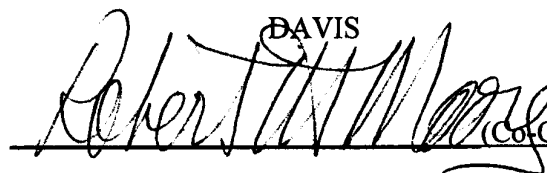
OFFICE OF GRADUATE STUDIES

of the


UNIVERSITY OF CALIFORNIA

DAVIS

Approved:

  
\_\_\_\_\_  
(Co-Chair)

  
\_\_\_\_\_  
(Co-Chair)

  
\_\_\_\_\_

  
\_\_\_\_\_

Committee in Charge

2004

To my husband

## TABLE OF CONTENTS

<b>NOMENCLATURE.....</b>	<b>V</b>
<b>ACKNOWLEDGEMENTS .....</b>	<b>VI</b>
<b>1 INTRODUCTION AND PROBLEM STATEMENT .....</b>	<b>1</b>
<b>2 LITERATURE REVIEW .....</b>	<b>3</b>
2.1 INTRODUCTION.....	3
2.2 REVIEW OF EXISTING COLD START STACK THERMAL MODELS .....	4
2.2.1 <i>Amphlett et al., 1996</i> .....	5
2.2.2 <i>Doss et al., 1998</i> .....	5
2.2.3 <i>Weisbrod et al., 2000</i> .....	6
2.2.4 <i>De Francesco and Arato, 2002</i> .....	7
2.2.5 <i>Gurski, 2002</i> .....	8
2.3 SUMMARY OF CHAPTER 2.....	9
<b>3 MODEL GENERATION.....</b>	<b>10</b>
3.1 CELL/STACK .....	11
3.1.1 <i>Assumptions</i> .....	13
3.1.2 <i>Model construction</i> .....	14
3.2 SYSTEM.....	17
3.2.1 <i>Assumptions</i> .....	19
3.2.2 <i>Model Construction</i> .....	19
3.3 CELL- AND SYSTEM-LEVEL WARMING METHODS.....	23
3.4 CELL- AND SYSTEM-LEVEL WATER MANAGEMENT METHODS.....	28
3.5 SUMMARY OF CHAPTER 3.....	29
<b>4 SIMULATION RESULTS AND DISCUSSION.....</b>	<b>29</b>
4.1 PRELIMINARY LUMPED ANALYSIS .....	30
4.2 STACK OPERATION AT 0°C, LAYERED MODEL.....	32
4.3 EXTREME CASE, LAYERED MODEL.....	38
4.4 COLD START ANALYSIS .....	40
4.5 SUMMARY OF CHAPTER 4.....	45
<b>5 CLOSING REMARKS .....</b>	<b>47</b>
5.1 CONCLUSIONS OF DISSERTATION.....	47
5.2 RECOMMENDATIONS FOR STARTUP STRATEGIES .....	49
5.3 FUTURE RESEARCH .....	50
<b>6 REFERENCES .....</b>	<b>50</b>
<b>7 APPENDIX.....</b>	<b>58</b>
7.1 PROPOSED STRATEGIES IN THE LITERATURE FOR COLD START HEAT AND WATER MANAGEMENT .....	58

7.1.1	<i>Review of warming strategies for direct hydrogen FCV fuel cell stack</i> .....	58
7.1.2	<i>Review of frozen water management strategies</i> .....	61
7.2	VALIDATION.....	63
7.3	EQUATIONS .....	65
7.4	PARAMETERS .....	99

## TABLE OF FIGURES

Figure 1:	Overview sketch of cell unit and endplates.....	12
Figure 2:	Model sketch of cell unit and endplates .....	13
Figure 3:	Stack temperature distribution.....	15
Figure 4:	Stack temperature distribution (enlarged).....	15
Figure 5:	Endplate/cell number effect on results – temp. distribution over time .....	16
Figure 6:	Endplate/cell number effect on results – relative energy .....	17
Figure 7:	Fuel cell system schematic.....	18
Figure 8:	Cooling loop schematic .....	18
Figure 9:	System component energy balance .....	19
Figure 10:	Small loop configuration.....	20
Figure 11:	System loop configuration without vehicle components .....	21
Figure 12:	System loop configuration with vehicle components.....	21
Figure 13:	Coolant temperature distribution.....	22
Figure 14:	Cell overpotential curve .....	23
Figure 15:	Electrode catalytic chemical reaction.....	24
Figure 16:	Electric resistance wire in membrane.....	26
Figure 17:	External heat source placement.....	27
Figure 18:	Heat source/heat exchanger.....	27
Figure 19:	Stack temperature distribution, trigger comparison .....	33
Figure 20:	Time Elapsed v. Simulation condition, 0°C case .....	34
Figure 21:	Energy Consumed v. Simulation condition, 0°C case.....	35
Figure 22:	Stack temperature distribution, 100 W.....	36
Figure 23:	Stack temperature distribution, heated endplates.....	36
Figure 24:	Stack temperature distribution, heated endplates, kept above 0°C.....	37
Figure 25:	Stack temperature distribution, extreme case, plot 1.....	39
Figure 26:	Stack temperature distribution, extreme case, plot 2.....	39
Figure 27:	Time elapsed, cold start analysis.....	41
Figure 28:	Energy consumption, cold start analysis .....	42
Figure 29:	Time elapsed, impact of HX efficiency.....	43
Figure 30:	Energy consumption, impact of HX efficiency.....	43
Figure 31:	Moles of ice formed and melted, fraction of GDL void volume occupied ....	44
Figure 32:	Temperature and power v. time, effect of melting ice .....	45
Figure 33:	Validation setup.....	64
Figure 34:	Validation results.....	64
Figure 35:	Linear coolant temperature distribution .....	65
Figure 36:	Model sketch of cell unit and endplates .....	66
Figure 37:	Illustration of areas used in equations .....	66
Figure 38:	Illustration for overall heat transfer coefficient derivation .....	67

Figure 39: Endplate energy balance.....	69
Figure 40: Bus energy balance.....	70
Figure 41: I/F plate energy balance .....	72
Figure 42: Anode channel energy balance.....	77
Figure 43: Anode gas diffusion layer energy balance .....	81
Figure 44: Anode catalyst energy balance .....	84
Figure 45: Membrane energy balance.....	86
Figure 46: Cathode catalyst energy balance .....	88
Figure 47: Cathode gas diffusion layer energy balance.....	91
Figure 48: Cathode channel energy balance .....	94
Figure 49: Plate energy balance.....	97

## **Nomenclature**

Unless indicated otherwise, the following nomenclature applies to the equations presented in this dissertation.

A: active area,  $m^2$  (or  $cm^2$ , where noted)

$A_{net}$ : net cell area (total area minus feedholes),  $m^2$

c: concentration,  $mol/cm^3$

$C_{p_{gas_i}}$ : gas specific heat, J/mol K, for i species

$C_{p_i}$ : material specific heat, J/kg K, i=each cell layer

$\dot{n}_i$ : flowrate, mol/sec for i species

F: Faraday's Law, 96485 Coulombs/mol electrons

$h_i$ : enthalpy, J/mol for i species

h: heat transfer coefficient,  $W/m^2K$

i: current density,  $Amps/m^2$  (when multiplied by active area, A) or  $Amps/cm^2$  where noted

I: current, Amps

k: thermal conductivity, W/m K

MW: molecular weight, kg/mol

$\bar{n}$ : specie quantity, mol

$\bar{R}$ : universal gas constant, 8.315 J/mol K

P: pressure, bars (except where noted)

$\dot{Q}$ : heat rate, J/sec

$SR_i$ : stoichiometric ratio, i = air or  $H_2$

$t_i$ : material thickness, m

T: temperature, K

$V_i$ : material volume,  $m^3$ , i=each cell layer

WEG: water/ethylene glycol (coolant)

X: mole fraction

Y: mass fraction

### **Greek symbols**

$\epsilon$ : factor used to determine volumetric vapor content

$\phi$ : relative humidity  
 $\eta$ : overpotential, volts  
 $\rho_i$ : material density, kg/m<sup>3</sup>, i=each cell layer  
 $\rho_{res_i}$ : specific resistance, ohm-m, i=each cell layer

### Subscripts

void: channel flowfield, porosity voids (e.g.  $A_{void} = A * \% \text{ porosity or \% contact area}$ )  
L: channel lands, solid portion of porous material (e.g.  $A_L = A*(1 - \% \text{ porosity or \% contact area})$ )  
liq: liquid  
gases: gases  
avg: average

## **Acknowledgements**

I am very grateful to the many individuals who have made the research discussed in this dissertation possible. I would like to acknowledge the members of my committee. Dr. Robert Moore provided expert technical advice and guidance throughout my years of research. I thank him for his interest in my academic and professional career. Professor Dan Sperling encouraged my pursuit of a doctorate and shared his experiences of living abroad. He enthusiastically convinced me to take the internship opportunity in Germany. Professor Myron Hoffman was the Chair of my Master's thesis committee and never wavered in his interest to continue to be a part of my research efforts. Professor Harry Dwyer was also on my Master's thesis committee. I appreciate his technical contributions to this dissertation and his first-hand advice on living in Germany.

I would also like to acknowledge various people who contributed to my research while at DaimlerChrysler from October 1, 2002 through September 30, 2003. I am indebted to Mr. Hans-Christian Winter and Dr. Dirk Walliser for opening the first doors to this opportunity. Without their assistance, this internship would not have been possible. Walter Baumgärtner, my supervisor and unofficial German language teacher, worked hard to make it possible for me to be a part of his group. I thank him for his openness and guidance throughout the internship. I consider Markus Schudy as the perfect role model for an aspiring doctorate. His time and patience were even more valuable than the technical knowledge he imparted, as he was also working hard to complete his own dissertation. I would also like to thank Dr. Stefan Reiff, Alexander Reelsen, Clemens Bögershausen, Ralf Koch, Alexander Schwank, and Christian Meyer-Delius for their assistance and encouragement. From Ballard Power Systems, Dr. Sven Schmalzriedt, Dr. Uwe Limbeck and Dr. Joachim Blum provided technical support. I appreciate their willingness to form this partnership.

I would also like to acknowledge the contributions in the very early stages made by some former UC Davis students. I want to thank Parvastu Badrinarayanan for our brainstorm sessions and water management discussions. I also want to thank Joshua Cunningham and Dr. Karl-Heinz Hauer who provided insight on system and vehicle issues.

The work was partially funded by DaimlerChrysler and the National Science Foundation's Integrative Graduate Education and Research Traineeship (IGERT) program. I am grateful to them for their support.

Finally, I want to express my heartfelt gratitude to my family and friends. I attribute the successes in my life to their constant encouragement and love.

## **Abstract**

For passenger fuel cell vehicles (FCVs), customers will expect to start the vehicle and drive almost immediately, implying a very short system warmup to full power. While hybridization strategies may fulfill this expectation, the extent of hybridization will be dictated by the time required for the fuel cell system to reach normal operating temperatures. Quick-starting fuel cell systems are impeded by two problems: 1) the freezing of residual water or water generated by starting the stack at below freezing temperatures and 2) temperature-dependent fuel cell performance, improving as the temperature reaches the normal range. Cold start models exist in the literature; however, there does not appear to be a model that fully captures the thermal characteristics of the stack during sub-freezing startup conditions. Existing models do not include stack internal heating methods or endplate thermal mass effect on end cells.

The focus of this research is the development and use of a sub-freezing thermal model for a polymer electrolyte fuel cell stack and system designed for integration within a direct hydrogen hybrid FCV. The stack is separated into individual cell layers to determine an accurate temperature distribution within the stack. Unlike a lumped model, which may use a single temperature as an indicator of the stack's thermal condition, a layered model can reveal the effect of the endplate thermal mass on the end cells, and accommodate the evaluation of internal heating methods that may mitigate this effect.

This research is designed to answer the following motivating questions:

- What detailed thermal model design will accurately characterize the fuel cell stack and system during the sub-freezing startup operation?
- What are the effects of different startup strategies on energy consumption and time to normal operation?

These questions are addressed in this dissertation. Major research findings include the following recommendations for the best startup strategies based on model parameter values and assumptions: 1) use internal heating methods (other than stack reactions) below 0°C, 2) circulate coolant for uniform heat distribution, 3) minimize coolant loop thermal mass, 4) heat the endplates, and 5) use metal such as stainless steel for the bipolar plates.



# **1 Introduction and Problem Statement**

In early 2002, the U.S. Department of Energy (DOE) announced a new partnership with USCAR (consortium of Big Three automakers DaimlerChrysler, Ford and General Motors) called FreedomCAR whose goal is to reduce U.S. dependence on petroleum through the development of hydrogen-powered fuel cell cars and light trucks. The primary focus of FreedomCAR is on basic research to provide fuel cell vehicles that use no petroleum. Considerable research and development effort has been funded through DOE under FreedomCAR's predecessor, the Partnership for a New Generation of Vehicles (PNGV), for hydrogen/air fuel cells powered directly by hydrogen and indirectly with other fuels. While much progress has been made on advancing fuel cell systems, the primary challenges for direct hydrogen systems are the lack of retail refueling infrastructure, on-board hydrogen storage, cost, durability, size and weight (U.S. DOE, 2001).

In addition to these challenges, reducing system startup time can produce interesting implications for the system configuration, such as the need to hybridize, which adds complexity and possibly cost. For passenger fuel cell vehicles, customers will expect to start the vehicle and drive almost immediately, implying a very short system warmup to full power. For the direct hydrogen system, the current DOE requirement for the 2010 goal of cold startup from  $-20^{\circ}\text{C}$  to maximum power is 30 seconds (U.S. DOE, 2002). While there is debate on the conditions in which hybridization would be useful, given complexity and added cost (Friedman, 1999), some studies concede that the cold start operation would require hybridization (Nadal and Barbir, 1996; Atwood et al., 2001; Rajashekar, 2000; Paganelli et al., 2002).

While hybridization strategies may fulfill the expectation of rapid driveaway, the extent of hybridization will be dictated by 1) the time required for the fuel cell system to reach normal operating temperatures, 2) packaging limits in real vehicles, and 3) effects of added weight. An analysis tool is developed and used in this dissertation to explore methods to minimize the startup time.

## ***Problem Statement***

A cold start fuel cell stack thermal model is a tool that can be used to analyze different warming strategies. However, a model that fully captures the thermal characteristics of the stack during sub-freezing cold start is not currently available. **Based on an evaluation of existing cold start stack thermal models in the literature, a new cold start stack thermal model is necessary to meet the criteria defined for an acceptable cold start simulation.**

Existing models lack the following features:

- Modeling of stack internal heating methods (other than stack reactions) and their impact on the stack temperature distribution.
- Modeling of endplate thermal mass effect on end cells and its impact on the stack temperature distribution.

Existing cold start stack thermal models address and model external heating methods as well as heat generated internally due to stack reactions. However, these

models consider the stack as a lumped mass and do not also accommodate the evaluation of other internal heating methods that are more easily included when the individual cell layers are modeled. Part of the evaluation of these heating methods includes observing the stack temperature distribution and even the cell temperature distribution to investigate temperature excursions within sensitive components such as the polymer electrolyte membrane (PEM). (PEM fuel cell stacks are considered suitable for transportation applications because they provide continuous electrical energy at high efficiency and power density (Thomas and Zalbowitz, 1999)).

Furthermore, these models do not explicitly account for the effect of the endplate thermal mass on the stack. The thermal mass of the endplates draws heat from the cells at both ends of the stack and affects the stack temperature distribution. Existing models use a single stack temperature or stack coolant outlet temperature, for example, as an indicator of the stack's thermal condition; however, in a model in which the cell layers are separate, the condition of each cell within the stack can be observed. For example, if the stack cannot operate until it is heated to 0°C, a single temperature may hide the fact that the end cells are lower than 0°C, resulting in ice formation if the stack is operated.

### ***New Model***

The one-dimensional, layered cell thermal model developed in this dissertation considers the features, in addition to those found in existing models, which form an analysis tool for sub-freezing cold start of a PEM fuel cell stack. Specifically, the main features of this new model are:

- Multi-layered structure (considers individual cell layers)
- Inclusion of transients and important physical effects,
- Inclusion of heat of fusion in energy balance to account for melting ice at 0°C (formed if stack operates at sub-freezing temperatures),
- Evaluation of external heating methods,
- Evaluation of internal heating methods, facilitated by a layered cell model,
- Consideration of endplate thermal mass to obtain a stack temperature distribution which will characterize a stack's condition more accurately than the simple surrogate of a single stack temperature, also facilitated by a layered model,
- Ability to set initial temperature to any temperature, especially sub-freezing temperatures, and
- Validation with experimental data.

The model includes those features not considered by existing cold start stack thermal models, namely the ability to observe the impact on the stack temperature distribution by stack internal heating methods (other than stack reactions) and the endplate thermal mass effect on end cells.

This new model was developed using Matlab<sup>®</sup>/Simulink<sup>®</sup> software. In a transportation application, such as a direct hydrogen hybrid fuel cell vehicle, the cold start operation generally includes the entire fuel cell system. Therefore, the layered cell thermal model is incorporated into a fuel cell system in which system component thermal masses have also been included. The fuel cell system used is one designed for integration into a direct hydrogen hybrid fuel cell vehicle model (DaimlerChrysler, Ballard Power Systems, 2003).

The cold start thermal model simulates startup for a non-moving vehicle. It is understood that the cooling loop heat fluxes may be different while the vehicle is being driven. However, these interactions are not within the scope of this dissertation.

### ***Organization of Dissertation***

This dissertation is organized in three main chapters. In Chapter 2, a review of existing cold start stack thermal models is presented. In Chapter 3, the model generation is described, including equations and non-proprietary component data, and a comparison is made between a lumped stack model and a layered cell model. In Chapter 4, simulation results are shown to highlight the capabilities of the layered cell thermal model and evaluate various warming methods using the model at the stack and system levels.

### ***Confidentiality***

The model has been validated against experimental data using DaimlerChrysler and Ballard Power Systems proprietary parameter values, but is used in this dissertation for simulations with literature-based and non-proprietary parameter values that do not necessarily represent the state-of-the-art. The purpose of the model is not to show how to attain the DOE goal of 30 seconds from  $-20^{\circ}\text{C}$  to “maximum power” (U.S. DOE, 2002), for example, but to demonstrate the benefits of this model as a tool for cold start analysis.

## **2 Literature Review**

This chapter analyzes different publicly available cold start fuel cell stack thermal models and makes a qualitative comparison among them. The qualitative comparison uses a set of criteria based on suggested design and operating guidelines to minimize startup time from sub-freezing temperatures (Weisbrod et al., 2000). Criteria for fuel cell vehicle models in general are discussed in Hauer (2001) and, while not considered here specifically, can be applied to the cold start stack thermal models. (A separate literature survey of cold start heat and water management is summarized in the Appendix, Section 7.1.)

Five cold start stack thermal models from the literature are described and their advantages and disadvantages are discussed. It is concluded that none of the investigated models 1) considers internal heating methods other than heat generated during stack operation or 2) explicitly considers the effect of the endplate thermal mass on the end cells of the stack. Both of these factors are important in determining the stack temperature distribution, which can be observed with a stack model sectioned in cell layers. Of the models investigated, all are transient and consider the energy and mass balances for the stack; however, the stack is modeled as a lumped mass and a temperature distribution cannot be obtained.

### **2.1 Introduction**

An outline of requirements for fuel cell vehicle models is found in Hauer (2001) which is a modification of general model criteria (such as: theoretical soundness,

completeness, practicality and valid results), as discussed in Bowman and Akiva (1996). These criteria are considered here in the context of cold start stack thermal models.

Theoretical soundness requires that the model considers relevant physical effects and be solid mathematically. For a cold start stack thermal model, thermal transients should be considered. Furthermore, energy and mass balances should be taken into account, which include sensible energy flows for coolant and anode and cathode gases. Water generation and phase changes (vapor, liquid and ice in the case of sub-freezing temperatures), stack heat losses to the environment, as well as internal heat generation by the electrochemical reactions and ohmic resistance should also be considered.

Completeness requires that a model has flexibility to evaluate several options. For a cold start stack thermal model, there should be a means by which a variety of stack internal and external warming methods can be compared using parameters such as energy consumption and startup time. In addition, there should exist the ability to observe the effect of the endplate thermal mass on the stack temperature distribution. This distribution can be used, for example, to observe the coldest cell (or the cell by the endplate) temperature and determine if it is below freezing even while the other layers are above freezing, a scenario that could generate ice if the stack was operated. Using a single stack temperature or the stack coolant outlet temperature, for example, may not be a good indicator of the actual stack thermal condition because it can hide the effect of the endplate thermal mass on the end cells. Even if the endplate thermal mass is considered in the calculation of the overall stack thermal mass used in the stack temperature calculation, the effect on the end cells is absent.

Practicality requires that a model has the necessary input data and can be validated. For a cold start stack thermal model, stack characteristic data is necessary, such as mass and specific heat, as well as electrochemical data which can determine stack internal heat and gas flows. In addition, a sub-freezing cold start stack thermal model should be functional at an initial temperature set by required technical targets, such as those outlined by the U.S. Department of Energy (U.S. DOE, 2002). Finally, results should be valid within error margins determined from experimental data.

The next section compares five cold start stack thermal models against the criteria explained above, and then describes a new cold start stack thermal model that is the focus of this dissertation. The comparison is summarized and it is concluded that a new cold start stack thermal model is necessary.

## **2.2 Review of existing cold start stack thermal models**

Five models were evaluated for their treatment of startup. These five models were chosen because they were the only ones in the literature that used a stack thermal model to specifically address cold start. The developers are listed below in chronological order:

- 1) Amphlett et al., 1996 - Royal Military College of Canada
- 2) Doss et al., 1998 - Argonne National Laboratory
- 3) Weisbrod et al., 2000 - Los Alamos National Laboratory
- 4) De Francesco and Arato, 2002 - Università di Genova
- 5) Gurski, 2002 - incorporated a transient model into Advisor (vehicle simulation program developed by National Renewable Energy Laboratory)

### 2.2.1 Amphlett et al., 1996

Amphlett et al. (1996) developed a steady state model (electrochemical coupled with thermal) that was transformed into a transient model that determines stack performance when the stack undergoes a disturbance, such as startup from room temperature. The general form of their transient model is

$$MC \frac{dT_{stack}}{dt} = \dot{q}_{theor} - \dot{q}_{elec} - \dot{q}_{sens} - \dot{q}_{loss}$$

where the left side of the equation is the accumulation term, and the right side terms are, respectively, the theoretical energy produced by the fuel cell reaction, the electric energy output, the energy from each of the fuel cell streams, and the heat loss from the stack surface.

Their model was validated against experimental data obtained from a Ballard Mark V stack. Model results were compared with experimental data for stack voltage, current, and temperature response to a load step of 0 to 20 Amps, for example. The authors determined that the model acceptably predicts the experimental data.

Strengths:

- Transient nature of cold start and physical effects are addressed.
- Internal warming by stack reactions is included.
- Model results are validated with experimental data.

Weaknesses:

- Lowest temperature evaluated is room temperature; sub-freezing temperature is not considered. Sub-freezing water management is not considered.
- External or internal heating methods other than stack reactions are not included.
- Stack temperature distribution is not possible and effect of endplate thermal mass on end cells is not considered.

### 2.2.2 Doss et al., 1998

Doss et al. (1998) perform a transient analysis of a 50-kW hydrogen-fueled polymer electrolyte fuel cell system starting from 27°C. The fuel cell is considered as a control volume with values for weight, surface area, heat transfer coefficient and specific heat. In their study they show the stack transient response in reaching its operating temperature of 80°C with and without the coolant bypassing the radiator. Mass and enthalpy balances are also part of the model and are detailed in an earlier study by other Argonne National Laboratory researchers (Kumar et al., 1994). It is unclear whether the stack model thermal response itself is compared to stack experimental data.

Strengths:

- Transient nature of cold start and physical effects are addressed.
- Internal warming by stack reactions is included.

Weaknesses:

- Lowest temperature evaluated is 27°C; sub-freezing temperature is not considered. Sub-freezing water management is not considered.
- External or internal heating methods other than stack reactions are not included.
- Stack temperature distribution is not possible and effect of endplate thermal mass on end cells is not considered.

- Validation of stack thermal model results with experimental results is unclear.

### 2.2.3 Weisbrod et al., 2000

Weisbrod et al. (2000a) addresses stack warm up through experimentation and transient model development. An overall heat and mass balance was defined around their stack. Their initial ambient temperature is  $-40^{\circ}\text{C}$ , and they obtained estimates of stack warm up time with and without an external heat source. Some of the assumptions they made for the configuration without the heat source are:

- there is no interaction with coolant system;
- dry air is available from compressor at  $78^{\circ}\text{C}$  (isentropic compression from  $-40^{\circ}\text{C}$ ); and
- the bipolar plates are thermally isolated from the end plates.

For the external heat source case, they used the above assumptions except they simulated waste heat from a fuel processor to warm stack coolant. Coolant comprised of a 60% ethylene glycol/water mixture was pumped through the stack cooling channels and returned to a reservoir until the stack reached operating temperature.

For the case without the heat source, they made the following conclusions:

- Reduce the thermal load of the end plates by thermal isolation or reduced heat capacity or thermal conductivity. The end plates can be an additional thermal mass that would need heating when warming up the stack. Furthermore, the end plates can draw heat away from within the stack.
- Operate the stack at a constant low stack voltage to maximize stack heat production.
- Compressor heat provides little benefit (Weisbrod et al., 2000b)
- Feed dry gases up to  $0^{\circ}\text{C}$  to unplug ice-packed feed lines and internal stack components.

For the external heat source case, they added the following conclusions:

- Minimize the coolant thermal mass.
- A large external heat source is required to bring stack startup times to a half minute.

Part of the authors' analysis included calculations determining the fraction of the gas diffusion layer (GDL) void volume that would be occupied by ice formed from water produced in the stack reactions. The porosity of the GDL ensures effective diffusion of the reactant gases to the catalyst. The GDL also allows permeation of water vapor to the membrane to keep it humidified and allows liquid water produced at the cathode to leave the fuel cell. The authors indicate that the impact of ice upon gas diffusion into the catalyst layer will be evaluated in future experiments.

Finally, the authors validated their model results with experiments conducted on an Energy Partners stack designed for cold start testing. Anode, cathode and coolant outlet temperatures were among the experimental results, as well as endplate and stack temperature. The measured and calculated coolant inlet and outlet temperatures were compared, the model results were deemed valid by the authors, and further predictions were made with the validated model.

Strengths:

- Transient nature of cold start and physical effects are considered.

- Water management issues such as purging ice and using dry gases up to 0°C are discussed. The model determines the portion of the GDL covered by ice.
- Internal warming by stack reactions and warming by an external heat source are included.
- It is assumed that the bipolar plates are thermally isolated from the endplates and methods are suggested to improve startup time (reducing the thermal load of the end plates by thermal isolation or reduced heat capacity or thermal conductivity).
- Temperature is initialized at -40°C.
- Model results are validated with experimental data.

Weaknesses:

- Internal heating methods other than stack reactions are not considered.
- Stack temperature distribution is not possible.

#### 2.2.4 De Francesco and Arato, 2002

In their work, De Francesco and Arato (2002) describe a model that evaluates various startup strategies considered for a hybrid fuel cell bus; however, the principles are applicable to a range of vehicles. They developed a transient, lumped stack model using the equation below.

$$M_t(C_p)_{stack} \frac{\partial T_{stack}}{\partial t} = h_{air}s_{air}(T_{air} - T_{stack}) + h_{est}s_{est}(T_{ext} - T_{stack}) - \left( \frac{\Delta H}{n_e F} + V^c \right) IS$$

where  $M_t$  is the total weight of the stack,  $s_{air}$  is contact area air per cell,  $h_{est}$  is the heat transfer coefficient for the external stack surface,  $s_{est}$  is the external stack surface area,  $T_{ext}$  is the temperature external to the stack,  $V^c$  is cathode voltage,  $I$  is current density and  $S$  is total internal cell surface area.

The authors considered four startup methods for the fuel cell system primarily related to the compressor and the stack heating itself. They evaluated the methods under worst-case system conditions, i.e. no external heating, heating by inlet gases during steady state compression, and no external humidification. They provide results and discussion for conditions below freezing, and discuss the possibilities for startup when environmental conditions obviate the need for humidification. However, under conditions when the stack requires humidification and heating, they discuss the use of an air humidifier and air heater.

Laboratory data were obtained in a procedure requiring a screw compressor run by a motor, which was connected to a tubing setup representing the pressure drop associated with a 30 kW fuel cell stack. While the data from this experiment is used in the model, it is unclear whether the stack model thermal response itself is compared to stack experimental data.

Strengths:

- Transient nature of cold start and physical effects are addressed.
- Internal warming by stack reactions is included. Use of external heat under certain conditions is discussed.

Weaknesses:

- Lowest temperature shown in plots is around -13°C, but not as low as -20°C. Sub-freezing water management is not considered.

- External or internal heating methods other than stack reactions are not included; however, it is recognized that the authors assumed a worst-case condition in which external heating is not available.
- Stack temperature distribution is not possible and effect of endplate thermal mass on end cells is not considered.
- Validation of model results with experimental results is unclear.

### 2.2.5 Gurski, 2002

Gurski (2002) describes in detail a transient fuel cell system and vehicle model developed to quantify the effects of cold start operation on performance and efficiency of a fuel cell system. The vehicle model was part of the Advisor vehicle simulator, developed by the National Renewable Energy Laboratory, in which the user can set data and characteristics of different vehicles. For Gurski's work, the vehicle model was based upon a hybrid fuel cell vehicle called Magellan (using the Ford Explorer platform) that was developed at Virginia Polytechnic Institute and State University. The transient model has two components – an electrochemical model which includes parasitic losses, and a thermal model that uses a finite difference lumped thermal capacity method to model the stack, reservoir and plumbing. The humidifier, condenser and radiator are also included in the thermal model.

The thermal stack model with the finite method energy and mass balance as found in Gurski (2002) is shown below.

$$T_{stack} = T_{previous} + \frac{timestep}{lumped\ capacitnce} (HeatGen - Q_{coolant} - Q_{ambient} - Q_{air} - Q_{water\_vapor} + Q_{condensng})$$

In Gurski's thermal stack model, inlet and outlet flows and internal heat and water generation are considered. Gurski provides cold start results for the stack, system and vehicle (by integrating his transient system model into the Advisor vehicle simulator), but only for temperatures at 0°C and above. Finally, data for the vehicle model was obtained from Magellan. While in general the models in Advisor are validated against real vehicle data (NREL, 2002), it is unclear whether the thermal model was validated against experiments conducted with Magellan.

Strengths:

- Transient nature of cold start and physical effects are considered.
- Internal warming by stack reactions is included.

Weaknesses:

- Lowest temperature evaluated is 0°C; sub-freezing temperature is not considered. Sub-freezing water management is not considered.
- External or internal heating methods other than stack reactions are not included.
- Stack temperature distribution is not possible and effect of endplate thermal mass on end cells is not considered.
- Validation of thermal model results with experimental results is unclear.



### 2.3 Summary of Chapter 2

In this chapter a review of existing cold start stack thermal models is provided. These models were evaluated against a set of criteria discussed at the beginning of the review. Table 1 summarizes the strengths and weaknesses of each model as they relate to theoretical soundness (criteria 1 and 2), completeness (criteria 3, 4 and 5), practicality (criterion 6) and validity (criterion 7) from a cold start stack thermal model standpoint.

Criterion 1, or *transient and physical effects*, is met by all of the models. This criterion is a good metric to determine whether or not the model adequately captures the processes present during the cold start operating condition. Criterion 2, or *water management at sub-freezing temperatures*, is met by one model. Humidification needs during stack operation are modeled by all the models, but only the model developed by Weisbrod et al. (2000) addresses sub-freezing water management issues such as blockage of ice formed from the water produced by the stack reactions.

Criterion 3, or *stack internal warming strategies*, is partially met by all the models because they only considered stack operation, and not other methods, for internal warming. Criterion 4, or *external warming strategies*, is actually modeled by Weisbrod et al. (2000) and only referred to by De Francesco and Arato (2002) as a necessary option under certain circumstances. Criterion 5, or *consideration of endplate thermal mass*, is only addressed by Weisbrod et al. (2000) via an assumption that the bipolar plates are thermally isolated from the endplates.

Criterion 6, or *sub-freezing initial temperature of -20°C*, is only met by Weisbrod et al. (2000), whose initial temperature was at -40°C. Finally, Criterion 7, or *validation with experimental data*, is only met by Weisbrod et al. (2000) and Amphlett, et al. (1996), while for the other models the validation of the thermal model with experimental data was unclear.

	Cold Start Stack Thermal Model	Amphlett et al., 1996	Doss et al., 1998	Weisbrod et al., 2000	De Francesco & Arato, 2002	Gurski, 2002
	Requirement					
Theoretical soundness	1. Transient, physical effects	+	+	+	+	+
	2. Water management at sub-freezing temperatures	-	-	+ <sup>1</sup>	-	-
Completeness	3. Stack internal warming strategies <sup>2</sup>	0	0	0	0	0
	4. External warming strategies	-	-	+	- <sup>3</sup>	-
	5. Consideration of endplate thermal mass	-	-	0 <sup>4</sup>	-	-
Practicality	6. Sub-freezing initial temperature of -20°C	- (room temp)	- (27°C)	+ (-40°C)	- (-13°C)	- (0°C)

Valid results	7. Validation with exper. data	+	-	+	-	-
---------------	--------------------------------	---	---	---	---	---

<sup>1</sup>discusses purging ice and feeding dry gases up to 0°C, calculations show percentage of gas diffusion layer void volume blocked by ice

<sup>2</sup>stack reactions only

<sup>3</sup>only discusses need for external heat under certain conditions

<sup>4</sup>model assumes bipolar plates are thermally isolated from endplates

**Table 1: Model eval. (+ meets req., - does not meet req., 0 partially meets req.)**

Based on this evaluation a new cold start stack thermal model is necessary to meet the criteria defined for an acceptable cold start simulation. The main features of this new model are:

- Multi-layered structure (considers individual cell layers)
- Inclusion of transients and important physical effects,
- Inclusion of heat of fusion in energy balance to account for melting ice at 0°C (formed if stack operates at sub-freezing temperatures),
- Evaluation of external heating methods,
- Evaluation of internal heating methods, facilitated by a layered cell model,
- Consideration of endplate thermal mass to obtain a stack temperature distribution which will characterize a stack's condition more accurately than the simple surrogate of a single stack temperature, also facilitated by a layered model,
- Ability to set initial temperature to any temperature, especially sub-freezing temperatures, and
- Validation with experimental data.

Several proposals for stack internal and external heating methods, as well as water management methods, were found in the literature and were useful in providing ideas for the new model development. A review of these literature sources can be found in Section 7.1. Other stack models that were reviewed in the literature are not specific to startup; however, those studies provide useful details related to the physics and assumptions made in their models' development (Rowe and Li, 2001; Argyropoulos et al., 1999a, 1999b; Dannenberg et al., 2000; Wöhr et al., 1998).

This new cold start stack thermal model could be useful to:

- Automakers and fuel cell stack and system designers, as a tool for evaluating materials, geometries, manufacturing feasibility, and other cell-, stack-, system-, and vehicle-level issues; and
- Universities, as an educational tool.

### **3 Model Generation**

This chapter is divided into two main parts: the fuel cell stack and fuel cell system cooling loop. Both parts include the assumptions, model construction, and parameters for the cell/stack and system components. The stack and system models were developed using Matlab<sup>®</sup>/Simulink<sup>®</sup> software. (The experimental validation of the

model, detailed presentation of equations, and summary of parameters are found in the Appendix, Sections 7.2-7.4.)

The stack is characterized on a cell basis, i.e. a layered cell thermal model is developed using first principles, duplicated and included with endplates to represent a stack. The model is built using energy and mass balances at each layer including sensible energy flows for coolant and anode and cathode gases. Water generation and phase changes (vapor, liquid and ice in the case of sub-freezing temperatures), stack heat losses to the environment, as well as internal heat generation by the electrochemical reactions and ohmic resistance are considered. The primary result of the calculations is the layer midpoint temperature as a function of time. Heat generation is not limited to stack reactions. Other heating methods as well as water management strategies considered on a cell/stack level in the model are those proposed in the literature (see Section 7.1).

The cold start operation generally includes the entire fuel cell system, specifically, the cooling loop; therefore, the layered cell thermal model is incorporated into a fuel cell system, in which system component thermal masses and energy calculations have also been included. External heating methods in the model as well as water management strategies considered on a system level are those proposed in the literature (see Section 7.1). The fuel cell system used is one designed for integration into a direct hydrogen hybrid fuel cell vehicle model (DaimlerChrysler, Ballard Power Systems, 2003). It must be noted that the model assumes the vehicle is not being driven. It is understood that the cooling loop heat fluxes may be different while the vehicle is being driven. However, these interactions are not within the scope of this dissertation.

Finally, due to confidentiality, stack and system parameters used in this dissertation have been obtained from the literature and non-proprietary data and do not necessarily represent the state-of-the-art; however, the stack model was validated against proprietary data as shown in Section 7.2. The purpose of the model is not to show how to attain the DOE goal of 30 seconds from  $-20^{\circ}\text{C}$  to “maximum power” (U.S. DOE, 2002), for example, but to demonstrate the benefits of this model as a tool for cold start analysis.

### **3.1 Cell/Stack**

The cell model assumes a proton exchange membrane (PEM) fuel cell for which the history and electrochemistry have been well documented in the literature (Larminie and Dicks, 2000; Appleby and Foulkes, 1989; Gottesfeld, 1997). As the fuel cell physical and electrochemical processes contribute to the heat generation that is considered in the cell model, a brief background of these processes is necessary to put the cell model generation and Section 7.3 equations into perspective.

Electrochemical reactions consist of half-reactions occurring at the anode and cathode. The electrodes are separated by an electrolyte, or in the case of a PEM fuel cell, the polymer electrolyte membrane. In the oxidation half-reaction at the anode,  $\text{H}^+$  ions from hydrogen gas travel through the membrane to the cathode, and electrons travel through an external circuit to the cathode. In the reduction half-reaction at the cathode, oxygen, which is provided by air supplied to the cathode, combines with the  $\text{H}^+$  ions and electrons to produce water and heat. Catalysts are used on both electrodes to increase the reaction rates. The half reactions are shown below:

Oxidation half-reaction	$2\text{H}_2$	$\rightarrow$	$4\text{H}^+ + 4\text{e}^-$
Reduction half-reaction	$\text{O}_2 + 4\text{H}^+ + 4\text{e}^-$	$\rightarrow$	$2\text{H}_2\text{O}$
Cell reaction	$2\text{H}_2 + \text{O}_2$	$\rightarrow$	$2\text{H}_2\text{O}$

Cooling is needed to maintain stack temperature at around 80°C during normal operation and the product water from the cathode reaction is both liquid and vapor. The product water is carried out of the fuel cell by the cathode airflow. Even with the formation of product water, additional humidification is necessary to ensure effective H<sup>+</sup> ion conduction through the membrane.

The layers in the cold start cell thermal model include bipolar plates (with cooling and gas channels), gas diffusion layer (GDL), catalyst support, and membrane, and a complete stack includes an endplate assembly (end plate, bus plate, and interface (I/F) plate) (see Figure 1). The cell model is one-dimensional (along the y-axis) in which the temperature at the center of each layer is calculated (see Figure 2). The equations and parameters involved in generating the cell model are found in Sections 7.3 and 7.4, respectively. All cells in the stack are built with the same ten layers (i.e. the middle section in Figure 1 is a repeating unit). Energy and mass balances are maintained within the model.

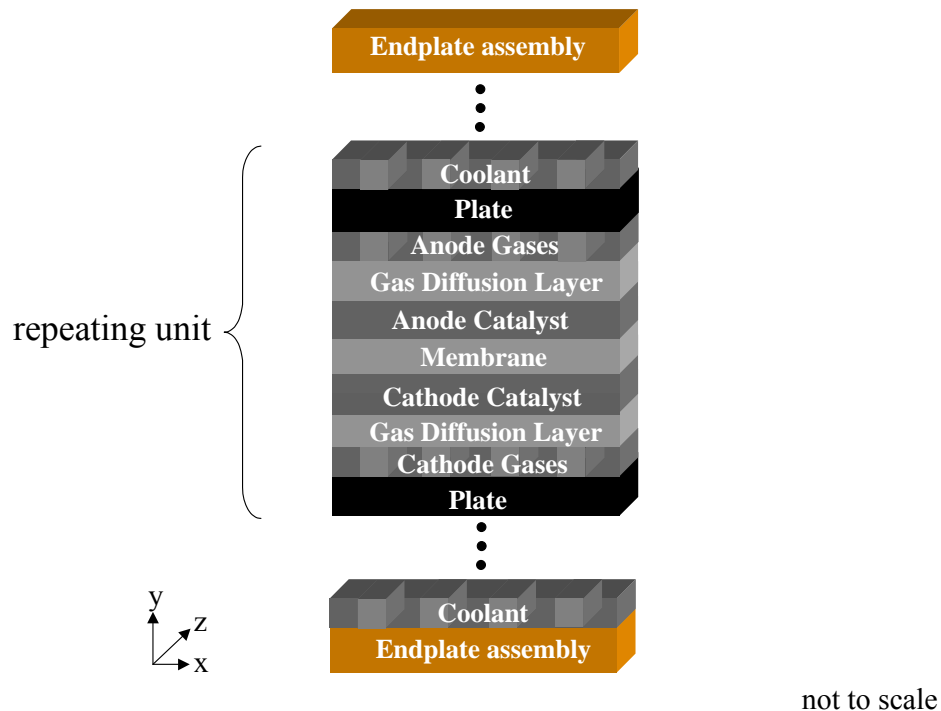


**Figure 1: Overview sketch of cell unit and endplates**

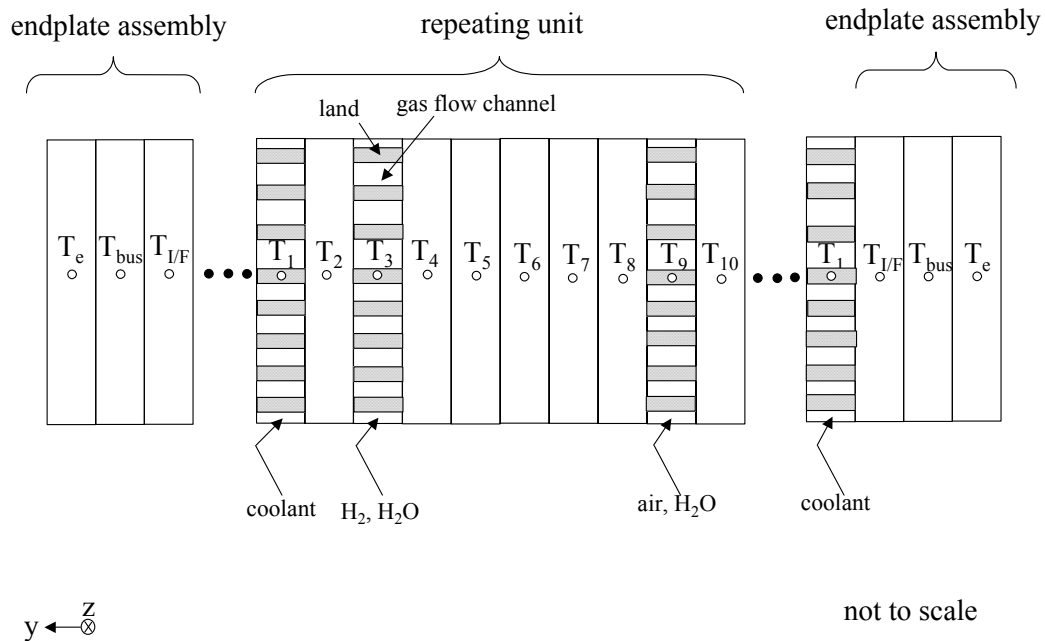


**Figure 2: Model sketch of cell unit and endplates**

### 3.1.1 Assumptions

The assumptions made in constructing the cell model are as follows:

- 1) Inlet temperatures of anode and cathode gases are linked to the inlet coolant temperature since the gases are cooled (or warmed) prior to entrance into the stack and are assumed to be in thermal equilibrium with the coolant.
- 2) A linear temperature distribution along cell in the  $z$ -direction is assumed for the coolant and gas flows.
- 3) The temperature distribution between layer centers has been linearized:  $dT/dy \rightarrow \Delta T/\Delta y$ .
- 4) In gas and coolant channels, the temperature of the land is equal to the temperature of the gas. The land is illustrated in Figure 2 and is defined as the solid portion of the fluid channels.
- 5) For fluid thermal mass calculations, flows (in and out) are averaged.
- 6) There is no slip (difference in velocity) between water vapor and liquid phases.
- 7) Current density,  $i$ , is homogeneously distributed over the active area.
- 8) The net water drag is assumed to be 0, i.e., the electro-osmotic drag through the membrane from anode to cathode and the back diffusion of product water from cathode to anode are assumed to be equal (refer to Sena et al., 1999).

- 9) Humidification of the anode and cathode is obtained from the ambient air; after the stack temperature reaches 30°C, external humidification begins at an assumed 100% inlet humidity.
- 10) Reaction water is assumed to be liquid.
- 11) Heat of vaporization is taken into account in the enthalpy equations.
- 12) Thermal conductivity,  $k$  for the materials is not a function of temperature as the change in  $k$  is small over the temperature range considered.
- 13) Enthalpy and specific heat are functions of temperature.
- 14) Ideal gas law is used for gases.
- 15) Entropy used in cell heat generation equation is not a function of temperature.
- 16) Spontaneous and complete condensation and vaporization are assumed.
- 17) Gas pressure is constant from inlet to outlet.
- 18) It is approximated that the membrane is gas tight (no O<sub>2</sub> or H<sub>2</sub> crossover).
- 19) Perfect air is assumed (79% N<sub>2</sub>, 21% O<sub>2</sub>) with no trace gases.
- 20) The membrane has constant resistance.
- 21) Heat of fusion is taken into account.
- 22) Contact resistance (thermal and electrical) between cell layers is neglected.

### 3.1.2 Model construction

#### ***Lumped stack v. Layered cell/stack model capabilities***

The benefit of a layered cell model is that a cell temperature distribution can be obtained. This distribution is not possible with a lumped model. This distribution can be used, for example, to observe the coldest cell (or the cell by the endplate) temperature and determine if it is below freezing even while the other layers are above freezing, a scenario that could generate ice within the channels if the stack was operated. See Figure 3 for a comparison of a lumped and layered stack temperature distribution while the stack is not on and is heated by an external heat source. Figure 4 is an enlarged view of the layered model of Figure 3 to show how the cells closest to the endplate can be above and below 0°C at a given point in time, while the lumped stack temperature is 0°C for all cells.

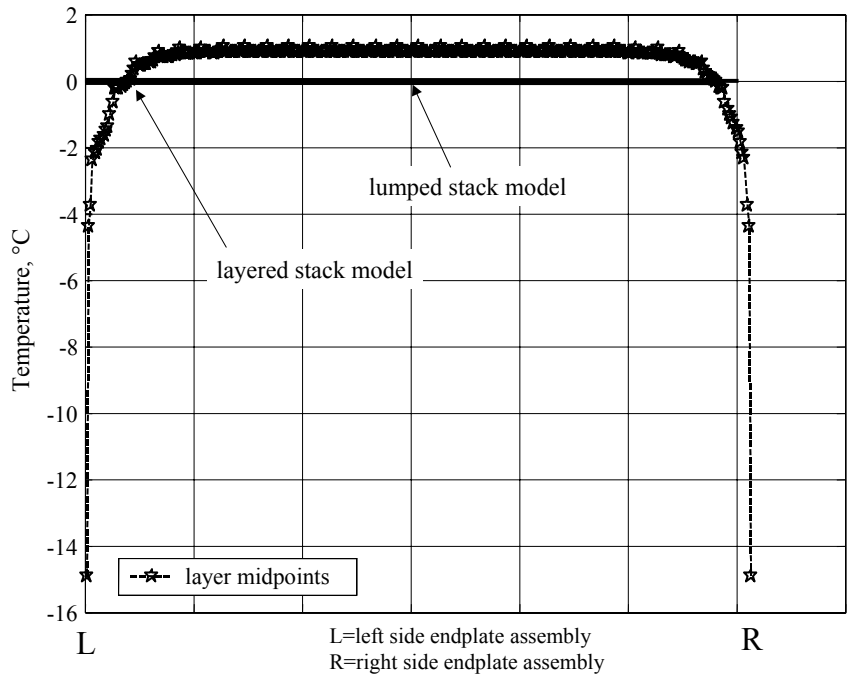


**Figure 3: Stack temperature distribution**

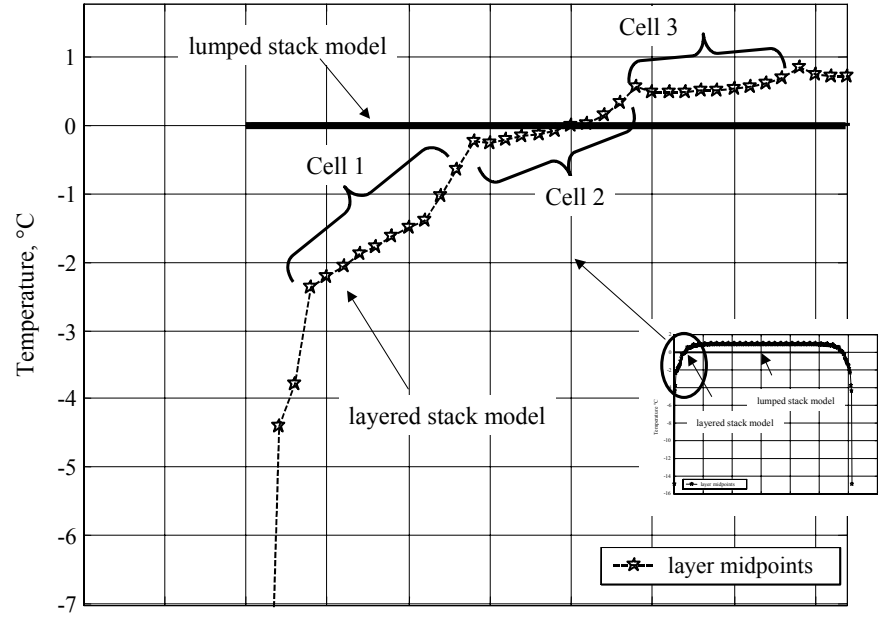


**Figure 4: Stack temperature distribution (enlarged)**

The distribution also can be used to determine the temperature differential across the stack and to monitor the membrane so that it does not exceed the allowable temperature. Furthermore, a layered cell model accommodates internal heating scenarios such as catalytic reactions at the anode and/or cathode or an electric wire at the membrane (see Section 3.3).

**Details of model construction**

Due to computational limitations, it was not possible to construct a model with the total number of cells considered in this dissertation. Therefore, it was necessary to determine the minimum number of cells which could accurately represent a full stack. This minimum number of cells would represent the full stack mass as the energy balance is performed on a cell layer basis, i.e. each layer of each cell increases in temperature over time given its own thermal mass and a normalized heat input.

Consider a case in which the fuel cell stack is off, an external heat source is provided until the coldest cell reaches a certain minimum temperature, and then turns off and the stack turns on until the coldest cell reaches a desired setpoint temperature. Figure 5 shows the temperature distribution over time for 5 and 30 cells. For the same conditions, 5 cells appear to take longer to reach the setpoint temperature. This behavior is a result of the endplate thermal mass. For the 5-cell case, the endplates affect the slope of the curve, thus lagging the 30-cell case and requiring longer time (and more energy) for the coldest cell to reach the desired temperature. As the cell number is increased to 30, the distribution approaches the assumed behavior of an n-cell stack.

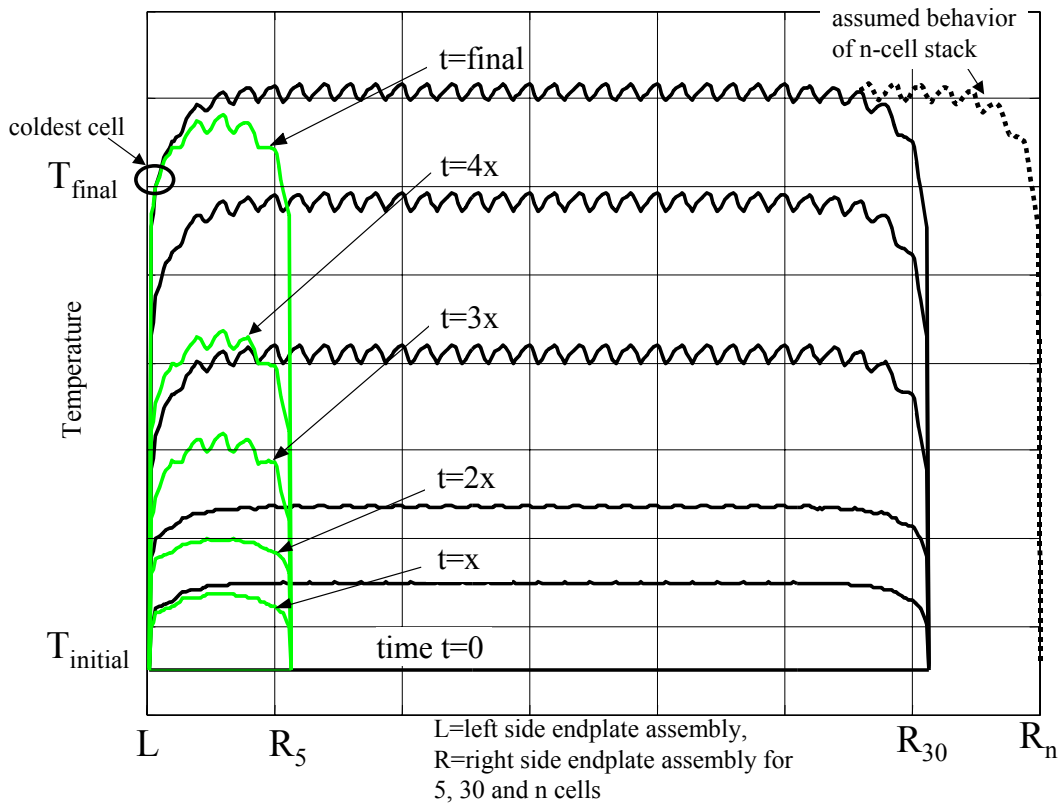


**Figure 5: Endplate/cell number effect on results – temp. distribution over time**



The model uses 30 cells as this number was shown to be the minimum necessary; Figure 6 illustrates the diminishing effect on energy consumption with increasing cell number. Note that this use of a 30-cell stack is a computational run time limitation, not an inherent limitation of the layered modeling methodology developed in this research.

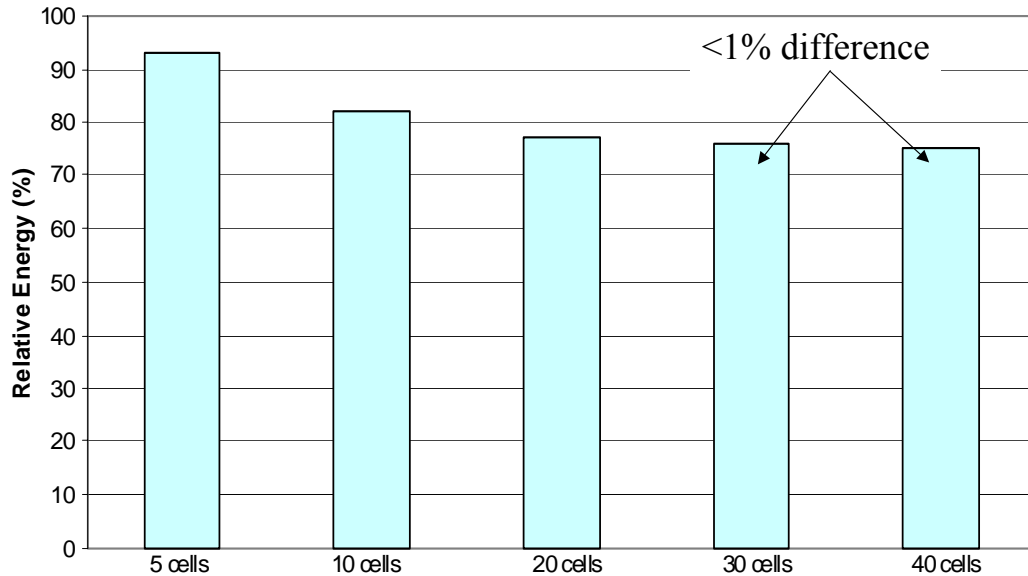


**Figure 6: Endplate/cell number effect on results – relative energy**

### 3.2 System

As the cold start operation generally includes the entire fuel cell system, particularly the system cooling loop, system component and coolant thermal masses (values shown in Section 7.4) and energy calculations have also been included and are discussed in this section. Energy and mass balances are maintained within the model. The components include the stack, compressor, humidifier, and startup heat exchanger (external heat source). Vehicle components such as the coolant pump are included, as well as the radiator fan motor, traction motor and radiator when they are not bypassed. However, the condenser is not included as it is not part of the cooling loop involved in cold start.

The warming method external to the fuel cell, i.e. burner or electric heater, represented by “external heat source” in Figure 7, is integrated into the cooling loop, but also has interactions with other components such as the battery and dc/dc converter (e.g. for an electric heater), and fuel and air supply (e.g. for a burner).

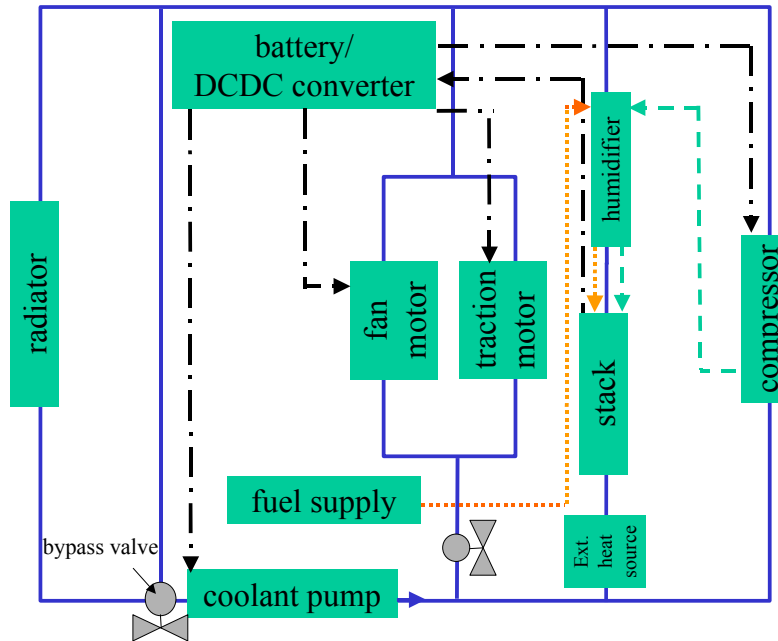


**Figure 7: Fuel cell system schematic**

Flow legend: .... H<sub>2</sub>, - - - air, -.- electrical energy, \_\_\_ coolant

The cooling model in the cold start model serves to carry heat from an external heat source to the stack and system components or circulate stack internal heat. A general schematic of the coolant loop is shown in Figure 8.

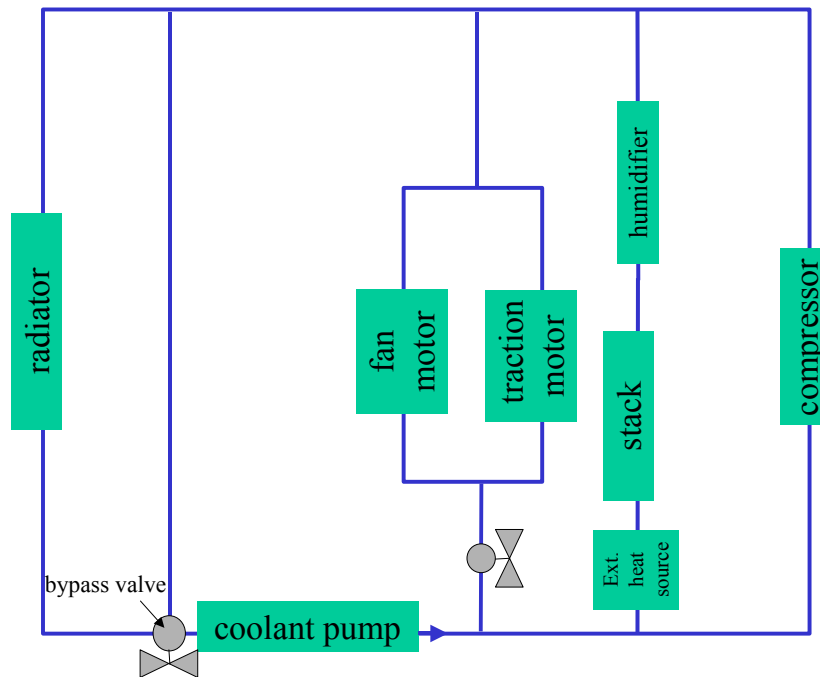


**Figure 8: Cooling loop schematic**

### 3.2.1 Assumptions

- 1) Heat losses from each component (except for the stack) to the environment are not taken into account.
- 2) The temperature calculated for each component is the average temperature and is equal to the component coolant temperature.
- 3) Flow resistances for determining the load on the coolant pump and the parasitic loss due to the pump current draw are considered.
- 4) The flow resistance of a heat exchanger for external heat sources is accounted for in the hydraulic losses.
- 5) The flowrate used in the coldstart model is the midpoint of the range shown in Section 7.4. It is assumed that the coolant pump output may be low in a sub-freezing condition and higher, but controlled by stack temperature, during normal operation. The middle of the pump flowrate range is used, to minimize the number of simulations required.
- 6) For the external warming methods, the heat transfer via a heat exchanger is assumed to be 100% efficient (efficiency is defined as ratio of heat exchanger output to power into heat source) and the full desired power is always available to the coolant. The simulations also include the impact of a heat exchanger that is a more realistic 50% efficient.

### 3.2.2 Model Construction

The cooling model follows the general equation energy shown in Figure 9 and in Equation 1. Component mass, component coolant and system piping coolant are taken into account. Vehicle components such as the fan motor and traction motor as well as the radiator and vehicle piping can be bypassed in the cold start model.

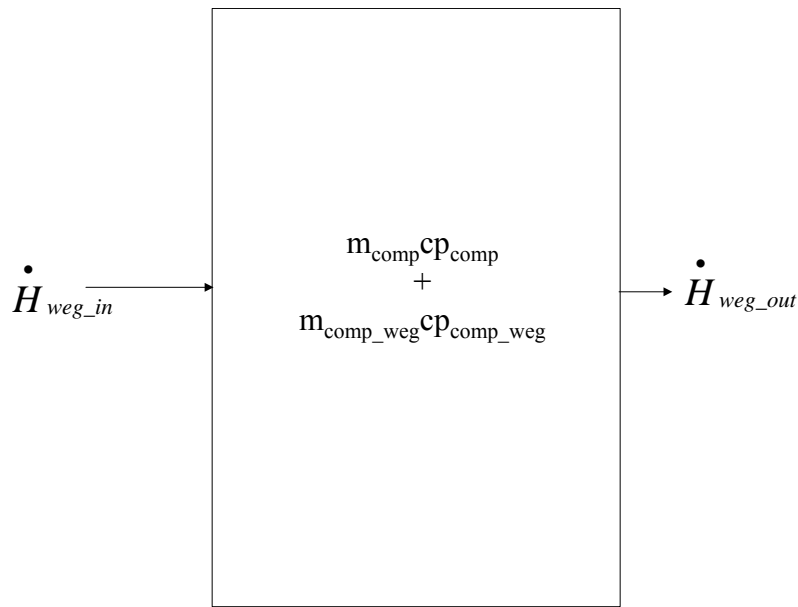


**Figure 9: System component energy balance**

$$\frac{dT_{comp}}{dt} = \frac{\dot{H}_{weg\_in} - \dot{H}_{weg\_out}}{m_{comp}cP_{comp} + m_{comp\_weg}cP_{comp\_weg}}$$

**Equation 1: System component energy equation**

The simulation results shown in Chapter 4 compare scenarios with the coolant circulation on and off to show the effect of both conditions on the stack's temperature distribution during warmup. In addition, for conditions in which the coolant is circulating, the results compare the impact on startup time and energy due to the addition of system and vehicle thermal masses.

Three coolant loop configurations are compared: 1) small loop, including the pump, stack, external heat source, and coolant for these components plus coolant in the stack manifold and system piping, 2) system loop without vehicle components, including the components in the small loop as well as compressor and humidifier component and coolant masses, and 3) the system loop with vehicle components, including all the above components plus the traction and radiator fan motors, the radiator, coolant in these components and coolant in the vehicle piping.

The small loop (with non-operating external heat source but with internally heated stack) is used as the simulation baseline configuration because it is the least thermally massive configuration that accommodates circulation. The system loop without and with vehicle components is used for comparison with the smaller loop (with operating external heat source plus internally heated stack) in the Chapter 4 simulations. An illustration of these coolant loop configurations is shown in dotted lines in Figure 10, Figure 11, and Figure 12.

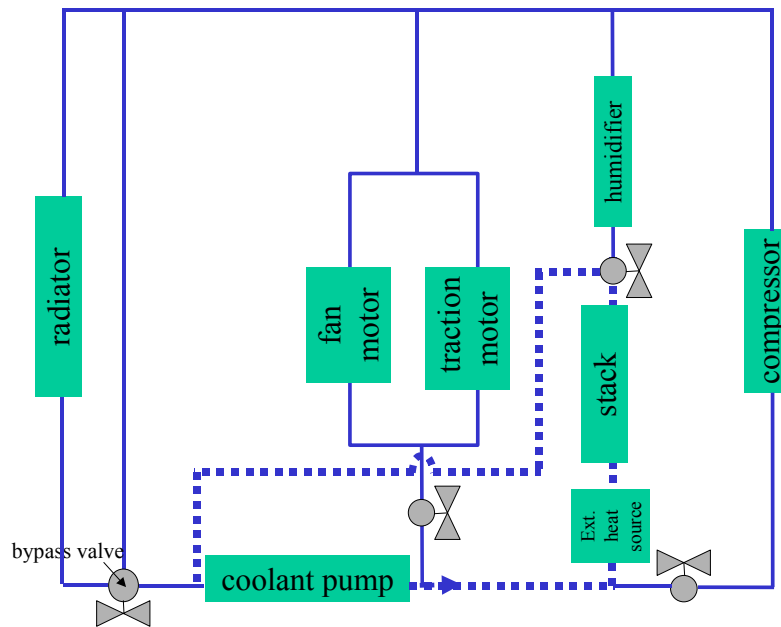


**Figure 10: Small loop configuration**

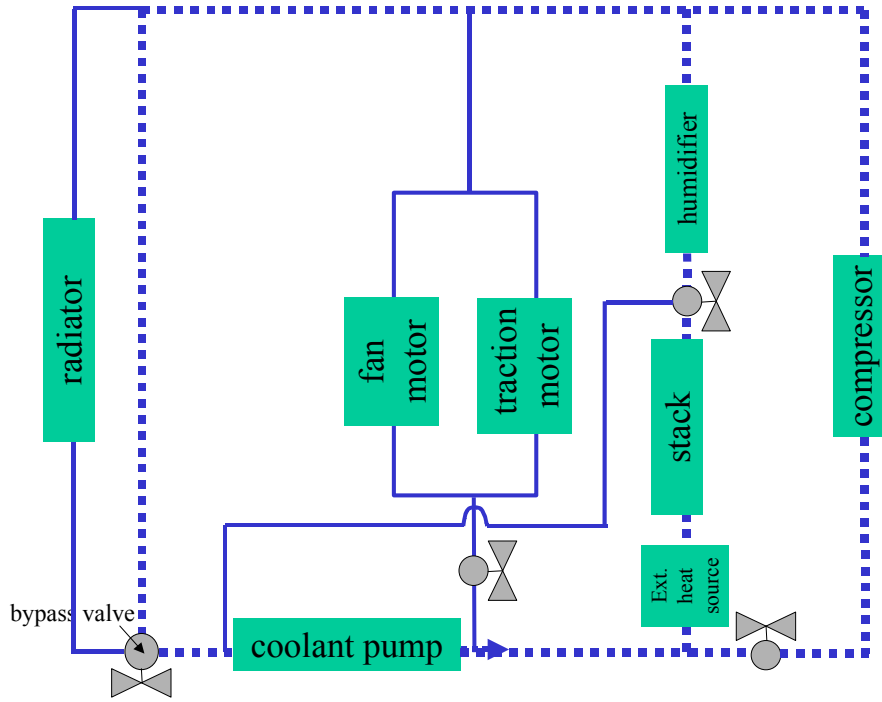


**Figure 11: System loop configuration without vehicle components**

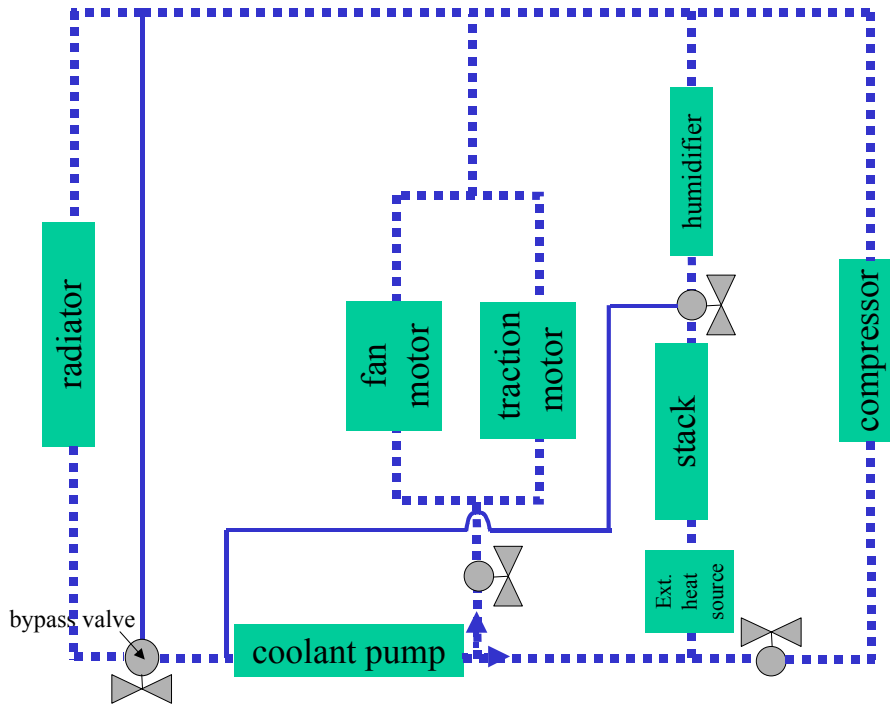


**Figure 12: System loop configuration with vehicle components**

When the coolant circulation is on, the stack coolant outlet temperature is calculated taking into account the fact that the model uses 30 cells to represent 225 cells (plus an extra cooling section for symmetry), for computational efficiency. The model calculates the midpoint temperature, or average, for each layer, including each cooling section. The total coolant flowrate used in the 30-cell model (with 31 cooling sections) is divided by 226 cooling sections and there is equal mass flowrate in all cells. To calculate the stack coolant outlet temperature, consider the following illustration and explanation.

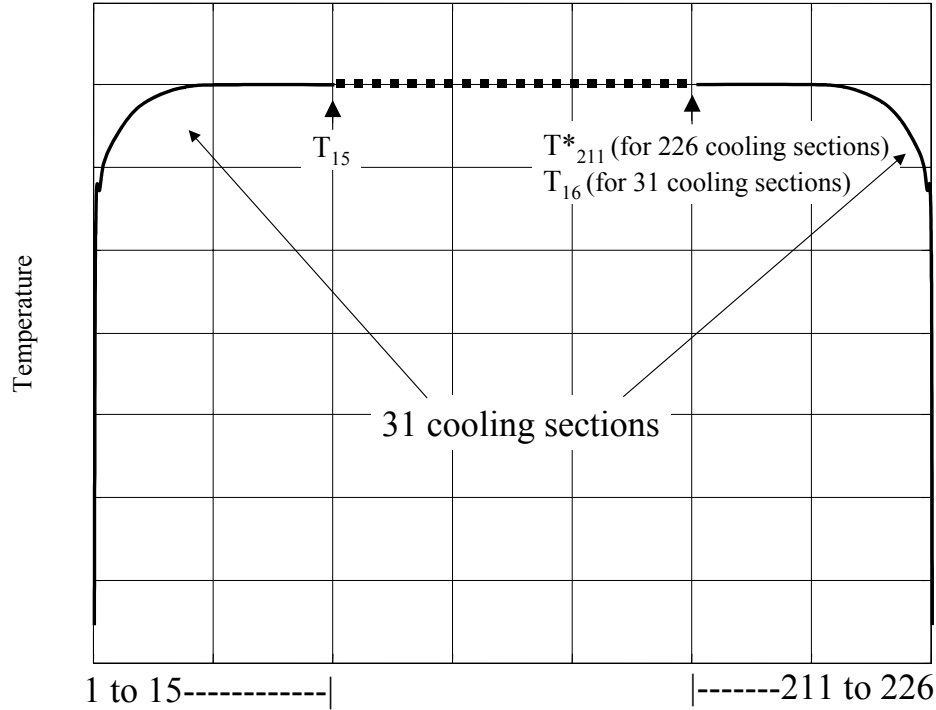


**Figure 13: Coolant temperature distribution**

In Figure 13, let  $T$  be the distribution of 31 cooling sections and  $T^*$  be the distribution of 226 cooling sections. Then  $T^*_1 = T_1$ ,  $T^*_2 = T_2$  and so forth until  $T^*_{15} = T_{15}$ . Since there is no change in the middle section, say starting from  $T_{15}$ , it can be used to represent the middle section of a 226-section distribution, i.e.,  $T^*_{16} = T_{15}$ ,  $T^*_{17} = T_{15}$  and so forth until  $T^*_{210} = T_{15}$ . Then, as shown in Figure 13,  $T^*_{211} = T_{16}$ ,  $T^*_{212} = T_{17}$  and so forth until  $T^*_{226} = T_{31}$ .

The result of the above explanation is the stack coolant outlet temperature for 226 coolant sections and is shown in Equation 2.

$$T^*_{stack\_coolant\_outlet} = \frac{(\sum_{i=1}^{14} T_{out\_i}) + T_{out\_15}(226 - 30) + (\sum_{j=16}^{31} T_{out\_j})}{226}$$

where  $T_{out} = 2T_{avg} - T_{in}$

**Equation 2: Calculation of stack coolant outlet temperature**

### 3.3 Cell- and system-level warming methods

This section will discuss cell- and system-level warming methods found in the literature (see Section 7.1.1) and describe how some cell-level methods are investigated using the cold start stack thermal model.

#### Cell

The methods considered are the following, in which the heat is generated via: a) the fuel cell stack itself when in operation, b) catalytic chemical reactions at the anode and/or cathode (with fuel cell stack off) and c) an electric wire laminated in the membrane (with fuel cell stack on or off). These possibilities are discussed below.

#### A. Stack itself

The stack is a source of heat when it is operating, due to entropy, ohmic and activation losses (including reaction and transport losses). These components are illustrated in the cell overpotential curve in Figure 14.

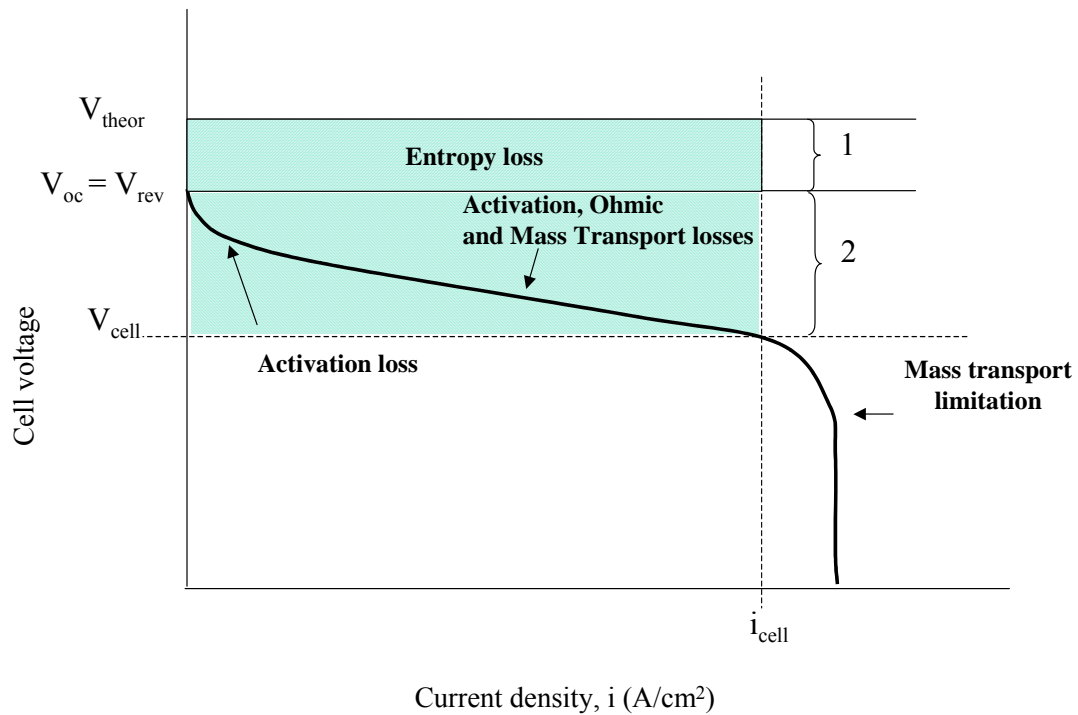


**Figure 14: Cell overpotential curve**

(legend: 1 = entropy loss, 2 = ohmic loss and activation loss including reaction and transport losses)

The cell equations found in Section 7.3 detail the sources of heat generated at the anode and cathode catalysts (Layers 5 and 7) when the stack is operating. The model accommodates the stack operating below  $0^\circ C$ ; however,  $H_2O$  sensible heat flow is not

considered, while H<sub>2</sub> and O<sub>2</sub> sensible heat flows, internal energy, and the heat of fusion are included. Above 0°C, sensible heat flow due to liquid water and water vapor is introduced.

Two sets of literature data are used to determine the stack internal energy. For temperatures from 25°C and above, the expressions found in Amphlett et al. (1995a, b) are used. It was shown in the startup-related paper by Amphlett et al. (1996) that the model presented in the earlier paper produced valid results for initial temperatures around 25°C. For temperatures below 25°C, the data presented by Datta et al., (2002) yields values for current as a function of temperature given the operating voltage. The data in their study is usable to -25°C, which accommodates a starting temperature of -20°C used in this dissertation. This initial temperature was selected to reflect the current United States Department of Energy cold startup requirement for 2010 (U.S. DOE, 2002).

B. Catalytic chemical reactions at electrodes (stack off)

Using controlled amounts of hydrogen and oxygen, it is possible to achieve a temperature rise at the anode and/or cathode catalyst layers. See Figure 15.

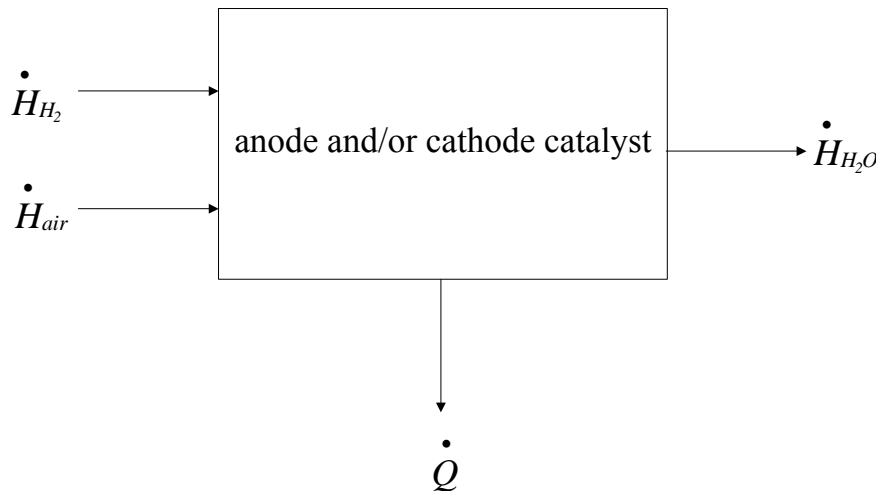
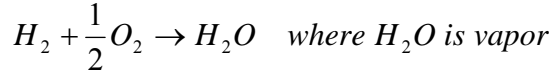


**Figure 15: Electrode catalytic chemical reaction**

The model uses a fixed value for heat flow calculated given a fuel and air concentration. According to Rock and Plant (2001), for a reaction at the anode, the O<sub>2</sub> concentration should be around 1-7% by volume in the anode H<sub>2</sub> flow and for a reaction at the cathode, the H<sub>2</sub> concentration should be 0.5-3.5% by volume in the cathode airflow. Their values are based on an initial temperature of below -25°C. Wheeler and Bonville (2000) and Fuller and Wheeler (2000a) discuss reactions on the cathode side only and suggest that the H<sub>2</sub> concentration should be around 1-2% by volume to less than 4% by volume in the cathode airflow. Their values are based on an initial temperature of -40°C. If O<sub>2</sub> is introduced on the anode side, however, there may be unburned H<sub>2</sub> that



must be dealt with in some way, such as by venting. An example calculation for 1% by volume hydrogen introduced on the cathode side at an initial temperature of  $-20^{\circ}\text{C}$  is shown in the following equations. The reaction is assumed to be steady state, steady flow and adiabatic in this example.



$$\dot{n}_{air\_cell} = \frac{i}{4F} \frac{SR_{air}}{0.21} A = 0.0074 \text{ mol/s}$$

where

$$i = 1 \frac{\text{Amp}}{\text{cm}^2}$$

$$SR_{air} = 2$$

$$A = 300 \text{ cm}^2$$

$$F = 96485 \text{ C/mol}$$

$$\dot{n}_{H_2\_cathode} = 0.01 \dot{n}_{air\_cell} = (7.4e-5) \text{ mol/s}$$

$$\Delta \dot{H}_{react} = \dot{n}_{H_2\_cathode} LHV_{H_2} = 18 \text{ W per cell}$$

react.:

$$H_2 : \dot{n}_{H_2\_cathode} = (7.4e-5) \text{ mol/s}$$

$$O_2 : \dot{n}_{O_2\_cathode} = 0.21 \dot{n}_{air\_cell} = (1.6e-3) \text{ mol/s}$$

$$N_2 : \dot{n}_{N_2\_cathode} = 3.76 \dot{n}_{O_2\_cathode} = (5.8e-3) \text{ mol/s}$$

only  $(3.7e-5) \text{ mol/s } O_2$  required to completely burn  $H_2$  prod.:

$$O_2 : \dot{n}_{O_2\_cathode} = 1.6e-3 - 3.7e-5 \approx (1.6e-3) \text{ mol/s}$$

$$N_2 : \dot{n}_{N_2\_cathode} = (5.8e-3) \text{ mol/s}$$

$$H_2O : \dot{n}_{H_2O\_cathode} = (7.4e-5) \text{ mol/s}$$

$$\Delta \dot{H}_{react} = \Delta \dot{H}_{prod} \quad (\text{with adiabatic assumption})$$

$$\Delta \dot{H}_{prod} = \sum_i (\dot{n} cp)_i (T_{ad} - T_o)$$

where  $T_{ad} = \text{unknown}$ ,  $T_o = -20^{\circ}\text{C} = 253\text{K}$

assume  $cp$  values at  $350\text{K}$  and solve for  $T_{ad}$

$$T_{ad} = 335\text{K} = 62^{\circ}\text{C}$$

**Equation 3: Example calculation for cathode side catalytic chemical reaction**

The example calculation in Equation 3 results in an adiabatic temperature of 62°C, or the highest possible temperature that can be obtained for the given reactant flows in a reaction in which no heat is transferred. The adiabatic temperature could be used as a “worst case” when considering that the temperature must not be higher than, for example, 80°C to prevent membrane drying. Given that heat will transfer from the electrode to adjoining layers, the reaction temperature will be lower.

C. Electric wire in membrane (stack on or off)

Gebhardt and Waidhas (2000) discuss integrating a wire into the cell membrane (see Figure 16). This heating method is modeled simply with a fixed power value in the membrane layer energy balance equation (see Section 7.3).

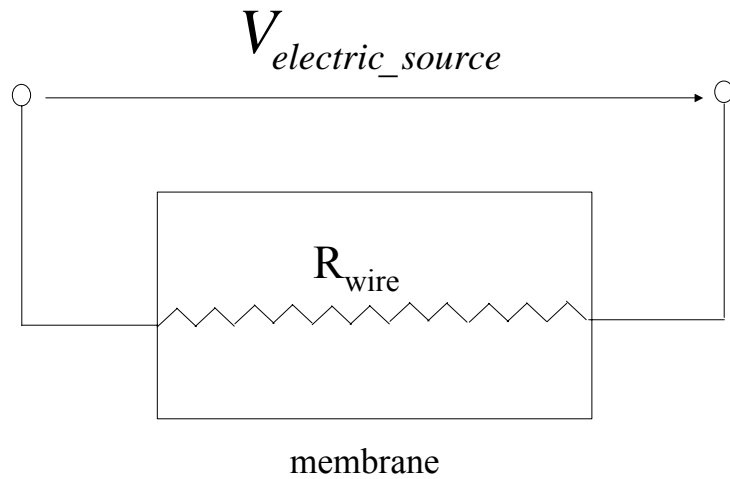


**Figure 16: Electric resistance wire in membrane**

System

Methods which can be used to facilitate fuel cell system startup are heating the coolant with external heat sources, such as a burner or an electric heater. Either component can be placed before or after the stack as shown in Figure 17. For the external warming methods, the heat transfer via a heat exchanger is assumed to be 100% efficient (efficiency is defined as ratio of heat exchanger output to power into heat source) and the full desired power is always available to the coolant. (The simulations also include the impact of a heat exchanger that is a more realistic 50% efficient.) The effect of temperature on a battery, and therefore on an electric heater, is considered in a separate battery thermal model; however, this analysis is outside the scope of this dissertation. The external heat source is illustrated in Figure 18 and the expression used to model the external heat source is shown in Equation 4.

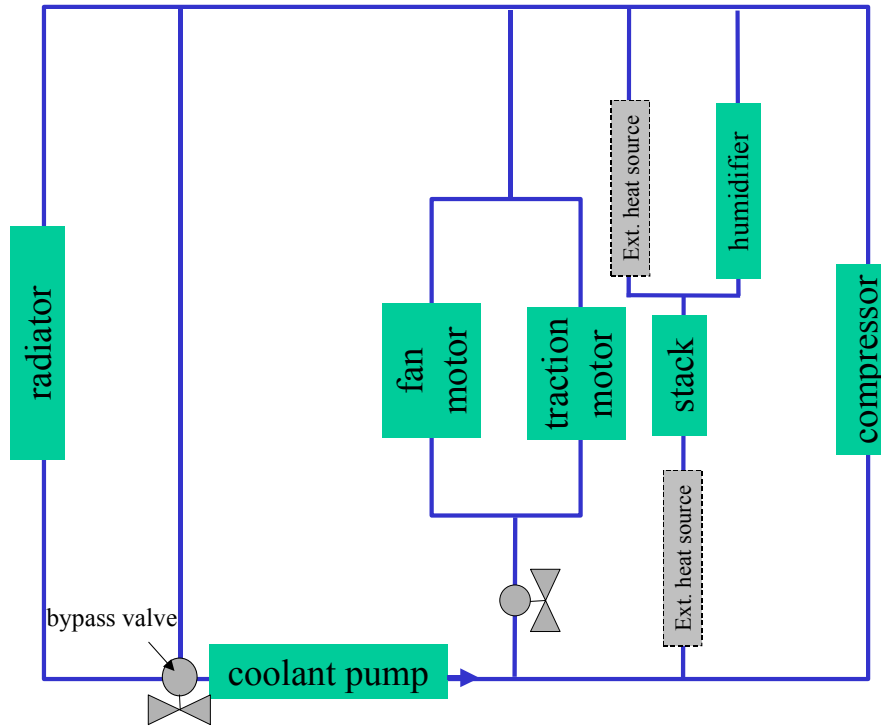


**Figure 17: External heat source placement**  
Before *or* after stack

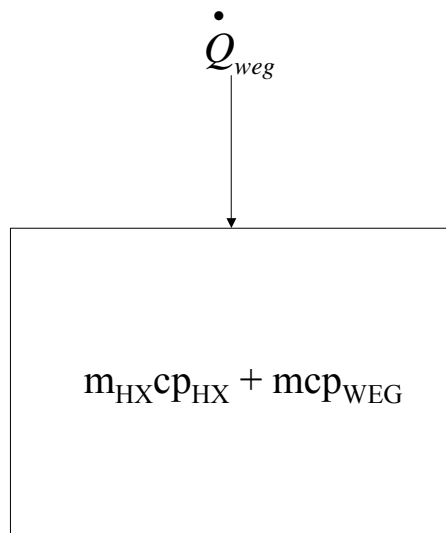


**Figure 18: Heat source/heat exchanger**

$$\dot{Q}_{weg} = (m_{HX} C_{p_{HX}} + m_{weg} C_{p_{weg}}) \frac{dT_{HX}}{dt}$$

**Equation 4: Energy balance**

### 3.4 Cell- and system-level water management methods

There are two cold start water management methods generally discussed in the literature as shown in Section 7.1.2: 1) purge water at shutdown and 2) keep the water from freezing. It is assumed that “water” refers to the de-ionized water used for stack humidification, and not the de-ionized water/ethylene glycol mixture typically used for the stack coolant. It is further assumed that the coolant remains on-board and does not freeze under the conditions considered in this dissertation. However, it is recognized that some fuel cell systems use water for both humidification and cooling functions, as shown in the literature, and have additional challenges as a result of the larger quantity of freezable water.

This section will generally discuss both water management methods on a cell- and system-level and provide details of how these methods are investigated on the cell level using the cold start stack thermal model.

#### *Purge water at shutdown*

This method can involve purging the stack and system of water that is then drained to a tank. The tank may expand to accommodate ice, or be kept above freezing. This method can also involve completely purging the water from the vehicle. However, expelling water from the vehicle to the ground can create icy patches in freezing conditions (Gaarder et al., 2002).

Even if the stack is purged, residual water can remain and freeze. Performing a simple calculation, one can determine the energy and time necessary at startup to melt the ice occupying the cathode GDL, for example.

Consider a stack operating below freezing which has a 300-cm<sup>2</sup> active area. Using the 0.4 mm cathode GDL with 40% porosity used in this dissertation, the total void volume is 4.8 cm<sup>3</sup>, and given the density of ice as 920 kg/m<sup>3</sup>, the mass of ice per cell is around 4.4 grams, or around 0.25 moles.

Using the specific heat,  $c_p$ , of ice of 2040 J/kgK, a temperature rise from -20°C to 0°C, the latent heat of fusion of 334444 J/kg, and an assumed 100 W heat input per cell, the energy and time required to melt the ice in the GDL is shown below:

$$\begin{aligned} \Delta E &= mc_p \Delta T + \Delta H_{fusion} = (0.0044 \text{ kg})(2040 \text{ J/kgK})(20 \text{ K}) + \\ &(0.0044 \text{ kg})(334444 \text{ J/kg}) = 1651 \text{ J} \\ \Delta t &= \frac{\Delta E}{P} = \frac{1651 \text{ J}}{100 \text{ J/s}} = 16.5 \text{ s} \end{aligned}$$

The above calculation assumes no heat transfer via conduction to adjoining layers. As discussed earlier, the cell model accounts for heat conduction between layers, therefore it is possible to observe the effect of the heat rate used for melting on the temperature rise of the layers during warmup. An example that considers melting ice is found in the simulation results, Chapter 4.

While various methods of replenishing humidification water after a complete purge are not actually modeled, the following methods could be considered: 1) melting ice in the tank, 2) relying on stack reaction product water, and 3) generating water from an on-board source, such as a burner which can also be an external heat source for the cold start operation.

### ***Keep the water from freezing***

If water is drained to a tank, it can be kept above freezing by an external heat source. If the water is kept within the stack, however, the stack must be continuously heated or operated at low levels to just exceed the freezing point.

Section 3.3 describes the heating methods that can be used to keep the stack above freezing, if this strategy is used. For example, at shutdown, the stack temperature could be monitored as it is decreasing, so that once a temperature just above freezing, for example, is reached, an on- or off-board heat source can turn on to maintain the stack at an above-freezing state. The stack itself can remain on at a low operation level to achieve the above-freezing state. The caveat to this method, however, is the energy impact of the duration of temperature maintenance.

The cell model accommodates a heat input at the membrane and the electrodes, as detailed in Section 3.3, and accounts for heat conduction to adjoining cell layers. Such an input in the model can be used to determine the energy necessary to maintain the cathode catalyst layer, for example, above freezing. An example of this “maintenance” scenario is found in the simulation results, Chapter 4.

## **3.5 Summary of Chapter 3**

This chapter described the model generation for the stack and system and included a discussion of various heating and water management methods, both on the cell and system levels. These methods may require some additional manufacturing processes, such as laminating a wire in the membrane, for example, or additional components, such as a burner or electric heater, all involving additional costs and packaging considerations. The next chapter describes the simulations performed to highlight the capabilities of the layered cell model and compares the results of these startup methods.

## **4 Simulation Results and Discussion**

The results of simulations performed with the layered cell cold start thermal model are detailed in this chapter. The results highlight the capabilities of a layered model when compared to a lumped analysis, and show the value of a layered model, especially for the cells by the endplates. The layered model is then used as a cold start model to evaluate various startup scenarios including, but not limited to, those considered by existing cold start models described in the literature.

The simulation boundary conditions are explained as follows. The conditions selected represent two distinct periods of interest: 1) sub-freezing ambient temperature ( $T_{amb}$ ) to stack operating temperature ( $T_{threshold}$ ), and 2) stack operating temperature

( $T_{\text{threshold}}$ ) to *vehicle propulsion* stack operating temperature ( $T_{\text{setpoint}}$ ). Condition 1 starts from  $T_{\text{amb}}$  and ends at  $T_{\text{threshold}}$ , and Condition 2 starts at  $T_{\text{threshold}}$  and ends at  $T_{\text{setpoint}}$ .

These conditions are met using one of the following two temperatures as a trigger: 1) a single stack temperature, a practical but incomplete metric to assess the stack's thermal condition, and 2) the cathode catalyst layer temperature. Some comparisons are made using the cathode catalyst layer temperature of the *middle* cell and of the *coldest* cell to distinguish the two when considering that fuel cell operation at  $T_{\text{threshold}}$  below  $0^{\circ}\text{C}$ , for example, can result in ice formation from product water at the cathode catalyst. In the investigations shown in the following sections, these temperatures are compared in terms of the useful information provided by them for control purposes.

The simulation results are divided into four sections:

- Section 4.1 shows a preliminary lumped analysis performed to establish a reference against which the layered model results can be compared.
- Section 4.2 investigates the stack thermal condition with the layered model showing how some cell layers or entire cells can be colder than expected as compared to a single lumped parameter temperature of  $0^{\circ}\text{C}$ . The simulations are performed with the stack off and warmed until the selected trigger reaches  $T_{\text{threshold}}$  of  $0^{\circ}\text{C}$  to determine if cell layers, especially cathode catalyst layers, are still below  $0^{\circ}\text{C}$  and could generate ice if the stack was subsequently operated.
- Section 4.3 investigates the stack thermal condition in an extreme case with the layered model showing how some cell layers or entire cells can be hotter than expected as compared to a single lumped parameter temperature of  $80^{\circ}\text{C}$ . The simulations are performed with the stack off and warmed until the selected trigger reaches  $T_{\text{threshold}}$  of  $80^{\circ}\text{C}$  to determine if cells exceed  $80^{\circ}\text{C}$  and by what magnitude.
- The benefits of a layered model, highlighted in Sections 4.2 and 4.3, are exploited in Section 4.4 as the layered model performs its intended function – as a cold start model used to evaluate various heating methods and to evaluate the effect of ice formation and melting.

Sections 4.2, 4.3 and 4.4 begin with a description of the simulation conditions and parameter (and parameter variation, if applicable) lists, followed by results and discussion.

#### **4.1 Preliminary lumped analysis**

Lumped parameter stack cold start analysis represents the literature state-of-the-art. The purpose of the preliminary lumped analysis here is to obtain a reference for the layered stack model and system model used in this dissertation.

Based on the parameters found in Section 7.4, a lumped analysis using Equation 5 is performed to determine energy consumption and time required for the stack and system thermal masses to reach a desired temperature. This analysis is divided into two parts: a *stack lumped case* and *system lumped case*. *Stack lumped case* is defined by the following points:

- 1) No effect on end cells (since there are no “end cells”) due to the endplate thermal mass (see Section 3.1.2 for more detail), although the endplate thermal mass itself is taken into account.
- 2) No losses to the environment. These losses are insignificant (~1%) relative to the heat draw of the endplate thermal mass determined by the layered model in this dissertation. Other studies neglect these losses altogether (Maggio et al., 1996; Zhang et al., 2004).
- 3) Temperature range is –20 to 0°C. The upper temperature limit of 0°C was selected for the lumped analysis to compare with the layered model for which several results are based on simulations with an upper limit of 0°C.
- 4) The thermal mass of the stack/endplates and stack and manifold coolant are considered. Note that the thermal mass calculations for the coolant use one value for the coolant specific heat (at -10°C, which is the middle of the temperature range specified in #3) unlike the layered model, which uses a curve fit of the temperature-dependent specific heat.

*System lumped case* includes the above conditions in the *stack lumped case*, plus the components in the small cooling loop as discussed in Section 3.2.2.

$$\Delta E = mcp\Delta T$$

$$\Delta E = P\Delta t$$

#### **Equation 5: Energy balance**

##### Stack lumped case

Using the thermal mass for the stack/endplates, stack coolant and manifold coolant found in Section 7.4, one can calculate the energy and time required by an 11250 W heat source (power level selected to match level used for internal heating in the model, i.e. 50 W x 225 cells) until  $T_{\text{threshold}}$ .

$$\Delta E = mcp\Delta T$$

$$1789880J = 89494 \frac{J}{K} (273 - 253)K$$

$$\Delta t = \frac{1789880 J}{11250 J/s} \approx 159 s$$

##### System lumped case

A similar calculation can be performed for the system lumped case, considering the components in the small loop. Using an 11250 W heat source (power level selected to match level used for internal heating in the model) until  $T_{\text{threshold}}$  results in the following time.

*small loop*

$$2083680J = 104184 \frac{J}{K} (273 - 253)K$$

$$\Delta t = \frac{2083680 J}{11250 J/s} \approx 185 s$$

The energy and time calculated in the stack and system lumped cases are compared with layered model results shown in the next section.

## 4.2 Stack operation at 0°C, layered model

### Simulation Conditions and Description

This section investigates the issue of starting the stack at 0°C when some cells are actually below 0°C, risking ice formation. A comparison is made between the single stack temperature used in the lumped analysis and the *middle* cell cathode catalyst layer temperature used in the layered model. Using Condition 1 of the boundary condition definitions described earlier, the layered model simulation runs with  $T_{amb}$  of -20°C until the trigger reaches  $T_{threshold}$  of 0°C by internal heating. The initial temperature,  $T_{amb}$ , was selected as -20°C to match the DOE requirements for 2010 (U.S. DOE, 2002). The stack operating temperature,  $T_{threshold}$ , is set at 0°C, and the stack in fact never turns on during these particular simulations. The purpose is to show how the stack may be colder than expected depending on the temperature used to determine stack readiness for operation. The layered model temperature distribution shows that by selecting the *middle* cell cathode catalyst layer temperature as the trigger, the end cells can still be below 0°C.

Then simulation results using the *coldest* cell cathode catalyst layer as the trigger show the additional time and energy required to bring this layer to 0°C. Further results illustrate the effect of independently varying parameters (e.g. bipolar plate material, endplate mass and condition, heat input level, and coolant flow) on the additional time and energy required. A summary of the parameters is shown in Table 2 and the variation on the parameters is shown in Table 3.

Parameter	Value
$T_{amb}$	-20°C
$T_{threshold}$	0°C
Trigger temperature	Middle cell cathode catalyst layer temperature vs. Coldest cell cathode catalyst layer temperature (used as baseline for variation runs)
Heat source	50 W in each cell membrane, e.g. power from electric wire (see Section 3.3)
Cell bipolar plate material (Cell layers 1, 2, 3, 9 and 10)	Graphite (see parameters in Section 7.4)
Endplate mass	from parameters in Section 7.4
Endplate condition	Unheated
Coolant flow	Off vs. On (small loop – see Section 3.2.2, used as baseline for variation runs), using middle of pump flowrate range (from parameters in Section 7.4)

**Table 2: Parameter summary, 0°C case**



Parameter	Baseline	Variation
Heat source	50 W per cell (in membrane, e.g. electric wire (see Section 3.3))	100 W per cell
Cell bipolar plate material (Cell layers 1, 2, 3, 9 and 10)	Graphite (see parameters in Section 7.4)	stainless steel (316L): <ul style="list-style-type: none"> <li>thickness, <math>t = 0.1</math> mm (source: Wind et al., 2003)</li> <li>thermal conductivity, <math>k = 13.4</math> W/mK</li> <li>density = <math>8238</math> kg/m<sup>3</sup></li> <li>specific heat, <math>c_p = 468</math> J/kgK</li> <li>specific resistance = <math>7.4e-7</math> ohm-m</li> </ul>
Endplate mass	from parameters in Section 7.4	50% less
Endplate condition	unheated	heated with power required to “flatten” temperature distribution (175 W each)

**Table 3: Parameter variation, 0°C case**

Results and Discussion

The results in this section are based on the parameters found in Table 2 and Table 3. The single stack temperature used in the lumped analysis and the layered model’s middle and coldest cell cathode catalyst layer temperatures, when used as the triggers, are compared in Figure 19.

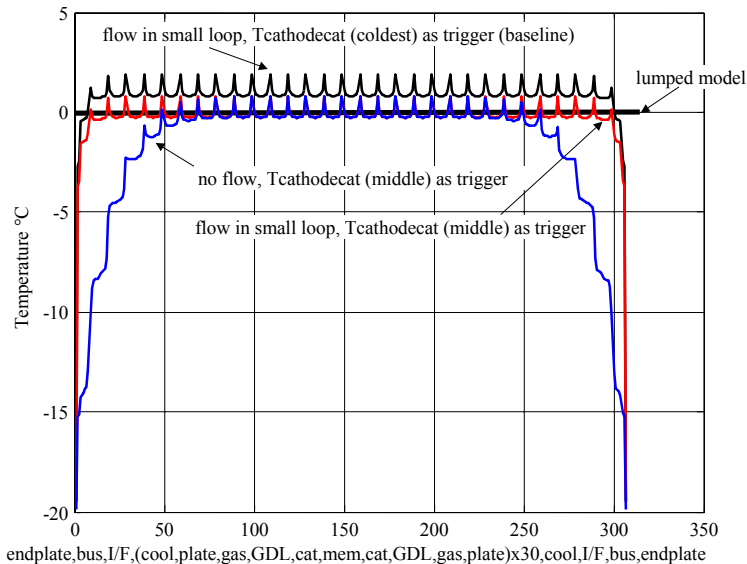


**Figure 19: Stack temperature distribution, trigger comparison**

Note the differences between the three cases shown in Figure 19. When there is coolant flow, heat from the middle cells is distributed to the end cells which are affected by the heat draw of the endplates. It is assumed that the coolant pump output may be low in a sub-freezing condition and higher, but controlled by stack temperature, during normal operation. As shown in Table 2, the middle of the pump flowrate range is used, to minimize the number of simulations required.

The effect of the endplate thermal mass is more pronounced in the no-flow condition. In both cases in which the middle cell cathode catalyst layer temperature is the trigger, there are end cell temperatures below 0°C. Keeping the flow on to maintain a more homogeneous temperature distribution, the trigger is changed to the coldest cell cathode catalyst layer temperature, ensuring that all cells are at or above 0°C. These conditions are used to establish a baseline for the next set of results.

For the baseline layered model, simulations are performed independently varying heat output, bipolar plate material, endplate mass, endplate condition (unheated or heated), and coolant flow (on or off). Figure 20 and Figure 21 compare time and energy for the lumped analysis and layered model, the trigger comparison, as well as the parameter variations against the baseline.

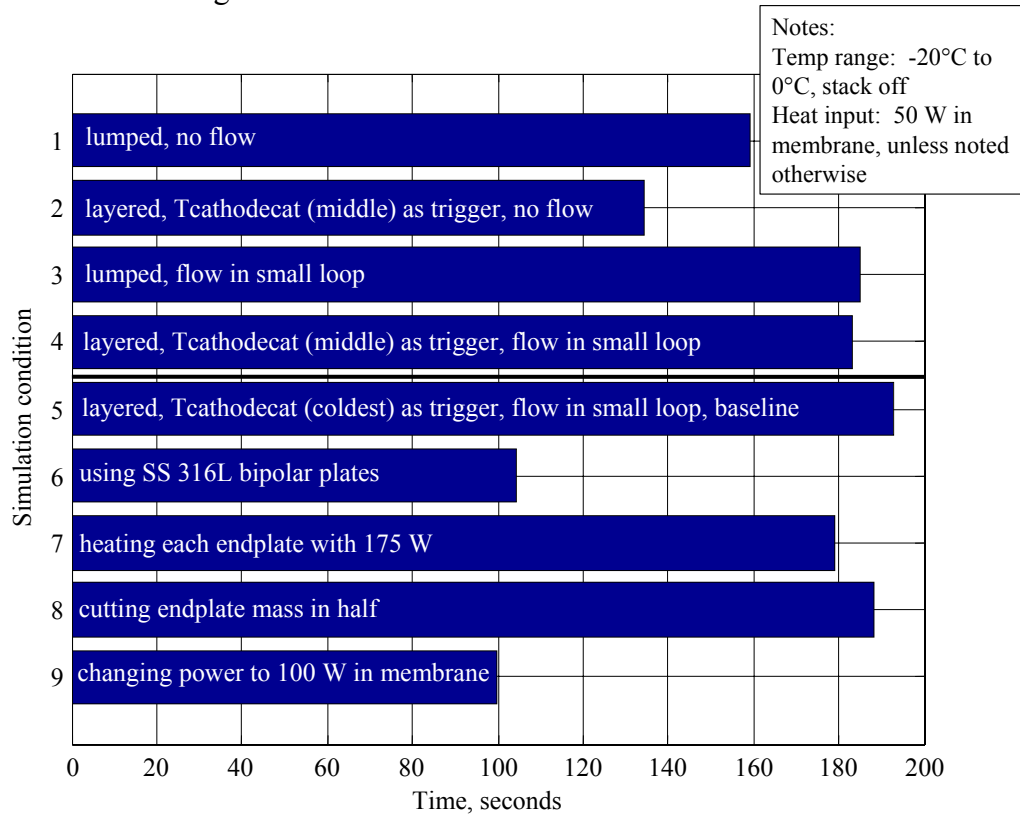


**Figure 20: Time Elapsed v. Simulation condition, 0°C case**

In Figure 20, the case with the layered model, no flow, and middle cell cathode catalyst layer as the trigger (bar 2) shows a time less than the 159 seconds previously determined in the lumped analysis (value from Section 4.1 shown in bar 1). The reason for this discrepancy lies in the coolant circulation. For the no-flow case, the middle cell

cathode catalyst layer heated to  $T_{\text{threshold}}$  quickly, while the end cells lagged, as shown in Figure 19.

In Figure 20, the case with flow in a small loop and middle cell cathode catalyst layer as the trigger (bar 4) shows a time slightly less than the 185 seconds found in the lumped analysis for the small loop (shown in bar 3) because the coolant circulation imparts heat to the end cells raising their temperatures much nearer to  $0^{\circ}\text{C}$ . This case shows that the lumped and layered models are actually similar in their times, indicating that the lumped model could be a sufficient tool under certain conditions. However, the lumped model lacks the information required to characterize the end cells for which a temperature gradient still exists.

Finally, the scenario in which the layered model uses the coldest cathode catalyst as the trigger (bar 5 and baseline for future simulations) shows an increase from the lumped analysis in time and energy, due to the continued heating up of the other cells in waiting for the coldest cell to reach  $T_{\text{threshold}}$ . This point is further illustrated in Figure 19.

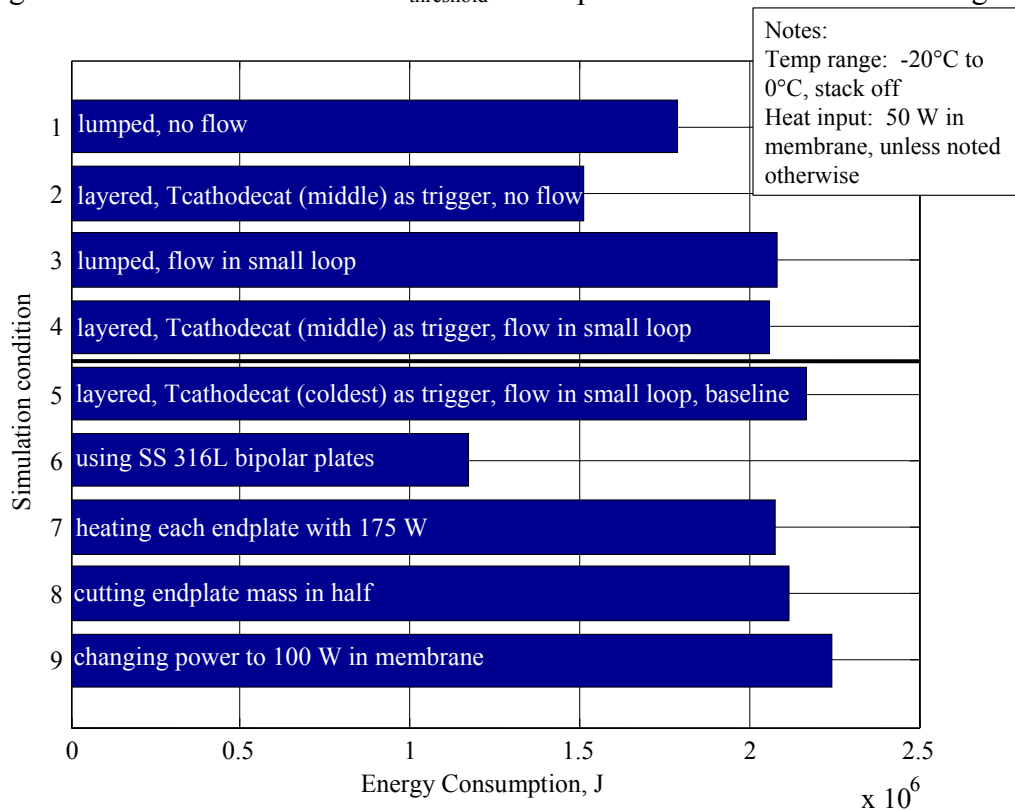


**Figure 21: Energy Consumed v. Simulation condition,  $0^{\circ}\text{C}$  case**

Some observations can be made about Figure 20 and Figure 21 compared to the baseline (bar 5), such as: 1) around the same energy is consumed for 100 W applied in the membrane in around half the time (bar 9) and the temperature rise in the membrane approximately doubled (see Figure 22), 2) there is a 46% reduction in time and energy for stainless steel bipolar plates (bar 6) due to a reduction in thickness and thermal mass, and 3) there is a 3% reduction in time and energy for cutting the endplate mass in half (bar 8).

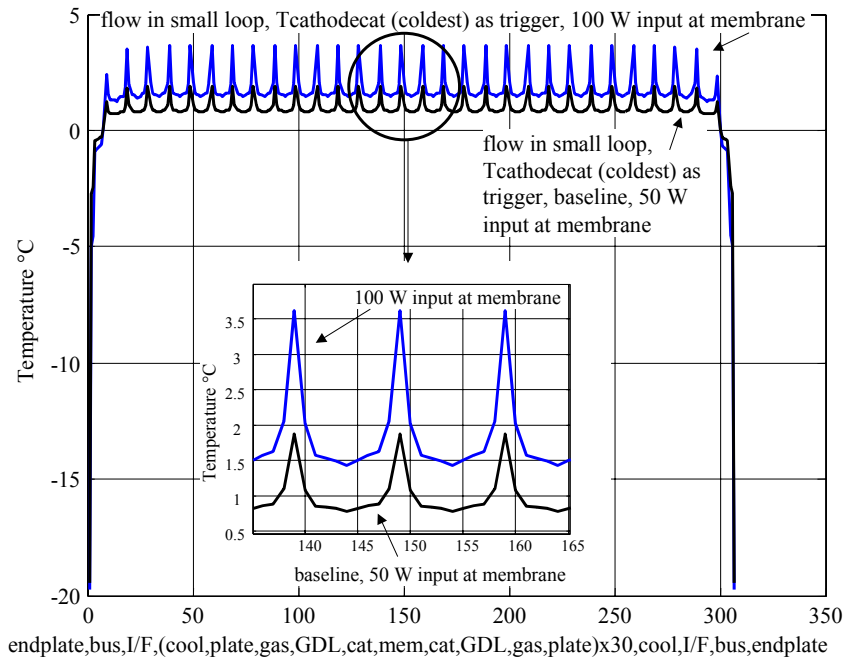


**Figure 22: Stack temperature distribution, 100 W**

It was found that using 175 W at each endplate (specifically, power applied to the copper bus layer of the endplate assembly) had the effect of bringing the end cells, especially the coldest cell, up to temperature faster, reducing the time by 7% and energy required by 4% (shown in bar 7 in Figure 20 and Figure 21). The temperature distribution in Figure 23 illustrates the effect of heating the endplates on the end cells.

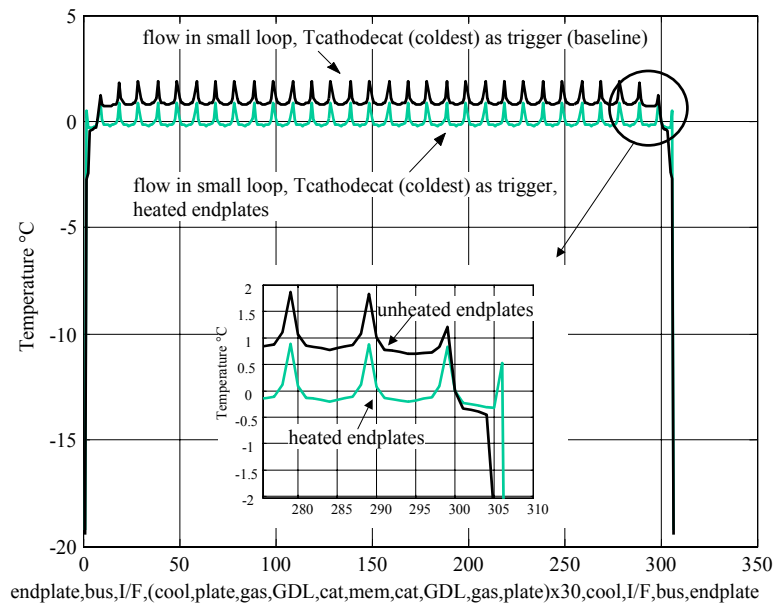


**Figure 23: Stack temperature distribution, heated endplates**

An application of heating the endplates can be in maintaining above-freezing conditions for the stack. A comparison in energy consumption can be made to a scenario in which the stack is not allowed to drop below 0°C, for example, by reducing the temperature at shutdown to just above 0°C and maintaining a low level of operation (requiring H<sub>2</sub> flow and air flow) or introducing an electrical heat input (requiring on- or off-board power). It was found in the model that a 0.05 W per cell internal heat input and 10 W at each endplate bus layer could maintain the coldest cell above 0°C, assuming the stack is uninsulated. Keeping the coolant off eliminates the need for pump power; however, if electrical power is used anyway for heating, it can be used for the pump.

Considering a 12-hour period of inoperation, for example, the total energy required would be 1,350,000 J, which is 0.375 kWh of electric source energy. The total energy required would be less than the amount shown in most of the scenarios in Figure 21, given the startup conditions and stack thermal characteristics. Of course, this analysis depends on the length of the inoperation period and may not be suitable, for example, for long-term vehicle parking. Figure 24 shows the temperature distribution for the 0.05 W per cell internal heat input and 10 W at each endplate bus layer for both coolant circulation conditions. Note that the ambient temperature is -20°C; therefore, the polymer endplate layer (the outermost layer of the endplate assembly) is below 0°C but has been heated to above -20°C.

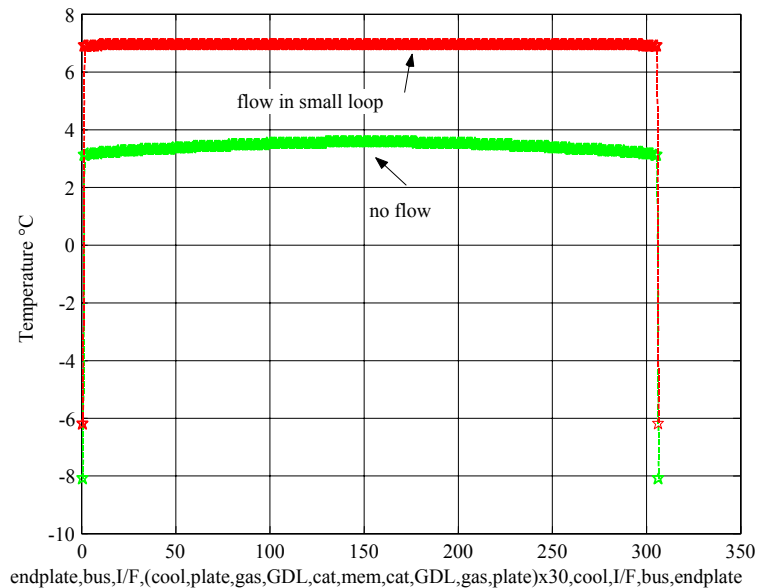


**Figure 24: Stack temperature distribution, heated endplates, kept above 0°C**

This section has illustrated the detailed information a layered model provides when considering a  $T_{\text{threshold}}$  of 0°C. The next section investigates the effect of an extreme case, such as an unusually high heat input within the cell, this time considering a  $T_{\text{threshold}}$  of 80°C.

### 4.3 Extreme case, layered model

#### Simulation Conditions and Description

This section investigates an extreme case of a 500 W per cell internal heat input using the layered model. Such a heat input could be, for example, a result of temperature excursions or hot spots from chemical reactions carried out on either or both electrodes (as discussed in Section 3.3). A 500 W internal input would obviously warm the stack within a shorter period of time than 50 W; however, the layered model illustrates the effect of such a heat input on each cell's internal temperature distribution. This case considers a temperature range from  $T_{amb}$  of  $-20^{\circ}\text{C}$  to the stack operating temperature  $T_{threshold}$  of  $80^{\circ}\text{C}$  reached by the selected temperature trigger.

As in the previous section, the stack never turns on during these particular simulations. A comparison is made between 1) a single stack temperature of  $80^{\circ}\text{C}$  and 2) the triggers of the middle and coldest cell cathode catalyst layer temperatures reaching  $80^{\circ}\text{C}$ . In this case, using the coldest cell cathode catalyst layer temperature is an extreme requirement for *all* cells to reach at least  $80^{\circ}\text{C}$  before the stack is operated. Coolant circulation is also compared, and, as later shown in the results, can have a significant impact on the overall stack temperature distribution. A summary of the parameters is shown in Table 4.

Parameter	Value
$T_{amb}$	$-20^{\circ}\text{C}$
$T_{threshold}$	$80^{\circ}\text{C}$
Trigger temperature	Middle cell cathode catalyst layer temperature vs. Coldest cell cathode catalyst layer temperature
Heat source	500 W in each cell membrane, e.g. as a result of possible temperature excursions from neighboring electrode chemical reactions (see Section 3.3)

**Table 4: Parameter summary, extreme case**

#### Results and Discussion

The effect on the membrane of a 500 W input is shown in Figure 25. The temperature difference between the low and high points within the cell is around  $11^{\circ}\text{C}$ , or about ten times the difference found in the 50 W cases shown earlier, reflecting the tenfold heat input.

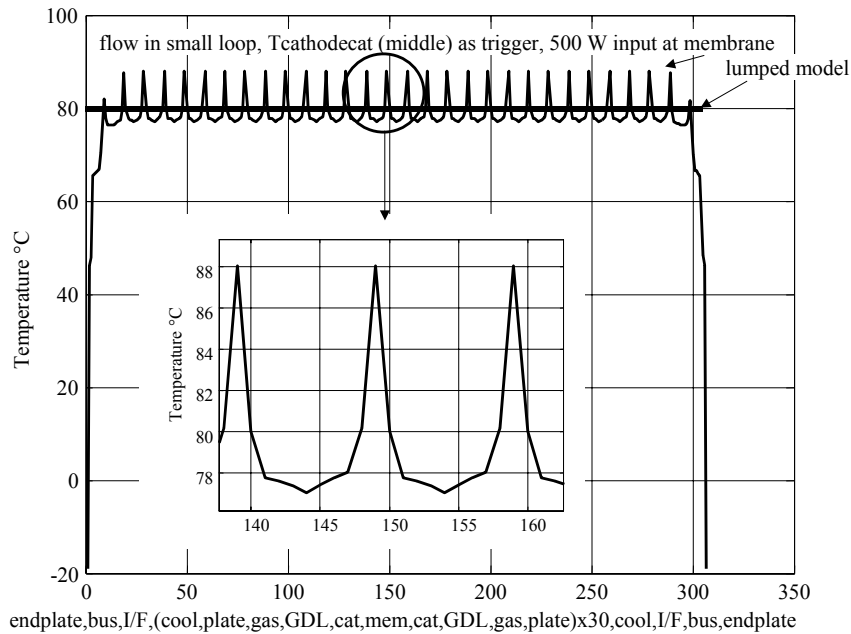


**Figure 25: Stack temperature distribution, extreme case, plot 1**

However, in Figure 26, in which the impact of the flow being on or off and of trigger temperature is compared, the cell temperature distribution for the middle portion of the cells remains the same. It is the lack of circulation and the (extreme) requirement for the coldest cell to reach 80°C that result in a catastrophic condition for the stack (namely, 250°C membrane temperature for no flow).

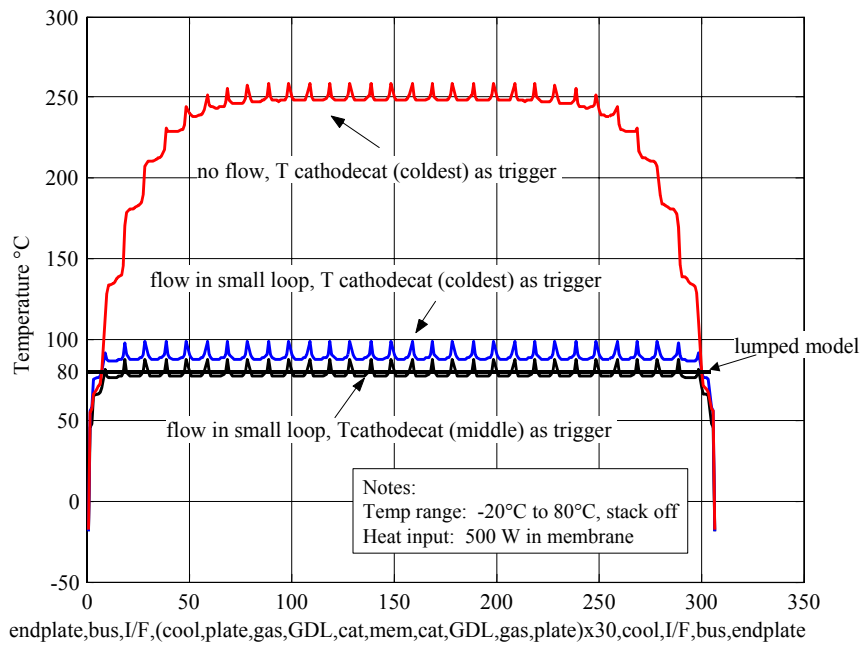


**Figure 26: Stack temperature distribution, extreme case, plot 2**

In Sections 4.2 and 4.3, two examples have been presented to illustrate the layered model’s capabilities to provide more information than a lumped model. In the next section, the layered model performs its intended function – as a cold start model used to evaluate various aspects of sub-freezing stack and system startup: stack- and system-level heating methods, stack operation below and above freezing, and stack ice formation due to residual and product water.

#### 4.4 Cold start analysis

##### Simulation Conditions and Description

In this section, the layered model is used to investigate the advantages and disadvantages of internal and external heating methods on a stack and system level, starting the stack alone or after a pre-heat period assisted by these heating methods, and the heat requirements for melting existing ice and/or ice formed from stack reactions. A summary of the parameters is shown in Table 5 and the simulation variations are listed in Table 6.

Parameter	Value
$T_{amb}$	-20°C
$T_{setpoint}$	80°C
Trigger temperature	Coldest cell cathode catalyst temperature
Heat source output	Internal heat input of 50 W per cell in membrane (e.g. power from electric wire (see Section 3.3))
Flow condition	Small loop (with non-operating external heat source)

**Table 5: Parameter summary, cold start analysis**

$T_{threshold}$	<ul style="list-style-type: none"> <li>• -20°C</li> <li>• 0°C</li> <li>• 20°C</li> </ul>
External heat source output (in addition to internal heat input in Table 5)	<ul style="list-style-type: none"> <li>• 5000 W</li> </ul>
Flow condition (with operating external heat source)	<ul style="list-style-type: none"> <li>• small loop</li> <li>• system loop with vehicle components bypassed</li> <li>• system loop with vehicle components included</li> </ul>

**Table 6: Simulation variation matrix, cold start analysis**

##### Results and Discussion

##### *Heating method comparisons*

Bar charts in Figure 27 and Figure 28 show the time elapsed and energy consumed for the parameters and conditions described in Table 5 and Table 6. The bars are divided into three groups, based on the temperature at which the the coldest cell cathode catalyst layer temperature reaches  $T_{threshold}$  and the stack begins to operate:



- 1)  $-20^{\circ}\text{C}$ , as shown in bar 1,
- 2)  $0^{\circ}\text{C}$ , as shown in bars 2-5, and
- 3)  $20^{\circ}\text{C}$ , as shown in bar 6.

When the stack begins operation at  $-20^{\circ}\text{C}$  (bar 1), no additional heat (internal or external) assists in the warmup process to  $T_{\text{setpoint}}$  of  $80^{\circ}\text{C}$  – the heat generated by the stack reactions is the sole source. However, for the other cases, internal heat of 50 W per membrane is used from  $T_{\text{amb}}$  of  $-20^{\circ}\text{C}$  up to the  $T_{\text{threshold}}$  (light-colored part of bars) at which the stack begins operation as indicated in the figures (dark-colored part of bars).

The baseline loop configuration used for bars 1, 2 and 6 is the small loop which includes the thermal mass of a non-operating external heat source. For the  $T_{\text{threshold}}$  of  $0^{\circ}\text{C}$  case (bars 2-5), comparisons are made when an additional 5 kW of heat input is obtained from the external source and when different cooling loop configurations are used. The internal stack heating plus external heating is used from  $T_{\text{amb}}$  of  $-20^{\circ}\text{C}$  up to the  $T_{\text{threshold}}$  at which the stack begins operation. The loop comparisons illustrate the impact of system and vehicle component thermal mass on the overall startup time and energy for the coldest cell cathode catalyst layer temperature to reach  $T_{\text{threshold}}$  of  $0^{\circ}\text{C}$  and  $T_{\text{setpoint}}$  of  $80^{\circ}\text{C}$  from  $T_{\text{amb}}$  of  $-20^{\circ}\text{C}$ . Bar 2 is compared with bar 3 in which the external heat source operates within the small loop. Then bar 3 is compared with bars 4 and 5 in which the external heat source operates within the system loop bypassing and including vehicle components, respectively.

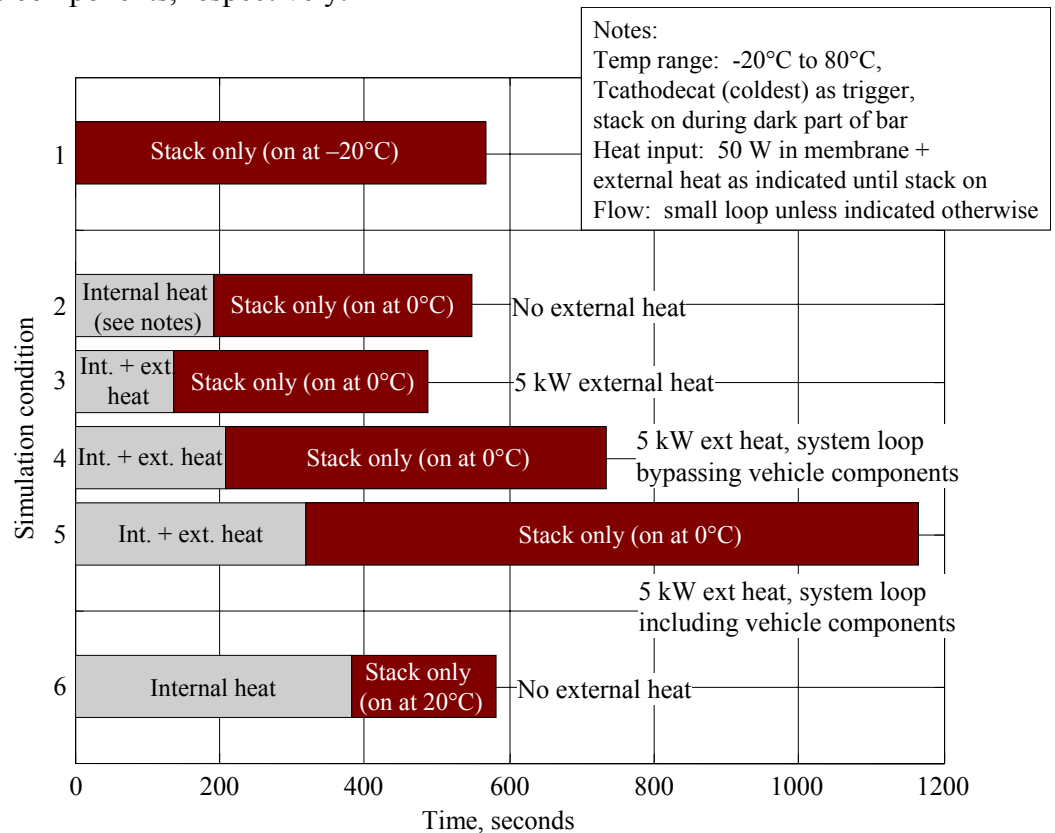


**Figure 27: Time elapsed, cold start analysis**

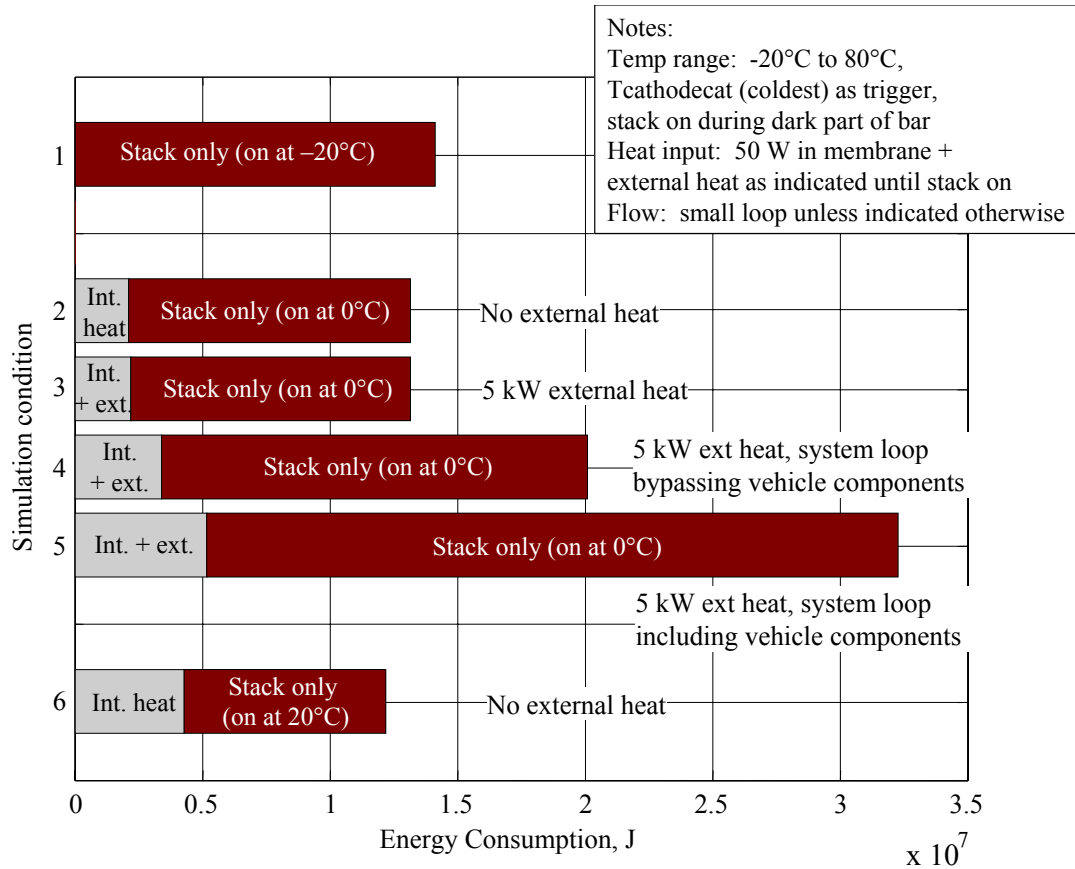


**Figure 28: Energy consumption, cold start analysis**

Note that the total energy consumed is a sum of two parts, separated by the light- and dark-colored parts of the bar chart: 1) the 100% efficient and constant internal heating power plus additional external heating power (if applicable) over time and 2) the H<sub>2</sub> energy consumed by the stack for which efficiency *as a heat source* changes over temperature and time.

When comparing bars 1, 2 and 6, it is shown that starting stack operation at 0°C and 20°C instead of -20°C results in a 4% reduction and 2% increase in overall time and a 7% and 14% reduction in overall energy, respectively.

As shown in bar 3 of Figure 27, the additional 5 kW external heating in the small loop improves the time by 11% compared with bar 2 with a negligible change in energy consumption, as shown in Figure 28.

However, the additional external heat in an expanded cooling loop increases overall time and energy by 52% for the system bypassing vehicle components (bar 4) and by 1.4 times for the system including vehicle components (bar 5) as compared to the small loop with external heat (bar 3).

As mentioned earlier, the external heat is assumed to be 100% efficient (efficiency is defined as ratio of heat exchanger output to power into heat source) and the full desired power is always available to the coolant. The following figures show the impact on time and energy of a heat exchanger that has a more realistic efficiency. Bar 3 in Figure 27 and Figure 28 in which 5 kW of external heat is transferred by a 100%

efficient heat exchanger is compared with the same scenario, but in which the heat exchanger is 50% efficient (shown as bar 3a in Figure 29 and Figure 30).

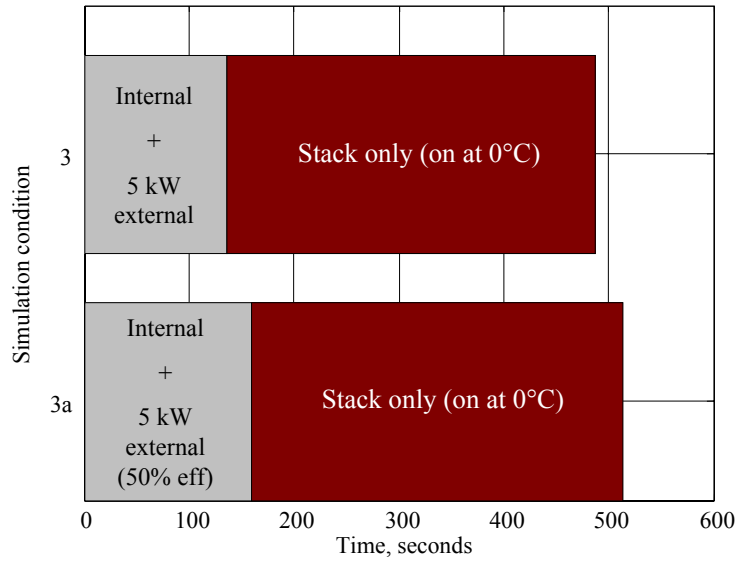


**Figure 29: Time elapsed, impact of HX efficiency**

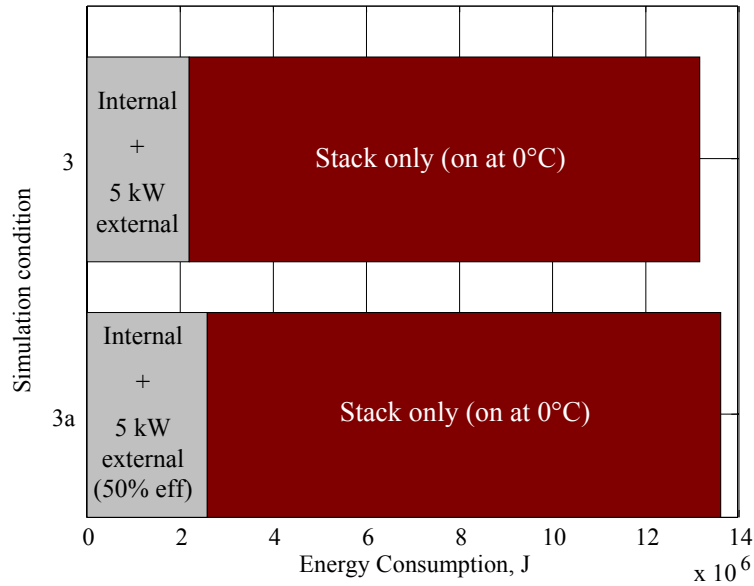


**Figure 30: Energy consumption, impact of HX efficiency**

The results in Figure 29 and Figure 30 show that both scenarios (bars 3 and 3a) use internal stack heating augmented by external heating until the stack turns on at 0°C; however, the external heating by a 50% efficient heat exchanger increases the pre-stack operation time and energy consumed by around 17% (light-colored parts of bars) and the overall time and energy by around 5%.

### Ice formation

Taking the case shown in bar 1 of Figure 27 and Figure 28, in which the stack starts operation at  $-20^{\circ}\text{C}$ , one can observe the impact of ice formation on startup characteristics. There are two assumptions that need to be reiterated: 1) the coldest cathode catalyst temperature is used in determining the ice formation and is applied to all cells, even though less ice may form in cells that warm up more quickly, thereby making this assumption a worst case (but “fail safe”), and 2) the impact of ice formation is limited to the thermal characteristics which result from cell current and voltage data for sub-freezing conditions found in the literature (see Section 3.3). No analysis is made in this dissertation of the impact of ice on gas diffusion to the catalyst layer.

Figure 31 shows the formation and melting of ice from product water, and from a combination of product water and ice that may exist from residual water after shutdown as calculated in Section 3.4. The scenario in which there is existing ice plus ice from product water yields a fraction of the GDL void volume above 1; this is showing that the existing ice completely fills the void volume and product water freezes as an additional layer. The time when melting begins corresponds to the time when the coldest cathode catalyst layer reaches  $0^{\circ}\text{C}$  as shown in Figure 32.

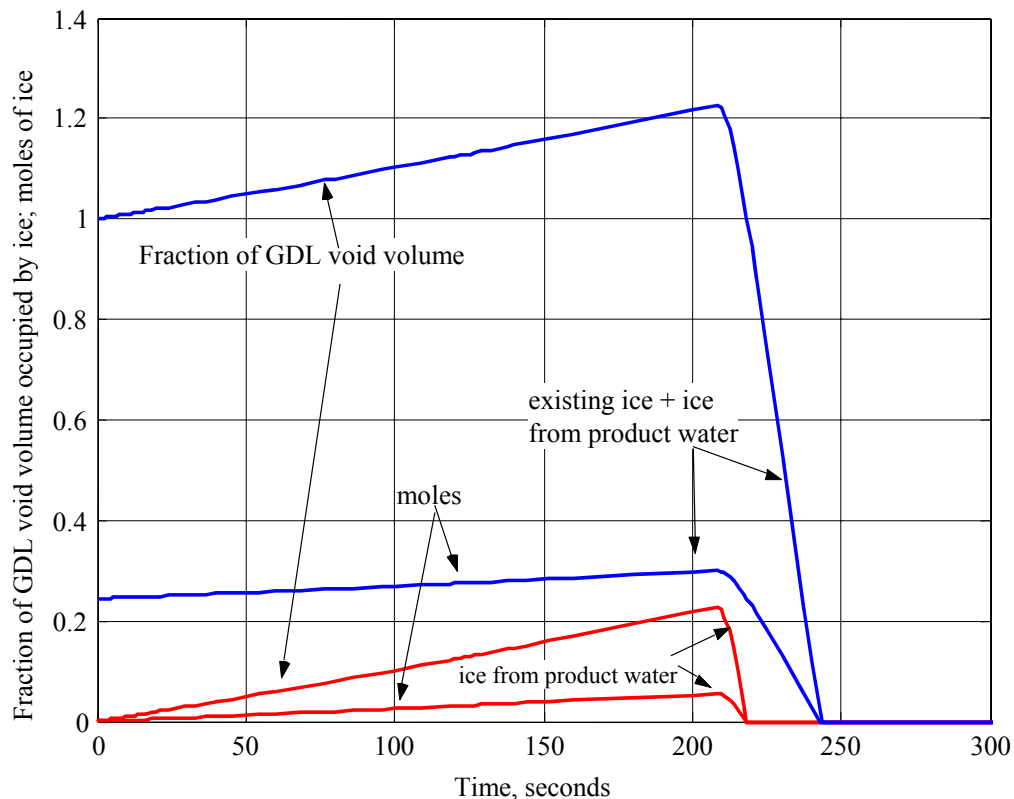


**Figure 31: Moles of ice formed and melted, fraction of GDL void volume occupied**

Figure 32 shows the corresponding power required to melt the ice and the effect on the coldest cathode catalyst temperature rise. As shown in the figure, the temperature ceases to rise for the period in which the power is required for melting and then resumes

its upward trajectory. As the cell voltage and current characteristics are switched from one set of data in the literature to another (see Section 3.3) based on the temperature ranges within which each was valid, the temperature rise occurs at a different slope at around 25°C.

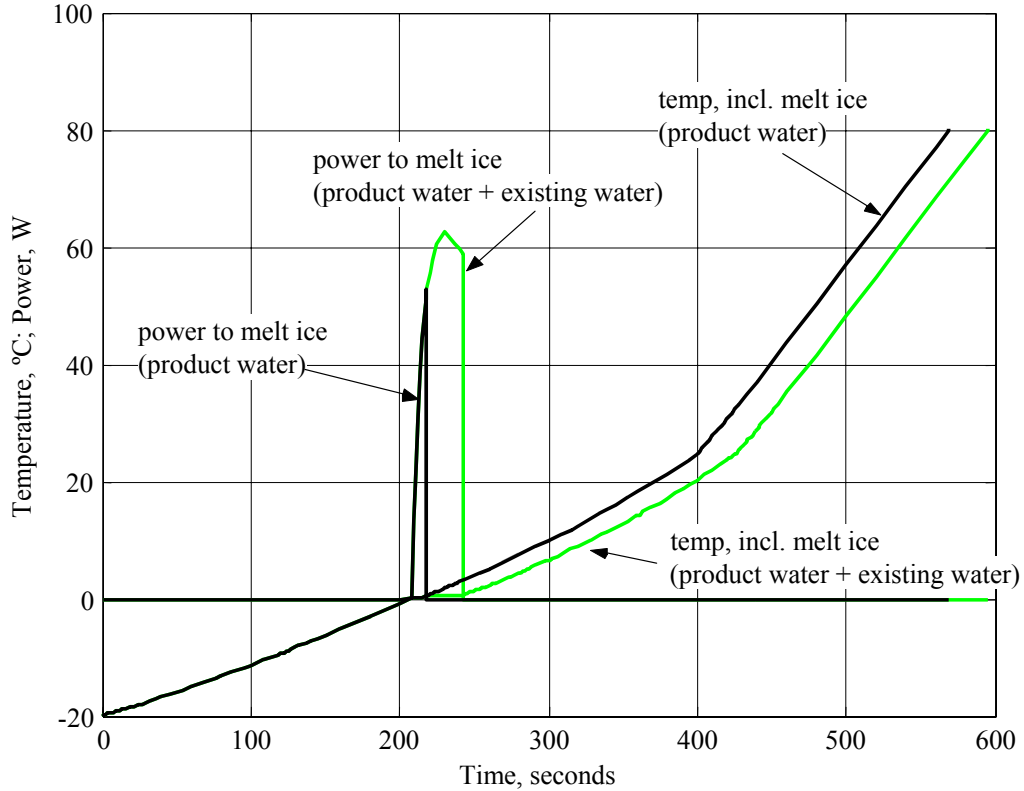


**Figure 32: Temperature and power v. time, effect of melting ice**

In this section, results were presented using the layered cell cold start thermal model to evaluate various aspects of sub-freezing startup: the advantages and disadvantages of internal and external heating methods, starting the stack alone or after a pre-heat period assisted by these heating methods, and the power requirements for melting ice.

#### 4.5 Summary of Chapter 4

Four sections in this chapter were presented: 1) a preliminary lumped analysis, 2) an analysis showing scenarios in which some cell layers or entire cells of the stack were colder than expected as compared to a single lumped parameter temperature of 0°C, depending on the temperature used in the layered model as the metric for the stack thermal control, 3) an analysis showing scenarios in which some cell layers or entire cells of the stack were hotter than expected as compared to a single lumped parameter temperature of 80°C, and 4) an evaluation of heating methods together with the impact of

ice formation and melting during a sub-freezing startup operation. Specific results are listed below.

- In section 4.1, a lumped energy balance was performed using the thermal mass values for the stack and system described in Section 7.4. The times were no less than two minutes for a temperature rise from  $-20^{\circ}\text{C}$  to  $0^{\circ}\text{C}$  using a heat input of 11250 W (total).
- In section 4.2, some of the major observations made using the layered model are described as follows:
  - The layered model temperature distribution revealed that the end cells were below  $0^{\circ}\text{C}$  even while a single stack temperature that may be used in a lumped model would show  $0^{\circ}\text{C}$ .
  - Coolant flow distributes heat from the hotter cells to the colder cells by the endplates. No coolant flow can cause a temperature lag in the end cells. With coolant flow, a comparison between the lumped and layered models of the time to reach a desired setpoint temperature showed that they are actually similar, indicating that the lumped model could be a sufficient tool under certain conditions. However, the lumped model lacks the information required to characterize the end cells for which a temperature gradient still exists.
  - Using stainless steel bipolar plates resulted in a 46% reduction in time and energy (compared with a baseline) due to a reduction in thickness and thermal mass.
  - Heating the endplates reduced the overall time and energy consumption (compared with a baseline) by mitigating the heat draw from the end cells.
- In section 4.3, some of the major observations made using the layered model in an extreme case are described as follows:
  - A heat input of 500 W per cell will result in an 11-degree spread among the layers within the cell temperature distribution.
  - If (with 500 W per cell) the coldest cell is also required to reach  $80^{\circ}\text{C}$ , and the coolant does not flow, the 11-degree spread within the cell remains; however, the overall stack temperature distribution rises to a level that would be catastrophic to stack components, particularly the membrane.
- In section 4.4, some of the major observations made using the layered model generally as a cold start thermal model are described as follows:
  - Starting stack operation at  $0^{\circ}\text{C}$  and  $20^{\circ}\text{C}$  instead of  $-20^{\circ}\text{C}$  results in an overall energy reduction of 7% and 14% and overall time reduction of 4% and increase of 2%, respectively.
  - Using a small cooling loop without and with external heating that augments internal heating of a stack until the stack operates at  $0^{\circ}\text{C}$  improves the overall time by 11% but negligibly changes the energy consumption.
  - Expanding the small cooling loop to the system level (with external heating that augments internal heating of a stack until the stack operates at  $0^{\circ}\text{C}$ ), bypassing vehicle component thermal masses,

increases overall time and energy by 52%. Similarly, expanding the small cooling loop to the system level, but including vehicle component thermal masses, increases overall time and energy by 1.4 times.

- Using a small cooling loop with 50% (versus 100%) efficient external heating that augments internal heating of a stack until the stack operates at 0°C increases the overall time and energy by 5% and the pre-stack operation time and energy by 17%.

## 5 Closing Remarks

### 5.1 Conclusions of dissertation

Chapter 2 provided a literature review that discussed existing models' treatment of startup. None of the five, lumped-stack models found in the literature fulfills the criteria for a theoretically sound, complete, practical and valid cold start stack thermal model and it was determined that a new, layered model was necessary. The criteria selected for the cold start thermal model evaluation are as follows.

- Criterion 1, or *transient and physical effects*, is met by all of the models. This criterion is a good metric to determine whether or not the model adequately captures the processes present during the cold start operating condition.
- Criterion 2, or *water management at sub-freezing temperatures*, is met by one of the models that addresses sub-freezing water management issues such as blockage of ice formed from the water produced by the stack reactions.
- Criterion 3, or *stack internal warming strategies*, is partially met by all of the models because they considered stack operation as an internal warming method, but not other internal warming methods, which are more conveniently evaluated through the use of a layered cell model.
- Criterion 4, or *external warming strategies*, is actually included in one model and referred to in another model as a necessary option under certain circumstances.
- Criterion 5, or *consideration of endplate thermal mass*, is only addressed by one model via an assumption that the bipolar plates are thermally isolated from the endplates. Endplate analysis is also more easily facilitated with a layered cell model.
- Criterion 6, or *sub-freezing initial temperature of -20°C*, is only met by one model with an initial temperature of -40°C.
- Criterion 7, or *validation with experimental data*, is met by two models, while for the other models the validation of the thermal model with experimental data is unclear.

Chapter 3 described the model generation for the stack and system and included a discussion of various heating methods, both on the cell level and system level. These methods may require some additional manufacturing processes, such as laminating a wire in the membrane, for example, or additional components, such as a burner or electric heater, all involving additional costs and packaging considerations.

Chapter 4 presented four sections: 1) a preliminary lumped analysis, 2) an analysis showing scenarios in which some cell layers or entire cells of the stack were colder than expected as compared to a single lumped parameter temperature of 0°C, depending on the temperature used in the layered model as the metric for the stack thermal control, 3) an analysis showing scenarios in which some cell layers or entire cells of the stack were hotter than expected as compared to a single lumped parameter temperature of 80°C, and 4) an evaluation of heating methods together with the impact of ice formation and melting during a sub-freezing startup operation. Specific results are listed below.

- In section 4.1, a lumped energy balance was performed using the thermal mass values for the stack and system described in Section 7.4. The times were no less than two minutes for a temperature rise from –20°C to 0°C using a heat input of 11250 W (total).
- In section 4.2, some of the major observations made using the layered model are described as follows:
  - The layered model temperature distribution revealed that the end cells were below 0°C even while a single stack temperature that may be used in a lumped model would show 0°C.
  - Coolant flow distributes heat from the hotter cells to the colder cells by the endplates. No coolant flow can cause a temperature lag in the end cells. With coolant flow, a comparison between the lumped and layered models of the time to reach a desired setpoint temperature showed that they are actually similar, indicating that the lumped model could be a sufficient tool under certain conditions. However, the lumped model lacks the information required to characterize the end cells for which a temperature gradient still exists.
  - Using stainless steel bipolar plates resulted in a 46% reduction in time and energy (compared with a baseline) due to a reduction in thickness and thermal mass.
  - Heating the endplates reduced the overall time and energy consumption (compared with a baseline) by mitigating the heat draw from the end cells.
- In section 4.3, some of the major observations made using the layered model in an extreme case are described as follows:
  - A heat input of 500 W per cell will result in an 11-degree spread among the layers within the cell temperature distribution.
  - If (with 500 W per cell) the coldest cell is also required to reach 80°C, and the coolant does not flow, the 11-degree spread within the cell remains; however, the overall stack temperature distribution rises to a level that would be catastrophic to stack components, particularly the membrane.
- In section 4.4, some of the major observations made using the layered model generally as a cold start thermal model are described as follows:
  - Starting stack operation at 0°C and 20°C instead of –20°C results in an overall energy reduction of 7% and 14% and overall time reduction of 4% and increase of 2%, respectively.



- Using a small cooling loop without and with external heating that augments internal heating of a stack until the stack operates at 0°C improves the overall time by 11% but negligibly changes the energy consumption.
- Expanding the small cooling loop to the system level (with external heating that augments internal heating of a stack until the stack operates at 0°C), bypassing vehicle component thermal masses, increases overall time and energy by 52%. Similarly, expanding the small cooling loop to the system level, but including vehicle component thermal masses, increases overall time and energy by 1.4 times.
- Using a small cooling loop with 50% (versus 100%) efficient external heating that augments internal heating of a stack until the stack operates at 0°C increases the overall time and energy by 5% and the pre-stack operation time and energy by 17%.

The model has been validated against experimental data (shown in the Appendix, Section 7.2) using DC and Ballard proprietary parameter values, but is used in this dissertation for simulations with literature-based and non-proprietary parameter values. The validation results reveal an interesting point about the assumption of linearity for the coolant channel along the direction of flow. While the model's validation is acceptable, a further improvement to better handle dynamic behavior would be to consider a second dimension of the cell/stack, i.e., discretize the cell/stack along the direction of coolant flow to determine the real temperature distribution along this dimension.

## 5.2 Recommendations for startup strategies

Based on the results of the model which use some strategies from the literature, parameter values from the literature and non-proprietary data (as shown in the Appendix, Section 7.4), several recommendations can be made on the best strategies for startup:

- 1) *Use internal stack heating other than stack reactions.* Starting stack operation below 0°C consumes more time and energy than starting the stack above 0°C due to ice formation and low heat generation at low temperatures. Even though at low temperatures the stack runs inefficiently and generates more heat than electricity, the amount of heat is insufficient to quickly warm up the stack. Therefore, it is recommended to utilize alternate internal stack heating methods up to 0°C or above. Such methods, as described in the dissertation, include using a resistance wire laminated in the cell membrane or chemical reactions at the electrodes.
- 2) *Circulate coolant during warmup.* The warming of the cells by the endplates lags the cells in the middle due to the heat draw by the endplate thermal mass. Circulating coolant ensures that the heat is distributed uniformly throughout the stack.
- 3) *Minimize thermal mass that is to be heated.* Even while it is recommended to circulate coolant, the thermal mass of the loop in which the coolant circulates should be minimized to ensure quick warmup of the stack.

- 4) *Heat the endplates.* Heating the endplates can mitigate the endplate thermal mass effect on the end cells and quickly bring the end cells to above 0°C, for example, to prevent ice formation when operating the stack.
- 5) *Use a metal-based material for the bipolar plates.* Using stainless steel, for example, can reduce the thickness and therefore the thermal mass of the bipolar plates, reducing time and energy consumption during warmup.

### 5.3 Future Research

There are several improvements that can be made to the model developed in this dissertation and to the evaluation of cold start. Possible avenues for future research include:

- 1) *Integrate cold start model into vehicle model to observe cold start operation while vehicle is moving.* Executing the cold start operation while the vehicle is moving introduces certain complexities. For example, the method employed in cold start may require current from the on-board electrical system at the same time as the vehicle traction motor. Further, the cooling loop heat fluxes, while the vehicle is being driven, may be different from when the vehicle is not being driven. These interactions would have to be considered.
- 2) *Extend this investigation to fuel processor-based systems.* In fuel cell vehicles for which H<sub>2</sub> is not carried on-board, a fuel processor is used to produce the H<sub>2</sub> from a hydrogen-rich fuel in a chemical reaction that requires heat. The cold start operation would have the increased complexity of warming the fuel processor as well as the fuel cell system.
- 3) *Develop a two- or three-dimensional (2D or 3D) cold start stack model.* Besides the obvious complications of adding another dimension, a 2D or 3D model may require the use of other software packages to model heat and mass flow distributions. However, as discussed in Section 7.2, future work could include discretizing the 1D layered model in a second dimension (along the direction of coolant fluid flow) to better account for dynamic behavior.

## 6 References

Adams, James A., Sulek, Mark S., and Saloka, George Steve, "Method for initiating a fuel cell," U.S. Patent 6,007,930, December 28, 1999.

Allmeasures.com, 1991-2001, website accessed February 2003, <[http://www.allmeasures.com/Formulae/static/formulae/electrical\\_conductivity/12.htm](http://www.allmeasures.com/Formulae/static/formulae/electrical_conductivity/12.htm)>.

Amphlett, J. C., Baumert, R. M., Mann, R. F., Peppley, B. A., Roberge, P. R., and Harris, T. J., "Performance Modeling of the Ballard Mark IV Solid Polymer Electrolyte Fuel Cell, I. Mechanistic Model Development, Journal of the Electrochemical Society, vol. 142, No. 1, pp. 1-8, January 1995a.

Amphlett, J. C., Baumert, R. M., Mann, R. F., Peppley, B. A., Roberge, P. R., and Harris, T. J., "Performance Modeling of the Ballard Mark IV Solid Polymer Electrolyte Fuel Cell, II. Empirical Model Development, Journal of the Electrochemical Society, vol. 142, No. 1, pp. 9-15, January 1995b.

Amphlett, J. C., Mann, R. F., Peppley, B. A., Roberge, Rodrigues, A., "A model predicting transient responses of proton exchange membrane fuel cells," Journal of Power Sources, vol. 61, pp. 183-188, 1996.

Andreoli, G. L. and Federici, F., "Supply system for fuel cells of the S.P.E. (solid polymer electrolyte) type for hybrid vehicles," U.S. Patent 5,605,770, February 25, 1997.

Appleby, A.J. and Foulkes, F.R., Fuel Cell Handbook, New York: Van Norstand Reinhold, 1989.

Arbin Instruments, "Dew Point Humidifier for Gas Streams," November 12, 2002, website accessed November 9, 2003, <<http://www.fuelcelltestingsystem.com/PDF/dph.pdf>>.

Argonne National Laboratory, "GCTool Computer Model Helps Focus Fuel Cell Vehicle Research," website accessed August 2002, <<http://www.transportation.anl.gov/ttrdc/modeling/gctool-new.html>>.

Argyropoulos, P., Scott, K., and Taama, W. M., "One-dimensional thermal model for direct methanol fuel cell stacks, Part I. Model Development," Journal of Power Sources, vol. 79, pp. 169-183, 1999a.

Argyropoulos, P., Scott, K., and Taama, W. M., "One-dimensional thermal model for direct methanol fuel cell stacks, Part II. Model based parametric analysis and predicted temperature profiles," Journal of Power Sources, vol. 79, pp. 184-198, 1999b.

Atbi, Abderrahmane, Fletcher, Nicholas J., Roberts, Joy A., St. Pierre, Jean, and Geest, Marian van der, "Methods for Improving the Cold Starting Capability of an Electrochemical Fuel Cell," WO 01/24296, April 5, 2001.

Atkins, P.W., Physikalische Chemie, VCH Verlagsgesellschaft mbH, 1990.

Atwood, Paul, Gurski, Stephen, Nelson, Douglas J., and Wipke, Keith B., "Degree of Hybridization Modeling of a Fuel Cell Hybrid Electric Sport Utility Vehicle," SAE Paper No. 2001-01-0236, 2001.

Baehr, Hans Dieter and Stephan, Karl, Waerme- und Stoffuebertragung, Berlin: Springer-Verlag, 1998, pp. 488-492.

Ballinger, Emily A., Reiser, Carl A., "Method and apparatus for the operation of a cell stack assembly during subfreezing temperatures," International Patent WO 02/081367, October 17, 2002.

Benz, Uwe, Fleck, Wolfram, and Hornburg, Gerald, "Process for supplying air to a fuel cell system," U.S. Patent 5,645,950, July 8, 1997.

Berning, T., Lu, D.M., and Djilali, N., "Three-dimensional computational analysis of transport phenomena in a PEM fuel cell," Journal of Power Sources, vol. 106, pp. 284-294, 2002.

Bonville, Leonard J., "Method and apparatus for thermal management of a fuel cell assembly," U.S. Patent 6,248,462, June 19, 2001.

Bowman, John L. and Ben-Akiva, Moshe, "Activity-Based Travel Forecasting," Activity-based travel forecasting conference, Document No. DOT-T-97-17, June 2-5, 1996.

Burch, Steven D., Potter, Thomas F., Keyser, Matthew A., Brady, Michael J., and Michaels, Kenton F., "Reducing Cold-Start Emissions by Catalytic Converter Thermal Management," SAE Paper No. 950409.

Condit, David A., Breault, Richard D., Van Dine, Leslie L., and Steinbugler, Margaret M., "Operating system for a direct antifreeze cooled fuel cell power plant," U.S. Patent 6,416,891, July 9, 2002.

DaimlerChrysler (DC) and Ballard Power Systems (BPS), fuel cell vehicle model, 2003.

Dannenberg, K., Ekdunge, P., and Lindbergh, G., "Mathematical model of the PEMFC," Journal of Applied Electrochemistry, vol. 30, pp. 1377-1387, 2000.

Datta, B.K., Velayutham, G. and Goud, A. Prasad, "Fuel cell power source for a cold region," Journal of Power Sources, v. 106, pp. 370-376, 2002.

De Francesco, M. and Arato, E., "Start-up analysis for automotive PEM fuel cell systems," Journal of Power Sources, vol. 108, pp. 41-52, 2002.

Doss, Ezzat Danial, Ahluwalia, Rajesh, and Kumar, Romesh, "Analytical Performance of Direct-Hydrogen-Fueled Polymer Electrolyte (PEFC) Fuel Cell Systems for Transportation Applications," 33<sup>rd</sup> Intersociety Engineering Conference on Energy Conversion, Colorado Springs, CO, August 2-6, 1998.

DuPont, "Nafion<sup>®</sup> perfluorinated polymer products," product information sheet, October 2000.

DuBose, Ronald Arthur, "Fuel cell gas management system," U.S. Patent 6,013,385, January 11, 2000.

EVworld, "Fuel Cell Ford Focus: Part 2," April 14, 2002, website accessed April 16, 2002, <<http://www.evworld.com/databases/storybuilder.cfm?storyid=337>>.

Fletcher, Nicholas J., Boehm, Gustav A., and Pow, Eric G., "Method and apparatus for commencing operation of a fuel cell electric power generation system below the freezing temperature of water," U.S. Patent 5,798,186, August 25, 1998.

Friedman, David J., "Maximizing Direct-Hydrogen PEM Fuel Cell Vehicle Efficiency – Is Hybridization Necessary?" SAE Paper No. 1999-01-0530.

Fuller; Thomas F., Wheeler; Douglas J., "Start up of frozen fuel cell," U.S. Patent 6,103,410, August 15, 2000a.

Fuller, Thomas F. and Wheeler, Douglas J., "Start up of cold fuel cell," U.S. Patent 6,068,941, May 30, 2000b.

Gaarder, Erik Hans, Spradlin, Gerald Ray, Borregard, Robert Charles, and Kempfer, Stephen Thomas, "Vehicles containing water-producing fuel cells, and methods for using water produced by the fuel cells," U.S. Patent 6,467,698, October 22, 2002.

Gardiner, Monterey R., Cunningham, J. and Moore, R. M., "Compressed Hydrogen Storage for Fuel Cell Vehicles," SAE Paper No. 2001-01-2531.

Gebhardt, U. and Waidhas, M., "Fuel Cell Battery with a Heating Element and Improved Cold Start Performance and Method for Cold-Starting a Fuel Cell Battery," abstract for WO 00/59058, October 5, 2000.

Goto, Sogo, "Fuel-cells system and method of regulating temperature in fuel-cells system," U.S. Patent 6,087,028, July 11, 2000.

Gottesfeld, Shimshon and Zawodzinski, Tom A., "Polymer Electrolyte Fuel Cells," In Alkire, Richard C., Gerischer, Heinz, Kolb, Dieter M., and Tobias, Charles W., (Eds.), Advances in Electrochemical Science and Engineering: Volume 5, Weinheim: Wiley-VCH, 1997, pp. 245-271.

Graage, Klaus, and Zur Megede, Detlef, "Starter device for fuel cell system," U.S. Patent 6,559,551, May 6, 2003.

Gurski, Stephen Daniel, Cold-start effects on performance and efficiency for vehicle fuel cell systems, Thesis, Virginia Polytechnic Institute and State University, December 19, 2002.

Hauer, Karl-Heinz, Analysis Tool for Fuel Cell Vehicle Hardware and Software (Controls) with an Application to Fuel Economy Comparisons of Alternative System Designs, Dissertation, University of California, Davis, 2001.

Herdeg, Wolfgang, and Zapp, Thomas, "Fuel cell system," U.S. Patent 6,440,595, August 27, 2002.

Hodgson, J. W., Irick, D.K., "Investigation and demonstration of a rich combustor cold-start device for alcohol-fueled engines," Golden, CO: National Renewable Energy Laboratory, April 1998.

Hsu; Michael S. and Ong; Robin Y. P., "Fuel cell power supply system," U.S. Patent 5,858,568, January 12, 1999.

Incropera, Frank P. and De Witt, David P., Fundamentals of Heat and Mass Transfer, 3<sup>rd</sup> edition, New York: John Wiley & Sons, 1990, Appendix A.

Kempton, Willett, Tomic, Jasna, Letendre, Steven, Brooks, Alec, and Lipman, Timothy, "Vehicle-to-Grid Power: Battery, Hybrid, and Fuel Cell Vehicles as Resources for Distributed Electric Power in California," 2001, website accessed October 2003, <<http://repositories.cdlib.org/itsdavis/UCD-ITS-RR-01-03>>.

Kralick, James H., "Cooling a fuel cell stack," U.S. Patent 6,316,137, November 13, 2001.

Kumar, R., Ahluwalia, R., Geyer, H. K., and Krumpelt, M., "Modeling of Polymer Electrolyte Fuel Cell Systems: Proceedings of the Annual Automotive Technology Development Contractor's Coordination Meeting, 1993, Society of Automotive Engineers, Inc., Warrendale, Pa., Report No. P-278, pp. 409-417, May 1994.

Larminie, James and Dicks, Andrew, Fuel Cell Systems Explained, Chichester: John Wiley & Sons, Ltd., 2000.

Le Roy, R. and Brown, C., "The Thermodynamics of Aqueous Water Electrolysis," Electrochem. Soc., vol. 127, Nr. 9, 1980.

Lide, David R., editor, CRC Handbook of Chemistry and Physics, Boca Raton: CRC Press, 1999.

Loctite, "Product 3565, Industrial Version," Technical data sheet, November 1999.

Lorenz, Helmut, Noreikat, Karl-Ernst, Klaiber, Thomas, Fleck, Wolfram, Sonntag, Josef, Hornburg, Gerald, and Gaulhofer, Andreas, "Apparatus and method for starting a fuel cell vehicle," U.S. Patent 5,794,732, August 18, 1998.

Matejcek, L., Untersuchungen zur Membranbeschichtung und zur Gasverteilerstruktur in Membran Brennstoffzelle, Dissertation, Universität Duisburg, 1999.

Maggio, G., Recupero, V., and Mantegazza, C., "Modeling of temperature distribution in a solid polymer electrolyte fuel cell stack," Journal of Power Sources, vol. 62, pp. 167-174, 1996.

Matson, D.W., Martin, P. M., Stewart, D. C., Tonkovich, A. Y., White, M., Zilka, J. L., and Roberts, G. L., "Fabrication of Microchannel Chemical Reactors using a Metal Lamination Process," presented at IMRET 3: 3rd International Conference on Microreaction Technology, Frankfurt, Germany, April 18-21, 1999, website accessed October 2003, <<http://www.pnl.gov/microcats/aboutus/publications/microfabrication/DWMFrankfurt.pdf>>.

Molin, A., Wester, L., Haraldsson, K., Gustafsson, M., Alvfors, P., and Martin, V., "Thermal Energy Storage for Fuel Cell Vehicle Systems," IEA, ECES IA Annex 17, Advanced Thermal Energy Storage Techniques -- Feasibility Studies and Demonstration Projects 2nd Workshop, Ljubljana, Slovenia, April 3-5, 2002.

Momoda, Leslie A. and Phelps, Amanda C., "Nanometer sized phase change materials for enhanced heat transfer fluid performance," U.S. Patent 6,447,692, September 10, 2002.

Mosig, J., Dreidimensionale mathematische Modellierung einer Brennstoffzelle mit Protonen-Austausch-Membran (PEMFC), Dissertation, Forschungszentrum Jülich, 1998.

Mufford, W. Edward, Strasky, Douglas G., and Gorbell, Brian N., "Temperature regulating system for a fuel cell powered vehicle," U.S. Patent 6,186,254, February 13, 2001.

Nadal, M. and Barbir, F., "Development of a Hybrid Fuel Cell/Battery Powered Electric Vehicle," International Journal of Hydrogen Energy, vol. 21, no. 6, pp. 497-505, 1996.

Naka, Takahiro, Hideaki, Sumi, Furuyama, Masataka, Isobe, Shoji, Hiramatsu, Yasushi, and Yoneoka, Mikio, "Method of starting and stopping methanol reforming apparatus and apparatus for supplying fuel to said apparatus," U.S. Patent 6,290,877, September 18, 2001.

National Institute of Standards and Technology (NIST), "Chemistry WebBook," 2003, website accessed February 2003, <<http://webbook.nist.gov/>>.

National Renewable Energy Laboratory, "Chapter 1: Introduction - Advisor Documentation," April 30, 2002, website accessed October 2003, <[http://www.ctts.nrel.gov/analysis/advisor\\_doc/advisor\\_ch1.htm](http://www.ctts.nrel.gov/analysis/advisor_doc/advisor_ch1.htm)>.

Ngu, Yan, Barbir, Frano, Husar, Attila, Neutzler, Jay K., and Snipas, Rachael, "Freeze Tolerant Fuel Cell System and Method," WO 00/65676, November 2, 2000.

Ogburn, Michael, Nelson, Douglas J., Luttrell, William, King, Brian, Postle, Scott, and Fahrenkrog, Robert, "Systems Integration and Performance Issues in a Fuel Cell Hybrid Electric Vehicle," SAE Paper No. 2000-01-0376, 2000a.

Ogburn, Michael, Boligitz, Alex, Luttrell, William, King, Brian, Postle, Scott, Fahrenkrog, Robert, and Nelson, Douglas J., "Integration of Fuel Cell Technology into a Hybrid Electric Vehicle," SAE Paper No. 2000-01-0592, 2000b.

Okamoto, Takafumi, "Gas humidifying device for use with a fuel cell," U.S. Patent 5,965,288, October 12, 1999.

Paganelli, Gino, Guezennec, Yann and Rizzoni, Giorgio, "Optimizing Control Strategy for Hybrid Fuel Cell Vehicle," SAE Paper No. 2002-01-0102.

Pettit, William Henry, "Fuel cell system combustor," U.S. Patent 6,232,005, May 15, 2001.

Rajashekara, K., "Propulsion System Strategies for Fuel Cell Vehicles," SAE Paper No. 2000-01-0369.

Roberts, Joy, Geest, Marian van der, St. Pierre, Jean, Wilkinson, David P., Lee, Alvin, and Moroz, Stephanie, "Method and apparatus for increasing the temperature of a fuel cell," U.S. Patent 6,329,089, December 11, 2001.

Rock, J.A. and Plant, L.B., "Method of cold start of a PEM fuel cell," European Patent 1113516A1, July 4, 2001.

Roeser, Thomas, Saling, Carlo, and Wolfsteiner, Matthias, "Method for shortening the starting time of CO oxidation catalytic converters in mobile fuel cell systems," U.S. Patent 6,536,546, March 25, 2003.

Rowe, Andrew and Li, Xianguo, "Mathematical modeling of proton exchange membrane fuel cells," Journal of Power Sources, vol. 102, pp. 82-96, 2001.

Sena, D.R., Ticianelli, E.A., Paganin, V.A., Gonzalez, E.R., "Effect of water transport in a PEFC at low temperatures operating with dry hydrogen," Journal of Electroanalytical Chemistry, vol. 477, pp. 164-170, 1999.

Siepierski, James S., Moore, Barbara S., and Hoch, Martin Monroe, "Water injected fuel cell system compressor," U.S. Patent 6,268,074, July 31, 2001.

Springer, T.E., Zawodzinski, T.A., and Gottesfeld, S., "Polymer Electrolyte Fuel Cell Model," Journal of the Electrochemical Society, vol. 138, no. 8, August 1991.

Springer, T.E., Wilson, M.S., and Gottesfeld, S., "Modeling and Experimental Diagnostics in Polymer Electrolyte Fuel Cells," Journal of the Electrochemical Society, vol. 140, no. 12, December 1993.



Sridar, P., Perumal, Ramkumar, Rajalakshmi, N., Raja, M., and Dhathathreyan, K.S., "Humidification studies on polymer electrolyte membrane fuel cell," Journal of Power Sources, vol. 101, pp. 72-78, 2001.

Tak2000, "Typical Material Properties," 2003, website accessed February 2003, <<http://www.tak2000.com/data/prop1.htm#Plastics>>.

The Engineering Toolbox, [http://www.engineeringtoolbox.com/24\\_146.html](http://www.engineeringtoolbox.com/24_146.html), website accessed March 2004.

Tran, D. and Cummins, M., "Development of the Jeep Commander 2 Fuel Cell Hybrid Electric Vehicle," SAE Paper No. 2001-01-2508.

U. S. Department of Energy, Fuel Cell for Transportation: 2001 Annual Progress Report, December 2001.

U. S. Department of Energy, Progress Report for Hydrogen, Fuel Cells, and Infrastructure Technologies Program, November 2002.

Ueno, Masataka, Kato, Kenji, Horiguchi, Munehisa, and Takada, Noriyuki, "Fuel cell system," U.S. Patent 6,294,277, September 25, 2001.

Unnasch, S and Drunert, V., Evaluation of Fuel Cell Reformer Emissions, Prepared by Arcadis Geraghty and Miller, Inc. for California Air Resource Board, Contract No. 95-313, 1999.

Vairex Corporation website, brochure, "Integrated Fuel Cell Air Management System," 2003, accessed November 9, 2003, <[http://www.vairex.com/products/vp\\_specs.html](http://www.vairex.com/products/vp_specs.html)>.

Weisbrod, Kirk, Hedstrom, Jim, Tafoya, José, Borup, Rod, and Inbody, Mike, "Cold Start Dynamics of a PEM Fuel Cell Stack," 2000 Fuel Cell Seminar, Portland, OR, October 30-November 2, 2000a.

Weisbrod, Kirk, Hedstrom, Jim, Tafoya, José, Borup, Rod, and Inbody, Mike, "Reformate Stack Operation Issues and Improved Designs," presentation at DOE Fuel Cell Program Review Meeting, June 7-8, 2000b.

Wheeler, D. J. and Bonville, L. J., "Start up of proton exchange membrane fuel cell," U.S. Patent 6,127,056, October 3, 2000.

Wind, Joerg, LaCroix, Annette, Braeuninger, Sigmar, Hedrich, Peter, Heller, Cosmas, and Schudy, Markus, "Metal bipolar plates and coatings," In Vielstich, W., Lamm, A., and Gasteiger H. (Eds.), Handbook of Fuel Cells – Fundamentals, Technology and Applications, Volume 3: Fuel Cell Technology and Applications, Chichester: John Wiley & Sons, Ltd., 2003.

Wöhr, M., Bolvin, K., Schnurnberger, W., Fischer, M., Neubrand, W., and Eigenberger, G., "Dynamic modeling and simulation of a polymer membrane fuel cell including mass transport limitation," International Journal of Hydrogen Energy, vol. 23, no.3, pp. 213-218, 1998.

Yamada, Shuji, Kanda, Motoya, Yoshizawa, Hiroyasu, and Sonai, Atsuo, "Fuel cell power generation system," U.S. Patent 5,482,790, January 9, 1996.

Zhang, Yangjun, Ouyang, Minggao, Lu, Qingchun, Luo, Jianxi, and Li, Xihao, "A model predicting performance of proton exchange membrane fuel cell stack thermal systems," Applied Thermal Engineering, vol. 24, pp. 501-513, 2004. (Available online at [www.sciencedirect.com](http://www.sciencedirect.com).)

Zilka-Marco, J.L, Tonkovich, A. Y., Powell, M., Roberts, G. L., Wang, Y., Fitzgerald, S. P., Wegeng, R. S., Martin, P. M., Matson, D. W. and Stewart, D. C., "Compact Microchannel Fuel Vaporizer." R&D 100 Award Entry, Pacific Northwest National Laboratory, Richland, Washington, February 1999, website accessed October 2003, <<http://www.pnl.gov/microcats/whatnew/r&dfuelvap.pdf>>.

Zur Megede, Detlef, "Hybrid vehicle having an ICE, fuel cell system and electric drive motor," U.S. Patent 6,276,473, August 21, 2001.

## **7 Appendix**

### **7.1 Proposed strategies in the literature for cold start heat and water management**

#### **7.1.1 Review of warming strategies for direct hydrogen FCV fuel cell stack**

Many sources (Lorenz et al., 1998; Tran and Cummins, 2001; Fletcher, 1998; Mufford, 2001) discuss relying on the fuel cell heating itself due to resistant heating, even if another method is used to assist the fuel cell before it generates heat internally. At around 20°C, the fuel cell begins to heat itself during low-efficiency operation until it reaches around 80°C.

For starting the stack below 0°C, Roberts et al. (2001) discuss a strategy in which the fuel cell temperature is increased by starving one or both electrodes of reactant. This starvation results in an increased overvoltage at the electrode and increased internal heat generation. Starvation conditions are obtained by reducing the reactant supply rate or by operating the fuel cell at a current density at which the reactant is consumed more quickly than it is supplied. Roberts et al. (2001) point out that the amount of reaction water produced during starvation is reduced, preventing ice blockage.

Typically, however, below the freezing point of water the fuel cell must be provided a heat source. This section describes strategies (as found in the literature) to warm up the fuel cell stack.

#### 7.1.1.1 Fuel cell stack coolant loop (warming loop)

Several studies discuss using a heat source to warm the fuel cell stack cooling loop or bypassing the radiator during startup. In their direct hydrogen fuel cell vehicle study, Doss et al. (1998) discuss the importance of bypassing the radiator until the coolant temperature approaches the design operating temperature for their 50 kW system. Hsu and Ong (1999) and Yamada et al. (1996) discuss pre-heating the fuel cell by circulating a heated fluid in the fuel cell cooling system and Rock and Plant (2001) specifically describe using a combustor as the heat source. Ballinger et al. (2002) discuss sending warm coolant through the coolant inlet and outlet manifolds only, and not through the actual coolant channels, to heat up the stack by conduction. In the study by Weisbrod et al. (2000a, 2000b) they point out the necessity to minimize the thermal mass of the coolant flow loop to minimize the need for a large external heat source. In their case, the heat source they model is waste heat from a fuel processor. While direct hydrogen systems do not include fuel processors, currently accepted system designs may require the use of a small hydrogen burner to serve as the heat source in this method of warming the fuel cell stack. Finally, in a vehicle having an internal combustion engine (ICE) drive and a fuel cell drive system, the ICE can start and move the vehicle immediately while heating the fuel cell system to operating temperature (Zur Megede, 2001).

The heat source for the cooling loop is not limited to combustor or fuel processor waste heat. Electric heaters have been considered as heat sources (Andreoli and Federici, 1997; Fletcher et al., 1998). Fletcher et al. (1998) discuss the use of electric heat, for which a battery may supply the power. The coolant stream may be water or a liquid that does not freeze at the freezing temperature of water.

Furthering the idea of using non-water based coolant, Goto (2000) discusses a method which obviates the need for melting the coolant at sub-zero temperatures and reduces warmup time by using an antifreeze solution which would require that the cooling flow is a closed system that circulates between the fuel cells and the radiator. Bonville (2001) outlines a similar approach in which the stack has two thermal management loops in which a primary loop is in thermal communication with the fuel cell stack for circulating water and a secondary loop is in thermal communication with the fuel cell stack for circulating an antifreeze solution, and each loop is diffusably isolated from one another. Section 7.1.2 provides more discussion on handling freezing conditions.

A method of improving the coolant's heat transfer characteristics, especially as it serves as a warming fluid, is in introducing nanometer-sized phase change material (nano-PCM) into the fluid (Momoda and Phelps, 2002). In addition to improving the heat transfer properties the nano-PCM particles can lower viscosity of the fluid at sub-freezing temperatures. The particle-filled fluid can be used to transfer heat to the system on start-up. The radiator would be bypassed and some of the fluid would be directed to a heat storage unit. The nano-PCM particles would be permitted to change phase after being released from the heat storage unit. Upon startup, if the temperature of the system is less than the phase change temperature, heat will be released to the system as the nano-PCM particles re-solidify.

In using a combustor as a heat source, in freezing conditions the burner itself must be heated up. There are several articles in the literature that describe methods to heat up

burners, or, more relevant to automobiles, catalytic converters for internal combustion engine vehicles. Electrical heating of inlet gases (Pettit, 2001) and ignition (Hodgson, 1998) are possible starting methods as well as maintaining heat by using insulation or other forms of thermal management (Burch, 1995). Furthermore, gas components that can delay startup, e.g. water that condenses from moist air and settles in the burner after shutdown, can freeze and delay burner ignition. Roeser et al. (2003) suggest that an adsorber can remove these gas components.

#### 7.1.1.2 Block heater, off- and on-board electricity

As with internal combustion engine (ICE) vehicles, block heaters in severe climates may be used to heat up the fuel cell stack in a direct hydrogen FCV. In their 2001 patent, Mufford et al. (2001) describe a scenario in which a resistor receiving electricity from off-board functions as a block heater to prevent the stack from freezing and assisting in startup. Similarly, in their patent Hsu and Ong (1999) discuss an off-board inverter that can be reversed to rectify alternating current from the utility grid, providing rectified power to warm up the fuel cell. The station would cut power to the fuel cell once it reached its operating temperature and could provide power. Fletcher et al. (1998) indicate that the power for pre-heating can be provided by an on-board source such as a battery. Gebhardt and Waidhas (2000) discuss using a heating element, i.e. wire to heat a portion of the fuel cell stack that can be powered by an on-board source.

#### 7.1.1.3 Exothermic chemical reactions on anode/cathode catalyst

A concept described by Rock and Plant (2001), Wheeler and Bonville (2000) and Fuller and Wheeler (2000a) is introducing hydrogen gas into the cathode stream (and possibly also oxygen into the anode stream) to produce exothermic chemical reactions at both electrodes for sub-freezing temperatures. Rock and Plant (2001) indicate that warm oxygen and/or hydrogen can be passed over the fuel cell cathode and anode flowfields for de-icing before sending in fuel and oxidant streams for the chemical reactions. Furthermore, they suggest higher gas flowrates than those used during normal operation of the fuel cell to ensure a uniform distribution of the heat generated by the chemical reactions. Finally, they suggest that for a reaction at the anode, the O<sub>2</sub> concentration should be around 1-7% by volume in the anode H<sub>2</sub> flow and for a reaction at the cathode, the H<sub>2</sub> concentration should be 0.5-3.5% by volume in the cathode airflow. These values are suggested to prevent temperature excursions within the electrodes and are based on an initial temperature of below -25°C.

Wheeler and Bonville (2000) and Fuller and Wheeler (2000a) discuss only sending hydrogen to the air side and note that the reaction should be carried out at subflame temperatures by limiting the hydrogen gas stream to a small volume percentage of the overall mixture, such as around 1-2% by volume to less than 4% by volume in the cathode airflow, to prevent explosion or membrane dehydration. Their suggested concentrations are based on an initial temperature of -40°C. They further discuss that in one embodiment, in which the cathode has catalytic hydrophobic regions in its structure to prevent flooding and freezing of water, the dilute fuel/oxygen reaction can enter and react. If necessary, catalyst can be introduced in these hydrophobic regions to initiate

reactions that will melt ice in other regions and diffuse the mixture into the catalyst of the entire cathode.

#### 7.1.1.4 Compressor start and compressor heating of fuel cell stack

A method to heat up the fuel cell stack can be feeding warm compressor air into the cathode side. Prior to the startup of the compressor itself (as it requires minimum flow and pressure conditions) an on-board supply of pressurized O<sub>2</sub> can provide oxidant for the fuel cell reactions (Adams et al., 1999), although pressurized O<sub>2</sub> will be an additional volume and weight on-board. The compressor can be started with an internal combustion engine (Graage and Zur Medege, 2003) or a starter motor until a minimum air volume flow and working pressure are achieved, and then the starter motor can be deactivated and an electric motor started to continue operating the compressor (Benz et al., 1997). The compressor can be operated dry to use the heat of compression transferred to the air to warm the fuel cell stack (Siepierski et al., 2001). However, it has been found by experiment that compressor heat provides little benefit (Weisbrod et al., 2000b).

#### 7.1.2 Review of frozen water management strategies

Of the many startup issues facing automakers, one that generates the most interest is how to deal with the system water in freezing conditions. Typically, the stack is cooled (or warmed) via a closed loop separated from the membrane using a non-water solution like antifreeze or other substances that have freezing points below the freezing point of water (Naka et al., 2001; Fuller and Wheeler, 2000b; Kralick, 2001; Okamoto, 1999; Ngu et al., 2000), but a typical PEM stack can only be humidified by de-ionized water. Humidification is necessary for H<sup>+</sup> ionic transport through the membrane. Substances like antifreeze will poison the stack by occupying catalyst sites. In freezing conditions, however, water that collects within the stack (but not necessarily within the membrane) can expand and damage stack components. Either the water must be purged or kept from freezing, which are activities that occur at shutdown. Note that some of the methods presented in Section 7.1.1 can be used in freezing and above-freezing conditions, and are related to the methods presented in this section.

##### 7.1.2.1 Water purge

Ngu et al. (2000), Atbi et al. (2001) and Unnasch (1999) suggest purging water from the stack. Atbi et al. (2001) discuss purging methods for the stack water and stack coolant (if the freezing point of the cooling fluid is above the anticipated stack storage temperature) by using oxidant or N<sub>2</sub>. They recommend to first interrupt electric current from the stack to the external circuit, reduce the stack temperature to below the operating temperature, preferably to as low as 10°C, then purge. Ngu et al. (2000) point out that even if the expansion of frozen water does not damage the stack, fuel system lines can be blocked. Water can accumulate in the gas diffusion layer and the flow channels of the collector plates. During shutdown, dry gases can be forced through the stack to purge out the channels and the gas diffusion layers.

Ngu, et al, further suggest that if at least one of the outlets is positioned below the channels, gravity will assist in removing the water. The drained water can be stored in a

tank, and the tank can be insulated or heated, or if allowed to expand, the water can freeze within the tank. Their recommended shutdown procedure includes reducing the stack temperature so that water vapor can condense, purging the water and reducing the system pressure to atmospheric. The shutdown procedure can also include a step in which the stack is operated to produce a pulsed current output to increase the heat of the stack at or just before shut down. Upon startup, dry gases can be flowed through reactant lines, and humidification of the gases can be initiated after the stack is above a predetermined temperature, which can be the freezing point of water at the ambient pressure. The startup procedure can include pressurizing to the maximum operating pressure to increase fuel cell heat and retain any thawing residual water. The humidification for the reactant gas flows is facilitated by a water reservoir, which, as mentioned earlier, may require a heat source to melt the water in the reservoir.

The water can also be purged from the vehicle, i.e., expelled onto the ground below the vehicle. However, according to Gaarder et al. (2002), who discuss using excess water in an on-board component such as the windshield washer, expulsion of water can lead to tire traction problems, or in the case of sub-freezing conditions, form ice patches and precarious driving conditions.

The Hybrid Electric Vehicle Team of Virginia Tech developed a fuel cell hybrid electric vehicle to meet the goals of the Department of Energy FutureCar Challenge and PNGV. The team describes the issues they encountered in system development (Ogburn et al., 2000a; Atwood et al., 2001; Ogburn et al., 2000b), especially those of water and thermal management during startup. Discrepancies between reactant temperatures and the fuel cell cooling loop can cause water condensation in the reactant streams or absorption by hot reactants, yielding undesirable flooding or drying conditions. These temperature discrepancies are more pronounced during startup when the system is cold: early acceleration would produce hot air at the compressor outlet and a system temperature imbalance.

While the Virginia Tech team did not address or analyze these startup issues, they did conduct testing to verify that humidification of the fuel cell during the warm up period can achieve humidity levels of 75%, above the 60% minimum recommended for stack startup. During normal operating conditions, the hydrogen vaporizes the water to provide the fuel cell with needed humidity levels. During the warm up period, the humidification chamber drains water to the water storage tank because the hydrogen is not hot enough to vaporize the water and some of the water is liquid.

#### 7.1.2.2 Water temperature maintenance above freezing point

Keeping a non-operating stack above the freezing point, especially for extended periods of time in sub-freezing conditions, has been shown to be possible with vacuum insulation or using phase change materials as latent heat storage that stores waste heat (generated during stack operation) combined with vacuum insulation (Molin et al., 2002).

Considering non-insulation strategies, Section 7.1.1 provided a discussion of heating methods that included the use of off- and on-board electricity. Keeping the temperature above the freezing point of water requires that some level of energy consumption takes place for an extended period of time, e.g. with a block heater as is used with internal combustion engines in severe climates. A burner may be used to

provide heat, or an on- or off-board electric source. For example, if the fuel cell vehicle is “plugged in” as might be possible in a vehicle-to-grid scenario (Kempton et al., 2001), the system may be kept at some minimum level for some hours to facilitate quick startup, e.g. a heater to keep the coolant passages within the stack warm. If the coolant circulates, power would need to be provided to a pump; however, the heater can also provide heat to the stack itself. As it may not always be possible to obtain off-board electricity, an on-board source would need to provide some level of continuous power.

Another option is to use anti-freeze in the water reservoir to prevent freezing (Herdeg and Zapp, 2002). To prevent anti-freeze from passing into the fuel cell during startup operation, a heater is used to heat the liquid and evaporate the anti-freeze in the liquid that is then collected, condensed and returned to the reservoir. Finally, Condit et al. (2002) discuss a “fine pore enthalpy exchange barrier” through which water vapor, but not the antifreeze solution (such as an alkanetriol), can pass to the fuel cell. During shutdown, the water in the electrolyte will evaporate and pass through the layers as vapor, and the antifreeze will evaporate and pass into the electrolyte to serve to lower the freezing point of the remaining solution in the electrolyte. Upon startup, any antifreeze in the electrolyte is oxidized at the anode and cathode catalysts.

The system may also be kept at some minimum level without a plug-in scenario, by keeping the fuel cell operating at some minimum level, such that internal resistance provides sufficient heat. However, this would require that the eductors (which incorporate a convergent-divergent nozzle and injection port for inducing hydrogen recirculation) have a high enough flow of high-pressure hydrogen for the motive force to circulate gaseous hydrogen. At startup or low level operation when little or no hydrogen is consumed, a “start-up eductor” (DuBose, 2000) powered by the injection of water or other fluid, which in turn is supplied by a pump requiring power, provides the motive flow and circulates and humidifies the anode loop. In startup, this second eductor would operate until sufficient hydrogen flow enables the primary eductor to work alone. In low operation mode, the second eductor would be the only means for circulation and humidification. The coolant may not need to be circulated, obviating the need for coolant pump power, since the fuel cell would be kept at a level of operation to just keep the water from freezing. The stack may also operate at atmospheric pressure using a blower instead of higher pressure, as may be the case during normal operation, in order to eliminate the need for powering a compressor.

## **7.2 Validation**

The validation of the cold start model has been made with DaimlerChrysler (DC) and Ballard Power Systems proprietary data; however, the results shown in Chapter 4 were obtained in simulations using literature parameter values and DC non-proprietary data within the validated model.

The DC experimental data included stack voltage and current, coolant flowrate, and stack inlet and outlet temperatures. Figure 33 shows the model inputs and outputs.

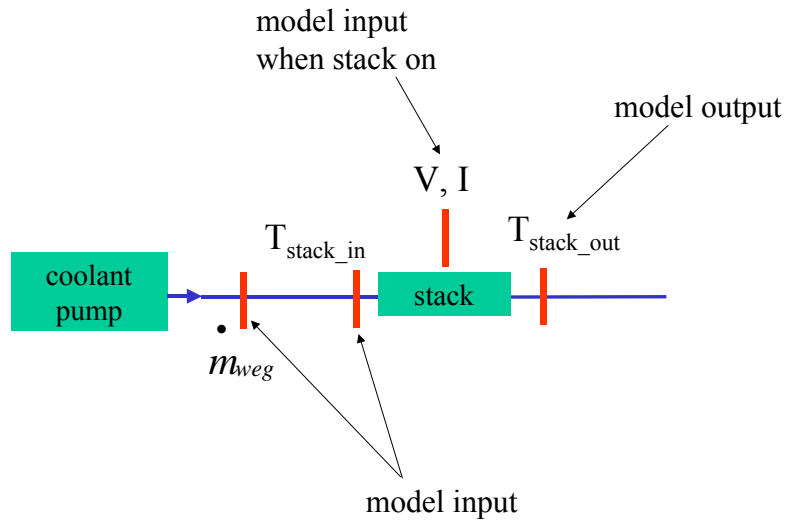


**Figure 33: Validation setup**

The test condition considered was *no external warming, stack on, idle to full power*. Given time constraints, the test was repeated three times and the experimental error was generated and used for the error bars for the model validation. Figure 34 compares DC experimental data with the model for the test condition. In this comparison, the model appears to correlate well with the experimental data.

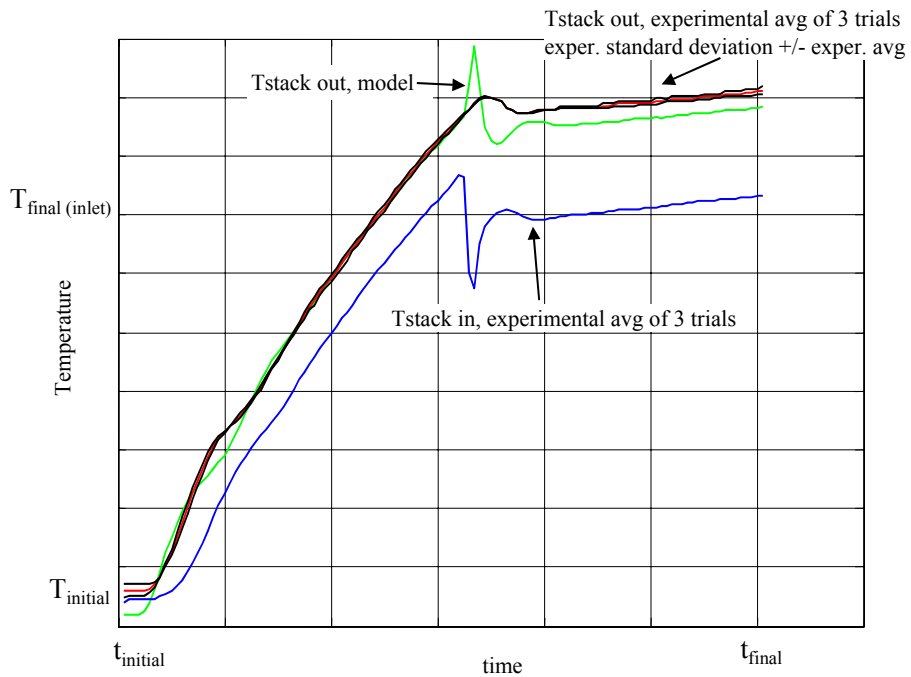


**Figure 34: Validation results**



The spiked response of the model output in Figure 34 to the dynamic behavior of the experimental input reveals an interesting point about the assumption of linearity for the coolant channel, discussed using the following figure (Figure 35) and explanation.

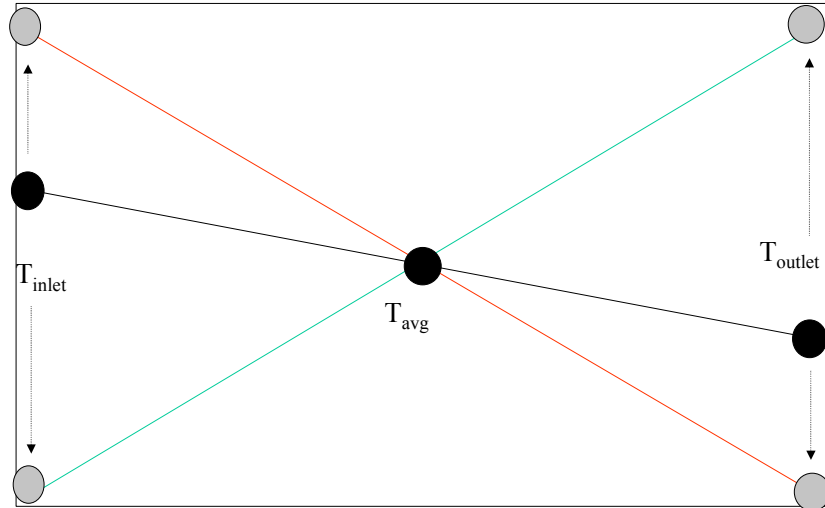


**Figure 35: Linear coolant temperature distribution**

In Figure 35, the outlet temperature is forced to assume high or low temperatures based on the inlet temperature dynamics. In the upward temperature ramp of Figure 34, the model smoothly follows the experiment. However, at the point of the sudden spike downward in the experimental stack inlet temperature, the model output spikes upward, unlike the experimental output, following the rigid behavior exhibited by the linear distribution. While the model's validation is acceptable, a further improvement to better handle dynamic behavior would be to consider a second dimension of the cell/stack, i.e., discretize the cell/stack along the direction of coolant flow to determine the real temperature distribution along this dimension.

### 7.3 Equations

#### Cell/Endplate

The equations in this section are organized in the following manner. Each layer shown in Figure 36 is separated, described, and illustrated with an energy balance. Equations then detail the illustration. Please note the explanation of areas used in the equations as illustrated in Figure 37. Please refer to Section 3.1.1 for the assumptions made in the cell model construction.

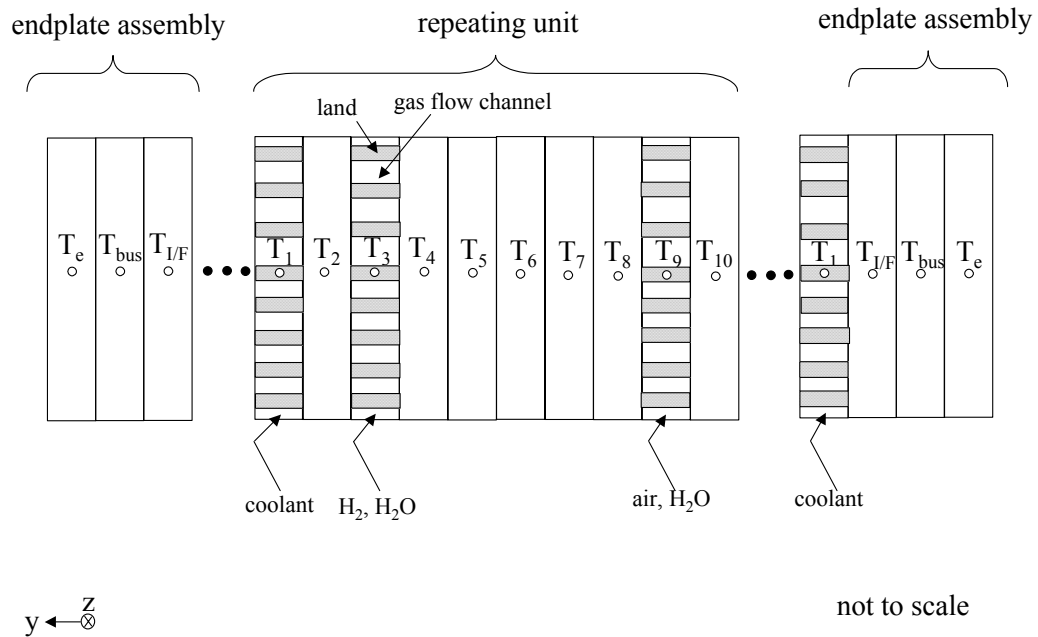


**Figure 36: Model sketch of cell unit and endplates**

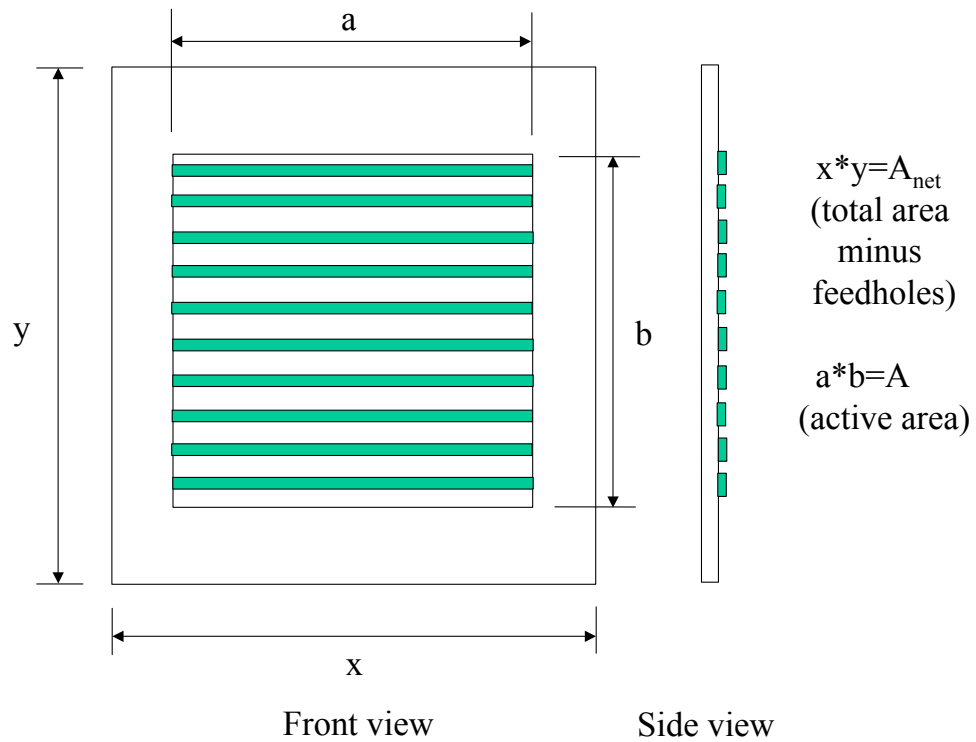


**Figure 37: Illustration of areas used in equations**

Figure 37 shows a general cell plate with channels.  $A$ , or the active area, is used in calculating stack current,  $I$ . It is also used, in conjunction with channel land contact area, in calculating the channel thermal mass or gas thermal mass in the flowfields. Finally,  $A$  is the area normal to the heat flow conducted from the channel land to the adjoining layers. Other layers use  $A_{\text{net}}$  in these calculations (with contact area or porosity as noted). For example,  $A_{\text{net5L}}$  is the net area multiplied by the fraction representing the solid portion of the porosity, or the “land” (L), for layer 5. See the Nomenclature section for detailed definitions.

Derivation of overall heat transfer coefficient,  $U$

Each energy balance equation includes a calculation for the overall heat transfer coefficient,  $U$ . Figure 38 provides the illustration for the following explanation.

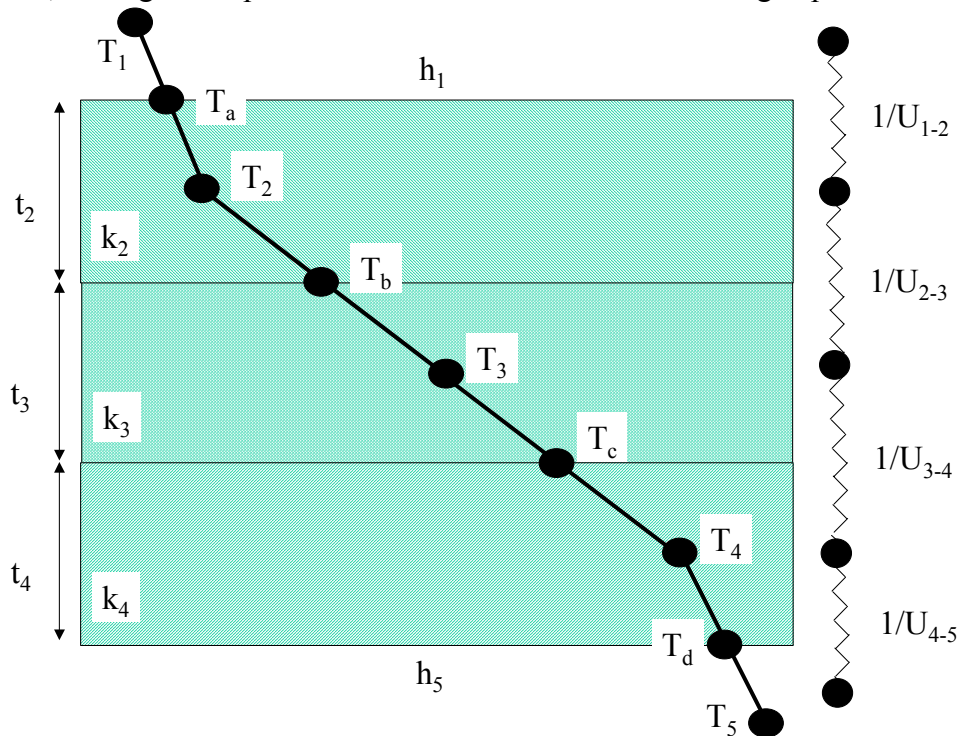


**Figure 38: Illustration for overall heat transfer coefficient derivation**

The thermal resistance for conduction and convection is shown in Figure 38. Note that the nodes defining the resistance boundaries are placed at the center of each section. This method was used in order to use the average temperature in the section, which was assumed to be in the center under steady state conditions.

The parameters  $k$  and  $t$  are the thermal conductivities and material thickness, respectively for the composite plates and  $h$  is the heat transfer coefficient of a fluid. An

arbitrary temperature profile is shown, represented by  $T_1, T_a, T_2, T_b, T_3, T_c, T_4, T_d$  and  $T_5$ . At steady state, the heat flux,  $q''$  is equal to  $U\Delta T$ , is identical in each section and can be described by the following equations. Take the segment represented by  $T_1, T_a$  and  $T_2$ :

$$\text{General equation : } q'' = U\Delta T$$

$$(1) \quad q'' = h(T_1 - T_a)$$

OR

$$q'' \frac{1}{h} = T_1 - T_a$$

$$(2) \quad q'' = \frac{k_2}{t_2/2} (T_a - T_2)$$

OR

$$q'' \frac{t_2/2}{k_2} = T_a - T_2$$

Adding heat flux equations (1) and (2) together yield:

$$q'' \left( \frac{1}{h} + \frac{t_2/2}{k_2} \right) = T_1 - T_2$$

$$\therefore U = \frac{1}{\frac{1}{h} + \frac{t_2/2}{k_2}}$$

For the segment represented by  $T_2, T_b$  and  $T_3$ :

$$\text{General equation : } q'' = U\Delta T$$

$$(1) \quad q'' = \frac{k_2}{t_2/2} (T_2 - T_b)$$

OR

$$q'' \frac{t_2/2}{k_2} = T_2 - T_b$$

$$(2) \quad q'' = \frac{k_3}{t_3/2} (T_b - T_3)$$

OR

$$q'' \frac{t_3/2}{k_3} = T_b - T_3$$

Adding heat flux equations (1) and (2) together yield:

$$q'' \left( \frac{t_2/2}{k_2} + \frac{t_3/2}{k_3} \right) = T_2 - T_3$$

$$\therefore U = \frac{1}{\frac{t_2/2}{k_2} + \frac{t_3/2}{k_3}}$$

Similar expressions can be derived for the other segments.

For clarification, the expressions used for heat rate in the layer equations on the following pages are of the form  $\dot{Q} = UA(T_1 - T_2)$ .

### ENDPLATE ASSEMBLY

LAYER: ENDPLATE – The endplate is placed on either end of the fuel cell stack and, with other hardware, serves to compress the cells together.

SKETCH:

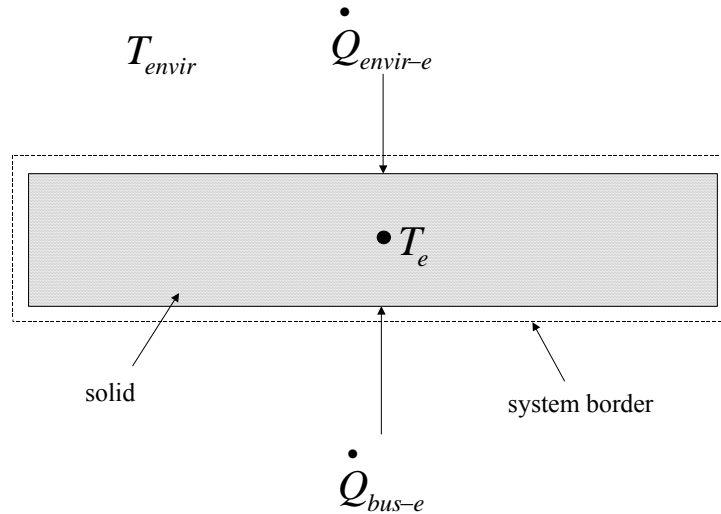


**Figure 39: Endplate energy balance**

EQUATIONS:

$$(\rho_e (A_{net} t_e) C p_e) \frac{dT_e}{dt} = \dot{Q}_{bus-e} + \dot{Q}_{envir-e}$$

### **Equation 6: Energy Balance**

The  $\dot{Q}$  expressions in Equation 6 are shown below.

$$\dot{Q}_{bus-e} = U_{bus-e} A_{net} (T_{bus} - T_e)$$

$$\dot{Q}_{envir-e} = U_{envir-e} A_{net} (T_{envir} - T_e)$$

**Equation 7: Set of heat flows**

The overall heat transfer coefficient terms are shown in Equation 8.

$$U_{bus-e} = \frac{1}{t_{bus}/2k_{bus} + t_e/2k_e}$$

$$U_{envir-e} = \frac{1}{t_e/2k_e + 1/h_{envir}}$$

**Equation 8: Set of overall heat transfer coefficients**

Note: For the convection term,  $1/h_{envir}$ ,  $A_{net}$  is used as the area, i.e. the term is used to represent convective losses from the endplate to the environment; however, it is assumed that  $h_{envir}A_{net}$  is represented by a combined parameter found in the literature (Amphlett et al., 1996) for the heat loss from the *stack* to the environment.

LAYER: BUS – The bus is part of the endplate assembly and is positioned between the endplate and interface (I/F) layer. This layer is the connection between endplates via the external circuit.

SKETCH:

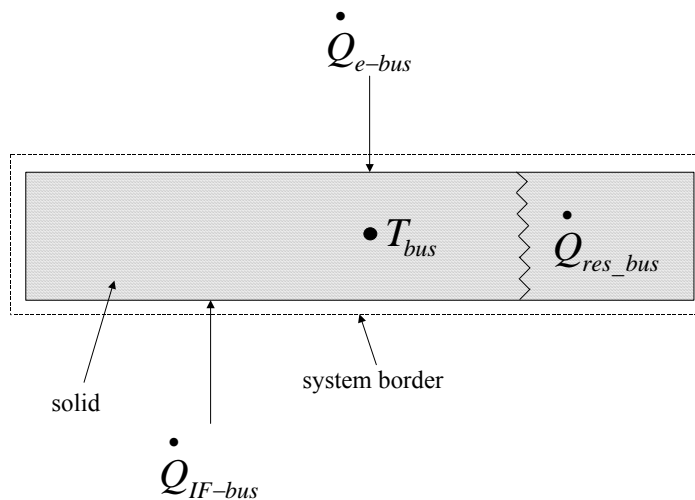


**Figure 40: Bus energy balance**

EQUATIONS:

$$(\rho_{bus} (A_{net} t_{bus}) Cp_{bus}) \frac{dT_{bus}}{dt} = \dot{Q}_{e-bus} + \dot{Q}_{IF-bus} + \dot{Q}_{res\_bus}$$

**Equation 9: Energy Balance**

The  $\dot{Q}$  expressions in Equation 9 are shown below.

$$\dot{Q}_{e-bus} = U_{e-bus} A_{net} (T_e - T_{bus})$$

$$\dot{Q}_{IF-bus} = U_{IF-bus} A_{net} (T_{IF} - T_{bus})$$

**Equation 10: Set of heat flows**

$$\dot{Q}_{res\_bus} = (iA)^2 \frac{\rho_{res\_bus} t_{bus}}{A_{net}}$$

**Equation 11: Heat generation**

The overall heat transfer coefficient terms are shown in Equation 12.

$$U_{e-bus} = \frac{1}{t_{bus}/2k_{bus} + t_e/2k_e}$$

$$U_{IF-bus} = \frac{1}{t_{IF}/2k_{IF} + t_{bus}/2k_{bus}}$$

**Equation 12: Set of overall heat transfer coefficients**

LAYER: I/F PLATE – The interface (I/F) plate is part of the endplate assembly and is positioned between the assembly and the end cell.

SKETCH:

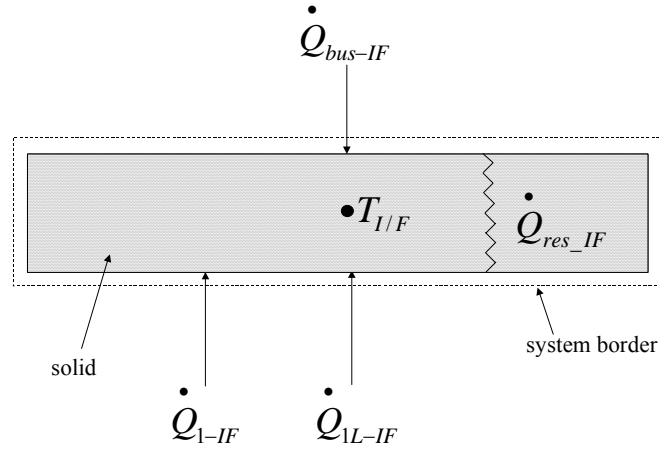


**Figure 41: I/F plate energy balance**

EQUATIONS:

$$(\rho_{IF} (A_{net} t_{IF}) C p_{IF}) \frac{dT_{IF}}{dt} = \dot{Q}_{1-IF} + \dot{Q}_{1L-IF} + \dot{Q}_{bus-IF} + \dot{Q}_{res-IF}$$

**Equation 13: Energy Balance**

The  $\dot{Q}$  expressions in Equation 13 are shown below.

$$\dot{Q}_{1-IF} = U_{1-IF} A_{1void} (T_1 - T_{IF})$$

$$\dot{Q}_{1L-IF} = U_{1L-IF} A_{1L} (T_1 - T_{IF})$$

$$\dot{Q}_{bus-IF} = U_{bus-IF} A_{net} (T_{bus} - T_{IF})$$

**Equation 14: Set of heat flows**

$$\dot{Q}_{res-IF} = (iA)^2 \frac{\rho_{res-IF} t_{IF}}{A_{net}}$$

**Equation 15: Heat generation**

The overall heat transfer coefficient terms are shown in Equation 16.

$$U_{1-IF} = \frac{1}{t_{IF}/2k_{IF} + 1/h_1}$$



$$U_{1L-IF} = \frac{1}{t_{IF}/2k_{IF} + t_1/2k_1}$$

$$U_{bus-IF} = \frac{1}{t_{IF}/2k_{IF} + t_{bus}/2k_{bus}}$$

**Equation 16: Set of overall heat transfer coefficients**

Note: For the convection term,  $1/h_1$ ,  $A_{1void}$  is used as the area; however, it is assumed that  $h_1A_{1void}$  is represented by a combined parameter found in the literature (Amphlett et al., 1996) for the heat transfer from the stack to the coolant.

CELL ASSEMBLY

LAYER 1: COOLANT - Within the cooling channels flows a water/ethylene glycol mixture, the medium by which heat is carried to or from the fuel cell.

SKETCH:

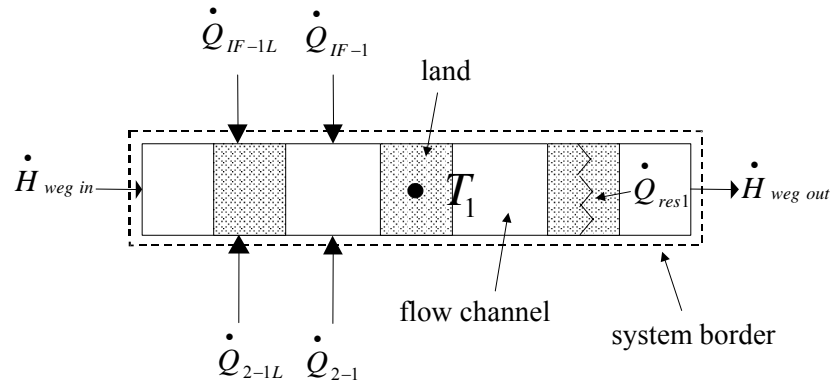


**Figure 43: Coolant layer energy balance**

EQUATIONS:

$$(m_{WEG} Cp_{WEG} + \rho_1(A_{1L}t_1)Cp_1) \frac{dT_1}{dt} = \dot{Q}_{IF-1} + \dot{Q}_{IF-1L} + \dot{Q}_{2-1} + \dot{Q}_{2-1L} + \dot{Q}_{res1} + \dot{H}_{weg in} - \dot{H}_{weg out}$$

**Equation 17: Energy Balance**

The  $\dot{Q}$  and  $\dot{H}$  expressions in Equation 17 are shown below.

$$\dot{Q}_{IF-1} = U_{IF-1} A_{1void} (T_{IF} - T_1)$$

$$\dot{Q}_{IF-1L} = U_{IF-1L} A_{1L} (T_{IF} - T_1)$$

$$\dot{Q}_{2-1} = U_{2-1} A_{1void} (T_2 - T_1)$$

$$\dot{Q}_{2-1L} = U_{2-1L} A_{1L} (T_2 - T_1)$$

$$\dot{H}_{WEGin} = \dot{m}_{WEG} c p_{WEG} T_{WEGin}$$

$$\dot{H}_{WEGout} = \dot{m}_{WEG} c p_{WEG} T_{WEGout}$$

### Equation 18: Heat flows

$$\dot{Q}_{res1} = (iA)^2 \frac{\rho_{res1} t_1}{A_{1L}}$$

### Equation 19: Heat generation

$$\dot{m}_{WEGin} = \dot{m}_{WEGout}$$

### Equation 20: Molar flows

The overall heat transfer coefficient terms are shown in Equation 21.

$$U_{IF-1} = \frac{1}{t_{IF}/2k_{IF} + 1/h_1}$$

$$U_{IF-1-L} = \frac{1}{t_{IF}/2k_{IF} + t_1/2k_1}$$

$$U_{2-1} = \frac{1}{t_2/2k_2 + 1/h_1}$$

$$U_{2-1-L} = \frac{1}{t_2/2k_2 + t_1/2k_1}$$

### Equation 21: Set of overall heat transfer coefficients

Notes:

- 1) For cooling layers not next to the interface plate (I/F), the “I/F” is replaced with “10” to represent the 10<sup>th</sup> layer of the previous cell, as seen in the repeating unit of Figure 37.

- 2) For the convection term,  $1/h_1, A_{1\text{void}}$  is used as the area; however, it is assumed that  $h_1 A_{1\text{void}}$  is represented by a combined parameter found in the literature (Amphlett et al., 1996) for the heat transfer from the stack to the coolant.

LAYER 2: PLATE - On either side of the plate exist channels for the coolant and anode gases. The plate is solid and non-permeable and serves to completely separate the two flows.

SKETCH:

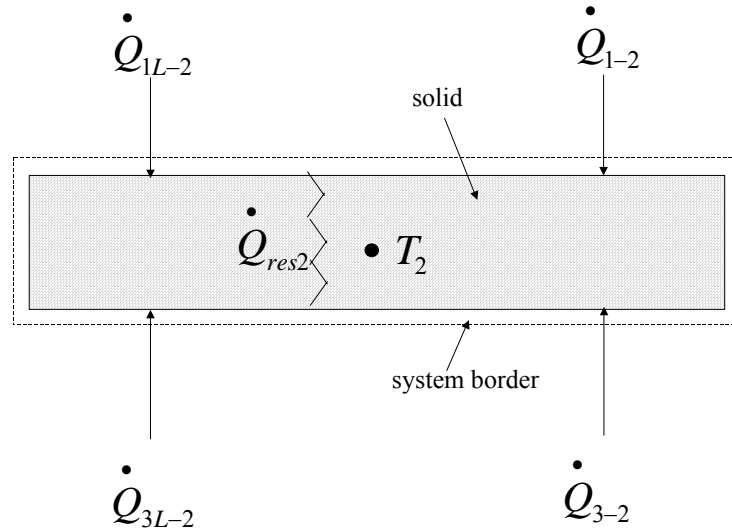


**Figure 44: Plate energy balance**

EQUATIONS:

$$(\rho_2(A_{net2})Cp_2) \frac{dT_2}{dt} = \dot{Q}_{1-2} + \dot{Q}_{1L-2} + \dot{Q}_{3-2} + \dot{Q}_{3L-2} + \dot{Q}_{res2}$$

**Equation 22: Energy Balance**

The  $\dot{Q}$  expressions in Equation 22 are shown below.

$$\dot{Q}_{1-2} = U_{1-2} A_{1\text{void}} (T_1 - T_2)$$

$$\dot{Q}_{1L-2} = U_{1L-2} A_{1L} (T_1 - T_2)$$

$$\dot{Q}_{3-2} = U_{3-2} A_{3\text{void}} (T_3 - T_2)$$

$$\dot{Q}_{3L-2} = U_{3L-2} A_{3L} (T_3 - T_2)$$

**Equation 23: Set of heat flows**

$$\dot{Q}_{res2} = (iA)^2 \frac{\rho_{res2} t_2}{A_{net}}$$

**Equation 24: Heat generation**

The overall heat transfer coefficient terms are shown in Equation 25.

$$U_{1-2} = \frac{1}{t_2/2k_2 + 1/h_1}$$

$$U_{1L-2} = \frac{1}{t_2/2k_2 + t_1/2k_1}$$

$$U_{3-2} = \frac{1}{t_2/2k_2 + 1/h_3}$$

$$U_{3L-2} = \frac{1}{t_2/2k_2 + t_3/2k_3}$$

**Equation 25: Set of overall heat transfer coefficients**

Notes:

- 1) For the convection term,  $1/h_1$ ,  $A_{1void}$  is used as the area; however, it is assumed that  $h_1 A_{1void}$  is represented by a combined parameter found in the literature (Amphlett et al., 1996) for the heat transfer from the stack to the coolant.
- 2) For the convection term,  $1/h_3$ ,  $A_{3void}$  is used as the area; however, it is assumed that  $h_3 A_{3void}$  is represented by a combined parameter found in the literature (Amphlett et al., 1996) for the heat transfer from the stack to the anode stream.

LAYER 3: ANODE GASES FLOWFIELD – The flowfield serves to carry the anode gases from the entrance point into the fuel cell to the gas exit.

SKETCH:

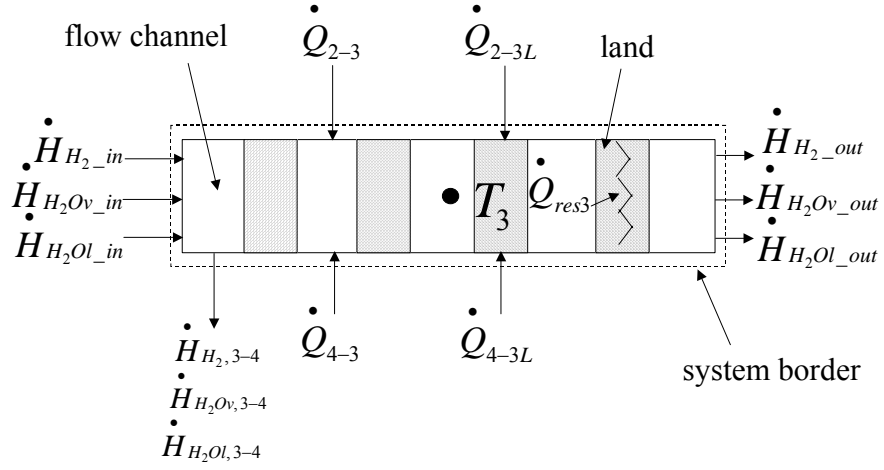


**Figure 42: Anode channel energy balance**

EQUATIONS:

$$(cp_{avg}(n_{gases} + n_{liq}) + \rho_3(A_{3L}t_3)Cp_3) \frac{dT_3}{dt} = \dot{Q}_{2-3} + \dot{Q}_{2-3L} + \dot{Q}_{4-3} + \dot{Q}_{4-3L} + \dot{Q}_{res3} +$$

$$\dot{H}_{H_2 in} + \dot{H}_{H_2Ov in} + \dot{H}_{H_2Ol in} - \dot{H}_{H_2 out} - \dot{H}_{H_2Ov out} - \dot{H}_{H_2Ol out} -$$

$$\dot{H}_{H_2,3-4} - \dot{H}_{H_2Ov,3-4} - \dot{H}_{H_2Ol,3-4}$$

**Equation 17: Energy Balance**

The  $\dot{Q}$  and  $\dot{H}$  expressions in Equation 17 are shown below.

$$\dot{Q}_{2-3} = U_{2-3} A_{3void} (T_2 - T_3)$$

$$\dot{Q}_{2-3L} = U_{2-3L} A_{3L} (T_2 - T_3)$$

$$\dot{Q}_{4-3} = U_{4-3} A_{3void} (T_4 - T_3)$$

$$\dot{Q}_{4-3L} = U_{4-3L} A_{3L} (T_4 - T_3)$$

$$\dot{H}_{H_2 in} = \dot{n}_{H_2 in} h_{H_2}(T_{3 in})$$

$$\dot{H}_{H_2Ov\ in} = \dot{n}_{H_2Ov\ in} h_{H_2Ov}(T_{3\ in})$$

$$\dot{H}_{H_2Ol\ in} = \dot{n}_{H_2Ol\ in} h_{H_2Ol}(T_{3\ in})$$

$$\dot{H}_{H_2\ out} = \dot{n}_{H_2\ out} h_{H_2}(T_{3\ out})$$

$$\dot{H}_{H_2Ov\ out} = \dot{n}_{H_2Ov\ out} h_{H_2Ov}(T_{3\ out})$$

$$\dot{H}_{H_2Ol\ out} = \dot{n}_{H_2Ol\ out} h_{H_2Ol}(T_{3\ out})$$

$$\dot{H}_{H_2\ 3-4} = \dot{n}_{H_2} h_{H_2}(T_3)$$

$$\dot{H}_{H_2Ov\ 3-4} = \dot{n}_{H_2Ov\ 3-4} h_{H_2Ov}(T_3)$$

$$\dot{H}_{H_2Ol\ 3-4} = \dot{n}_{H_2Ol\ 3-4} h_{H_2Ol}(T_3)$$

**Equation 18: Set of heat flows**

$$\dot{Q}_{res3} = (iA)^2 \frac{\rho_{res3} t_3}{A_{3L}}$$

**Equation 19: Heat generation**

$$\dot{n}_{H_2\ in} - \dot{n}_{H_2\ out} = \dot{n}_{H_2\ 3-4} = \dot{n}_{H_2} = \frac{iA}{2F}$$

$$\dot{n}_{H_2\ in} = SR_{H_2} \dot{n}_{H_2}$$

$$\dot{n}_{H_2O} = \dot{n}_{H_2Ov} + \dot{n}_{H_2Ol}$$

$$\dot{n}_{H_2O\ in} - \dot{n}_{H_2O\ out} = \dot{n}_{H_2O\ 3-4}$$

**Equation 20: Set of molar flows**

The overall heat transfer coefficient terms are shown in Equation 21.

$$U_{2-3} = \frac{1}{t_2/2k_2 + 1/h_3}$$

$$U_{2-3L} = \frac{1}{t_2/2k_2 + t_3/2k_3}$$

$$U_{4-3} = \frac{1}{t_4/2k_4 + 1/h_3}$$

$$U_{4-3L} = \frac{1}{t_4/2k_4 + t_3/2k_3}$$

**Equation 21: Set of overall heat transfer coefficients**

Note: For the convection term,  $1/h_3$ ,  $A_{3\text{void}}$  is used as the area; however, it is assumed that  $h_3 A_{3\text{void}}$  is represented by a combined parameter found in the literature (Amphlett et al., 1996) for the heat transfer from the stack to the anode stream.

The calculation for the vapor and liquid water molar flowrates is as follows:

*anode channel inlet (in) :*

$$P_{H_2Ov, in} = \phi_{in} P_{sat}(T_{in})$$

$$X_{H_2Ov, in} = \frac{P_{H_2Ov, in}}{P_{tot}}$$

$$X_{H_2O, in} = \frac{P_{sat}(T_{in})}{P_{tot}}$$

$$X_{H_2} = 1 - X_{H_2O, in}$$

$$\dot{n}_{tot, in} = \frac{SR \dot{n}_{H_2}}{X_{H_2}} = \frac{\dot{n}_{H_2, in}}{X_{H_2}}$$

$$\dot{n}_{H_2Ov, in} = X_{H_2Ov, in} \dot{n}_{tot, in} = \dot{n}_{H_2O, in}$$

$$\dot{n}_{H_2Ol, in} = 0$$

*anode channel middle (mid) :*

$$\dot{n}_{H_2O, mid} = \dot{n}_{H_2O, in} - \dot{n}_{H_2O, migration, mid}$$

$$\dot{n}_{tot, mid} = \dot{n}_{tot, in} - \dot{n}_{H_2, rxn} - \dot{n}_{H_2O, migration, mid}$$

$$X_{v, sat} = \frac{P_{sat}(T_{mid})}{P_{tot}}$$

$$X_{H_2O, mid} = \frac{\dot{n}_{H_2O, mid}}{\dot{n}_{tot, mid}}$$

$$\text{if } X_{H_2O, mid} \geq X_{v, sat}$$

$$X_{H_2O, v, mid} = X_{v, sat}$$

$$X_{H_2O, l, mid} = X_{H_2O, mid} - X_{v, sat}$$

$$\text{if } X_{H_2O, mid} \leq X_{v, sat}$$

$$X_{H_2O, v, mid} = X_{H_2O, mid}$$

$$X_{H_2O, l, mid} = 0$$

$$\dot{n}_{H_2O, v, migration, mid} = X_{H_2O, v, mid} \dot{n}_{H_2O, migration, mid}$$

$$\dot{n}_{H_2O, l, migration, mid} = X_{H_2O, l, mid} \dot{n}_{H_2O, migration, mid}$$

*anode channel outlet (out)*

$$\dot{n}_{H_2O, mid} = \dot{n}_{H_2O, out}$$

$$\dot{n}_{tot, mid} = \dot{n}_{tot, out}$$

$$\dot{n}_{H_2O, v, out} = X_{H_2O, v, out} \dot{n}_{tot, out}$$

$$\dot{n}_{H_2O, l, out} = \dot{n}_{H_2O, out} - \dot{n}_{H_2O, v, out}$$

Note: net migration water (or water drag) is assumed to be 0 in the model, i.e., electro-osmotic water drag through the membrane from anode to cathode is assumed to be equal to the back diffusion of product water from cathode to anode (refer to Sena et al., 1999).

The calculation of the thermal mass of the gas/liquid mixture is as follows:

$$\text{thermal mass} = cp_{avg} (n_{gases} + n_{liq})$$

$$n_{gases} = \frac{PV_{gases}}{RT_3}$$



$$n_{liq} = \frac{V_{liq} \rho_{liq}}{MW_{H_2O}}$$

$$V_{liq} = V_{3void} - V_{gases}$$

$$V_{3void} = A_{3void} t_3$$

$$V_{gases} = \varepsilon V_{3void}$$

$$\text{where } \varepsilon = \left( \frac{\rho_{gases}}{\rho_{liq}} \frac{1-Y}{Y} + 1 \right)^{-1} \quad (\text{Baehr and Stephan, 1998})$$

LAYER 4: ANODE GAS DIFFUSION LAYER (GDL) – The porosity of the GDL ensures effective diffusion of the reactant gases to the anode catalyst. The GDL also allows permeation of water vapor to the membrane to keep it humidified.

SKETCH:

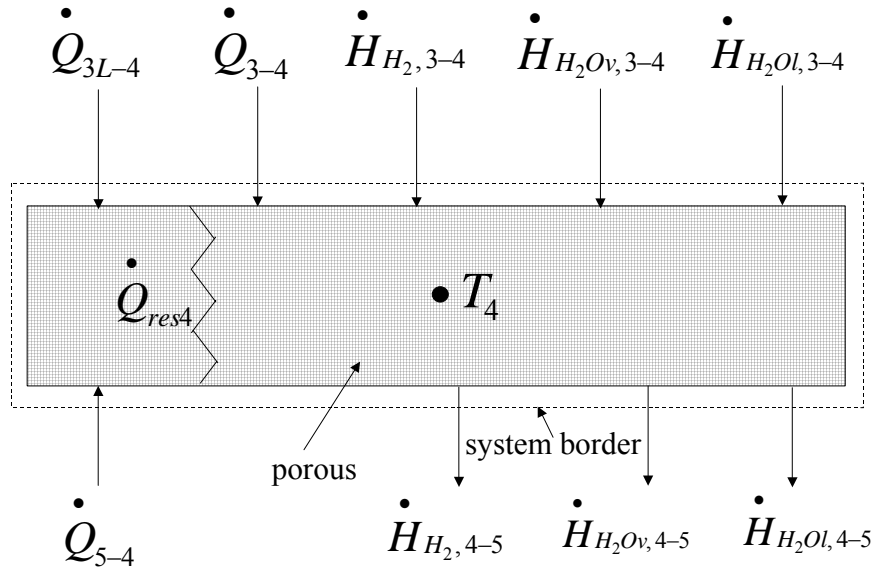


**Figure 43: Anode gas diffusion layer energy balance**

EQUATIONS:

$$(c_{p_{avg}} (n_{gases} + n_{liq}) + \rho_4 (A_{net} t_4) C_{p4}) \frac{dT_4}{dt} = \dot{Q}_{3-4} + \dot{Q}_{3L-4} + \dot{Q}_{5-4} + \dot{Q}_{res4} +$$

$$\dot{H}_{H_2,3-4} + \dot{H}_{H_2Ov,3-4} + \dot{H}_{H_2Ol,3-4} - \dot{H}_{H_2,4-5} - \dot{H}_{H_2Ov,4-5} - \dot{H}_{H_2Ol,4-5}$$

**Equation 22: Energy Balance**

(In Equation 22 the density,  $\rho_4$ , takes porosity into account so  $A_{net}$  is used.)

The  $\dot{Q}$  and  $\dot{H}$  expressions in Equation 22 are shown below.

$$\dot{Q}_{3-4} = U_{3-4} A_{3void} (T_3 - T_4)$$

$$\dot{Q}_{3L-4} = U_{3L-4} A_{3L} (T_3 - T_4)$$

$$\dot{Q}_{5-4} = U_{5-4} A_{net5L} (T_5 - T_4)$$

$$\dot{H}_{H_2,3-4} = \dot{n}_{H_2} h_{H_2} (T_3)$$

$$\dot{H}_{H_2Ov,3-4} = \dot{n}_{H_2Ov,3-4} h_{H_2Ov} (T_3)$$

$$\dot{H}_{H_2Ol,3-4} = \dot{n}_{H_2Ol,3-4} h_{H_2Ol} (T_3)$$

$$\dot{H}_{H_2,4-5} = \dot{n}_{H_2} h_{H_2} (T_4)$$

$$\dot{H}_{H_2Ov,4-5} = \dot{n}_{H_2Ov,4-5} h_{H_2Ov} (T_4)$$

$$\dot{H}_{H_2Ol,4-5} = \dot{n}_{H_2Ol,4-5} h_{H_2Ol} (T_4)$$

### Equation 23: Set of heat flows

(Note:  $A_{net5L}$  represents the area of the solid portion of the porous catalyst. Convective heat transfer is neglected for the void portion of the porous catalyst.)

$$\dot{Q}_{res4} = (iA)^2 \frac{\rho_{res4} t_4}{A_{net}} (\rho_{res4} \text{ accounts for porosity so } A_{net} \text{ is used})$$

### Equation 24: Heat generation

$$\dot{n}_{H_2,3-4} = \dot{n}_{H_2,4-5}$$

$$\dot{n}_{H_2O,3-4} = \dot{n}_{H_2O,4-5}$$

### Equation 25: Set of molar flows

The overall heat transfer coefficient terms are shown in Equation 26.

$$U_{3-4} = \frac{1}{t_4/2k_4 + 1/h_3}$$

$$U_{3L-4} = \frac{1}{t_4/2k_4 + t_3/2k_3}$$

$$U_{5-4} = \frac{1}{t_5/2k_5 + t_4/2k_4}$$

**Equation 26: Set of overall heat transfer coefficients**

Note: For the convection term,  $1/h_3$ ,  $A_{3\text{void}}$  is used as the area; however, it is assumed that  $h_3A_{3\text{void}}$  is represented by a combined parameter found in the literature (Amphlett et al., 1996) for the heat transfer from the stack to the anode stream.

The calculation for the vapor and liquid water migration molar flowrates is the same as shown in Layer 3 for the middle section.

The calculation of the thermal mass of the gas/liquid mixture is as follows:

$$\text{thermal mass} = cp_{\text{avg}} (n_{\text{gases}} + n_{\text{liq}})$$

$$n_{\text{gases}} = \frac{PV_{\text{gases}}}{RT_4}$$

$$n_{\text{liq}} = \frac{V_{\text{liq}}\rho_{\text{liq}}}{MW_{\text{H}_2\text{O}}}$$

$$V_{\text{liq}} = V_{4\text{void}} - V_{\text{gases}}$$

$$V_{4\text{void}} = A_{\text{net}4\text{void}}t_4$$

$$V_{\text{gases}} = \varepsilon V_{4\text{void}}$$

LAYER 5: ANODE CATALYST SUPPORT – The anode catalyst support is a platinum-loaded carbon layer on which the  $\text{H}_2$  molecule is dissociated. Two hydrogen (H) atoms bond to two platinum (Pt) atoms that allow each H atom to release an electron to form a  $\text{H}^+$  ion. The ions pass through the membrane while the electrons pass through the outer circuit from the anode to the cathode.

SKETCH:

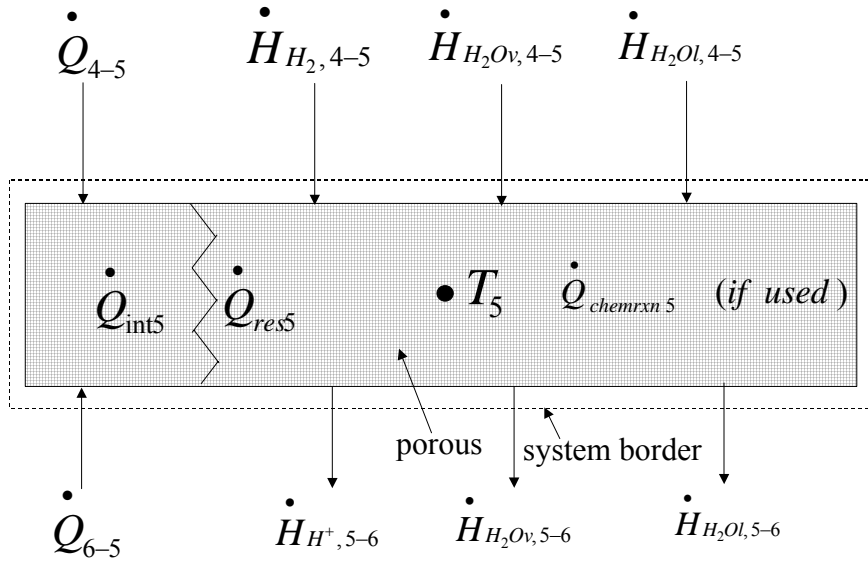


**Figure 44: Anode catalyst energy balance**

EQUATIONS:

$$(cp_{avg}(n_{gases} + n_{liq}) + \rho_5(A_{net5L}t_5)Cp_5) \frac{dT_5}{dt} = \dot{Q}_{4-5} + \dot{Q}_{6-5} + \dot{Q}_{int5} + \dot{Q}_{res5} + \dot{H}_{H_2,4-5} + \dot{H}_{H_2Ov,4-5} + \dot{H}_{H_2Ol,4-5} - \dot{H}_{H^+,5-6} - \dot{H}_{H_2Ov,5-6} - \dot{H}_{H_2Ol,5-6}$$

**Equation 27: Energy Balance**

The  $\dot{Q}$  and  $\dot{H}$  expressions in Equation 27 are shown below.

$$\dot{Q}_{4-5} = U_{4-5} A_{net5L} (T_4 - T_5)$$

$$\dot{Q}_{6-5} = U_{6-5} A_{net5L} (T_6 - T_5)$$

$$\dot{H}_{H_2,4-5} = \dot{n}_{H_2} h_{H_2}(T_4)$$

$$\dot{H}_{H_2Ov,4-5} = \dot{n}_{H_2Ov,4-5} h_{H_2Ov}(T_4)$$

$$\dot{H}_{H_2Ol,4-5} = \dot{n}_{H_2Ol,4-5} h_{H_2Ol}(T_4)$$

$$\dot{H}_{H^+5-6} = \dot{n}_{H_2} h_{H_2}(T_5)$$

$$\dot{H}_{H_2Ov5-6} = \dot{n}_{H_2Ov5-6} h_{H_2Ov}(T_5)$$

$$\dot{H}_{H_2O|5-6} = \dot{n}_{H_2O|5-6} h_{H_2O}(T_5)$$

**Equation 28: Set of heat flows**

(Note:  $A_{net5L}$  represents the area of the solid portion of the porous catalyst. Convective heat transfer is neglected for the void portion of the porous catalyst.)

$$\dot{Q}_{res5} = (iA)^2 \frac{\rho_{res5} t_5}{A_{net5L}}$$

$$\dot{Q}_{chemrxn5} = \text{arbitrary} \text{ (based on information presented in Section 3.3)}$$

$$\dot{Q}_{int5} = iA \left( \frac{T\Delta S}{2F} + \eta_5 + (iA)R_{elec} + \frac{\Delta H_{H_2O}}{iA} \right), \text{ for layer 5: anode catalyst}$$

where

1st term = entropy loss, Anode  $\Delta S = -130.7 \text{ J/molK}$ , (Wöhr et al, 1998)

2nd term = activation overpotential (assumed 0)

3rd term = electrical resist. loss (of layer 5, included separately as  $\dot{Q}_{res5}$ )

4th term = heat of vaporization (already accounted for in the enthalpy equations)

**Equation 29: Heat generation**

$H_2$  properties are assumed for  $H^+$

$$\dot{n}_{H_2O4-5} = \dot{n}_{H_2O5-6}$$

**Equation 30: Molar flow**

The overall heat transfer coefficient terms are shown in Equation 31.

$$U_{4-5} = \frac{1}{t_4/2k_4 + t_5/2k_5}$$

$$U_{6-5} = \frac{1}{t_6/2k_6 + t_5/2k_5}$$

**Equation 31: Set of overall heat transfer coefficients**

The calculation for the vapor and liquid water migration molar flowrates is the same as shown in Layer 3 for the middle section.

The calculation of the thermal mass of the gas/liquid mixture is as follows:

$$\text{thermal mass} = cp_{avg} (n_{gases} + n_{liq})$$

$$n_{gases} = \frac{PV_{gases}}{RT_5}$$

$$n_{liq} = \frac{V_{liq}\rho_{liq}}{MW_{H_2O}}$$

$$V_{liq} = V_{5void} - V_{gases}$$

$$V_{5void} = A_{net5void}t_5$$

$$V_{gases} = \varepsilon V_{5void}$$

LAYER 6: MEMBRANE – The polymer electrolyte membrane (after which the PEM fuel cell stack is named) is the medium by which the  $H^+$  ions travel from anode to cathode.

SKETCH:

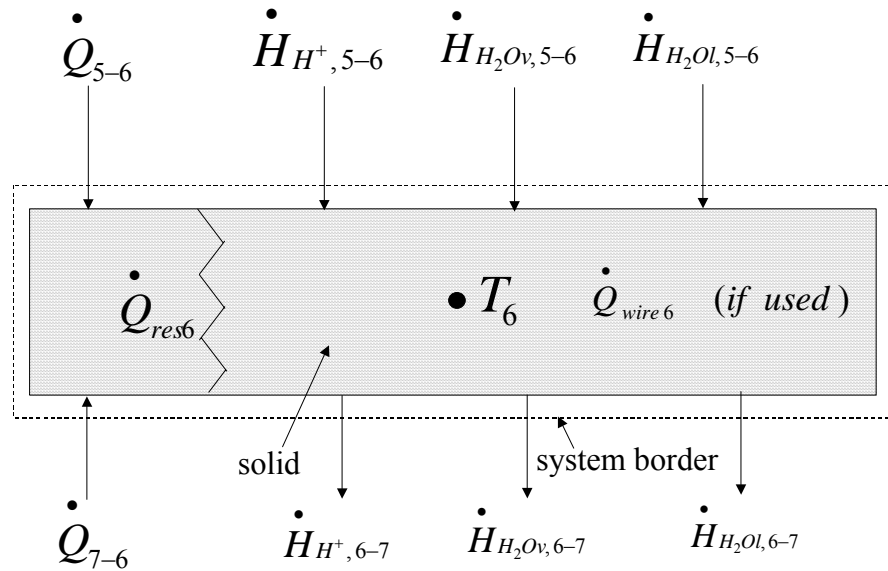


**Figure 45: Membrane energy balance**

EQUATIONS:

$$(cp_{avg}(n_{gases} + n_{liq}) + \rho_6(A_{net}t_6)Cp_6) \frac{dT_6}{dt} = \dot{Q}_{5-6} + \dot{Q}_{7-6} + \dot{Q}_{res6} + \dot{H}_{H^+,5-6} + \dot{H}_{H_2Ov,5-6} + \dot{H}_{H_2Ol,5-6} - \dot{H}_{H^+,6-7} - \dot{H}_{H_2Ov,6-7} - \dot{H}_{H_2Ol,6-7}$$

**Equation 32: Energy Balance**

The  $\dot{Q}$  and  $\dot{H}$  expressions in Equation 32 are shown below.

$$\dot{Q}_{5-6} = U_{5-6} A_{net5L} (T_5 - T_6)$$

$$\dot{Q}_{7-6} = U_{7-6} A_{net7L} (T_7 - T_6)$$

$$\dot{H}_{H^+, 5-6} = \dot{n}_{H_2} h_{H_2} (T_5)$$

$$\dot{H}_{H_2Ov, 5-6} = \dot{n}_{H_2Ov, 5-6} h_{H_2Ov} (T_5)$$

$$\dot{H}_{H_2Ol, 5-6} = \dot{n}_{H_2Ol, 5-6} h_{H_2Ol} (T_5)$$

$$\dot{H}_{H^+ 6-7} = \dot{n}_{H_2} h_{H_2} (T_6)$$

$$\dot{H}_{H_2Ov 6-7} = \dot{n}_{H_2Ov 6-7} h_{H_2Ov} (T_6)$$

$$\dot{H}_{H_2Ol 6-7} = \dot{n}_{H_2Ol 6-7} h_{H_2Ol} (T_6)$$

### Equation 33: Set of heat flows

(Note:  $A_{net5L}$  and  $A_{net7L}$  represent the area of the solid portion of the porous catalyst. Convective heat transfer is neglected for the void portion of the porous catalyst.)

$$\dot{Q}_{res6} = (iA)^2 \frac{\rho_{res6} t_6}{A_{net}} \text{ (protonic resistance)}$$

$$\dot{Q}_{wire6} = \text{arbitrary}$$

### Equation 34: Heat generation

$H_2$  properties are assumed for  $H^+$

$$\dot{n}_{H_2O 5-6} = \dot{n}_{H_2O 6-7}$$

### Equation 35: Molar flow

The overall heat transfer coefficient terms are shown in **Error! Reference source not found.**

$$U_{5-6} = \frac{1}{t_6/2k_6 + t_5/2k_5}$$

$$U_{7-6} = \frac{1}{t_6/2k_6 + t_7/2k_7}$$

### Equation 36: Set of overall heat transfer coefficients

Note: The calculation for the vapor and liquid water migration molar flowrates is the same as shown in Layer 3 for the middle section. It is assumed that there is no liquid or vapor within the membrane so no gas/liquid mixture thermal mass calculation is performed.

LAYER 7: CATHODE CATALYST SUPPORT – The cathode catalyst support is a platinum-loaded carbon layer on which the oxygen combines with the  $H^+$  ions and electrons to form water and heat.

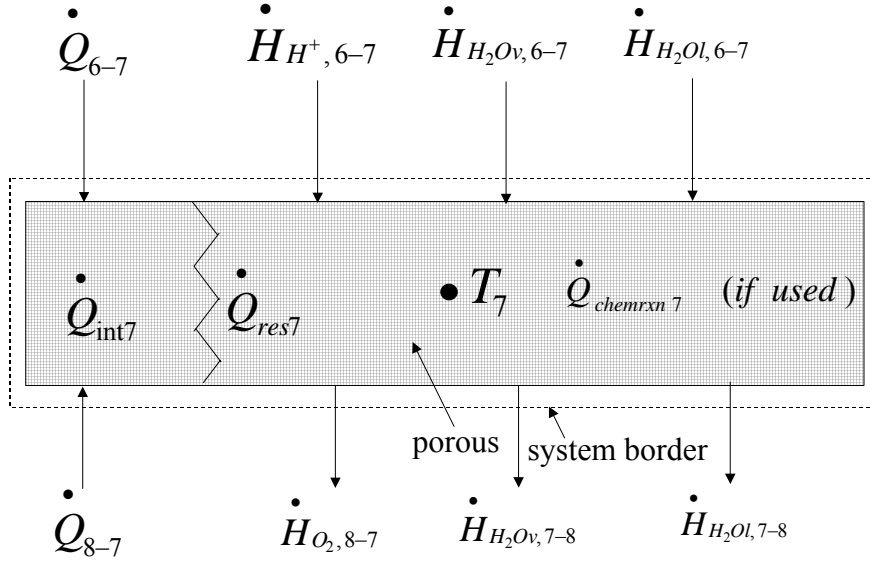


**Figure 46: Cathode catalyst energy balance**

EQUATIONS:

$$(cp_{avg} (n_{gases} + n_{liq}) + \rho_7 (A_{net7L} t_7) Cp_7) \frac{dT_7}{dt} = \dot{Q}_{6-7} + \dot{Q}_{8-7} + \dot{Q}_{res7} + \dot{Q}_{int7}$$

$$\dot{H}_{H^+, 6-7} + \dot{H}_{H_2Ov, 6-7} + \dot{H}_{H_2Ol, 6-7} + \dot{H}_{O_2, 8-7} - \dot{H}_{H_2Ov, 7-8} - \dot{H}_{H_2Ol, 7-8}$$

**Equation 37: Energy Balance**

The  $\dot{Q}$  and  $\dot{H}$  expressions in Equation 37 are shown below.

$$\dot{Q}_{6-7} = U_{6-7} A_{net7L} (T_6 - T_7)$$

$$\dot{Q}_{8-7} = U_{8-7} A_{net7L} (T_8 - T_7)$$

$$\dot{H}_{H^+, 6-7} = \dot{n}_{H_2} h_{H_2} (T_6)$$



$$\dot{H}_{H_2Ov,6-7} = \dot{n}_{H_2Ov,6-7} h_{H_2Ov}(T_6)$$

$$\dot{H}_{H_2Ol,6-7} = \dot{n}_{H_2Ol,6-7} h_{H_2Ol}(T_6)$$

$$\dot{H}_{O_2,8-7} = \dot{n}_{O_2} h_{O_2}(T_8)$$

$$\dot{H}_{H_2Ov,7-8} = \dot{n}_{H_2Ov,7-8} h_{H_2Ov}(T_7)$$

$$\dot{H}_{H_2Ol,7-8} = \dot{n}_{H_2Ol,7-8} h_{H_2Ol}(T_7)$$

### Equation 38: Set of heat flows

(Note:  $A_{net7L}$  represents the area of the solid portion of the porous catalyst. Convective heat transfer is neglected for the void portion of the porous catalyst.)

$$\dot{Q}_{res7} = (iA)^2 \frac{\rho_{res7} t_7}{A_{net7L}}$$

$$\dot{Q}_{chemrxn7} = \text{arbitrary (based on information presented in Section 3.3)}$$

$$\dot{Q}_{int7} = iA \left( \frac{T\Delta S}{4F} + \eta_7 + (iA)R_{elec} + \frac{\Delta H_{H_2O}}{iA} \right), \text{ for layer 7 : cathode catalyst}$$

where

1st term = entropy loss, Cathode  $\Delta S = -65.0 \text{ J/molK}$ , for liquid water in products, (Wöhr et al, 1998)

2nd term = activation overpotential

$$\eta_7 = V_{rev} - V_{cell} - IR_{membrane, protonic}$$

where  $V_{rev}$  is found in Amphlett et al. (1995a), for temperatures 25°C and above, assuming fixed  $i = 0.5 \text{ A/cm}^2$  :

$$V_{rev} = 1.229 - (0.85e - 3)(T_7 - 298.15) + (4.3085e - 5)(T_7)(\ln(p_{H_2}) + 0.5(\ln(p_{O_2})))$$

derived from the general Nernst equation :

$$V_{rev} = V^0 - \frac{\bar{R}T}{nF} \ln \left[ \sqrt{p_{O_2} p_{H_2}} \right] \text{ where } V^0 \text{ can vary with temperature :}$$

$$V^0 = V^0_{ref} + (T - T^0) \left( \frac{\Delta S^0}{nF} \right)$$

$$IR_{membrane, protonic} = \dot{Q}_{res6} / I$$

activation overpotential from Amphlett et al. (1995b) :

$$\eta_7 = -0.9514 + 0.00312T_7 - (0.000187)(T_7)(\ln(I)) + (7.4e - 5)(T_7)(\ln(c_{O_2}))$$

where the concentration of O<sub>2</sub> at the gas/liquid interface is derived from Henry's Law

$$c_{O_2} = \frac{P_{O_2}}{(5.08e + 6) \exp\left(\frac{-498}{T_7}\right)}$$

(constant in denominator : Perry et al. (1963) as seen in Amphlett et al. (1995a))

for temperatures below 25° C, from Datta et al. (2002):

with operation cell voltage, V<sub>cell</sub>, fixed at 0.67 V;

current density, with active area assumed to be 100 cm<sup>2</sup> (for stack considered in Datta et al.),

as fn(T) :

[-25 -16 -7 2 10 15 20] °C

[0.14 0.16 0.18 0.2 0.23 0.27 0.30] A/cm<sup>2</sup>

3rd term = electrical resist. of layer 7 (included separately as  $\dot{Q}_{res7}$ )

4th term = heat of vaporization (already accounted for in the enthalpy equations)

### Equation 39: Heat generation

H<sub>2</sub> properties are assumed for H<sup>+</sup>

$$\dot{n}_{O_2\ 8-7} = 0.5 \dot{n}_{H_2}$$

$$\dot{n}_{H_2O\ rxn} = \dot{n}_{H_2}$$

$$\dot{n}_{H_2O\ 7-8} = \dot{n}_{H_2O\ 6-7} + \dot{n}_{H_2O\ rxn}$$

### Equation 40: Set of molar flows

The overall heat transfer coefficient terms are shown in Equation 41.

$$U_{6-7} = \frac{1}{t_6/2k_6 + t_7/2k_7}$$

$$U_{8-7} = \frac{1}{t_8/2k_8 + t_7/2k_7}$$

### Equation 41: Set of overall heat transfer coefficients

The calculation for the vapor and liquid water migration molar flowrates is the same as shown in Layer 3 for the middle section.

The calculation of the thermal mass of the gas/liquid mixture is as follows:

$$\text{thermal mass} = cp_{avg} (n_{gases} + n_{liq})$$

$$n_{gases} = \frac{PV_{gases}}{RT_7}$$

$$n_{liq} = \frac{V_{liq}\rho_{liq}}{MW_{H_2O}}$$

$$V_{liq} = V_{7void} - V_{gases}$$

$$V_{7void} = A_{net7void}t_7$$

$$V_{gases} = \varepsilon V_{7void}$$

LAYER 8: CATHODE GAS DIFFUSION LAYER (GDL) – The porosity of the GDL ensures effective diffusion of the reactant gases to the cathode catalyst. The GDL also allows liquid water produced at the cathode to leave the fuel cell.

SKETCH:

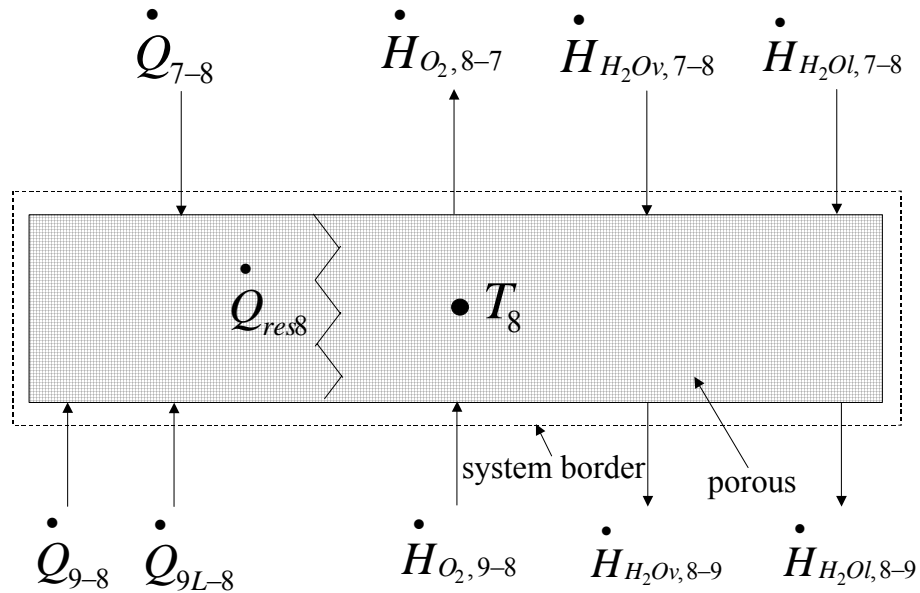


**Figure 47: Cathode gas diffusion layer energy balance**

EQUATIONS:

$$(cp_{avg}(n_{gases} + n_{liq}) + \rho_8(A_{net}t_8)Cp_8) \frac{dT_8}{dt} = \dot{Q}_{7-8} + \dot{Q}_{9-8} + \dot{Q}_{9L-8} + \dot{Q}_{res8} + \dot{H}_{H_2Ov, 7-8} + \dot{H}_{H_2Ol, 7-8} + \dot{H}_{O_2, 9-8} - \dot{H}_{H_2Ov, 8-9} - \dot{H}_{H_2Ol, 8-9} - \dot{H}_{O_2, 8-7}$$

#### Equation 42: Energy Balance

(In Equation 42 the density,  $\rho_8$ , takes porosity into account so  $A_{net}$  is used.)

The  $\dot{Q}$  and  $\dot{H}$  expressions in Equation 42 are shown below.

$$\dot{Q}_{7-8} = U_{7-8} A_{net7L} (T_7 - T_8)$$

$$\dot{Q}_{9-8} = U_{9-8} A_{9void} (T_9 - T_8)$$

$$\dot{Q}_{9L-8} = U_{9L-8} A_{9L} (T_9 - T_8)$$

$$\dot{H}_{H_2Ov, 7-8} = \dot{n}_{H_2Ov, 7-8} h_{H_2Ov} (T_7)$$

$$\dot{H}_{H_2Ol, 7-8} = \dot{n}_{H_2Ol, 7-8} h_{H_2Ol} (T_7)$$

$$\dot{H}_{O_2, 8-7} = \dot{n}_{O_2} h_{O_2} (T_8)$$

$$\dot{H}_{H_2Ov, 8-9} = \dot{n}_{H_2Ov, 8-9} h_{H_2Ov} (T_8)$$

$$\dot{H}_{H_2Ol, 8-9} = \dot{n}_{H_2Ol, 8-9} h_{H_2Ol} (T_8)$$

$$\dot{H}_{O_2, 9-8} = \dot{n}_{H_2} h_{H_2} (T_9)$$

#### Equation 43: Set of heat flows

(Note:  $A_{net7L}$  represents the area of the solid portion of the porous catalyst. Convective heat transfer is neglected for the void portion of the porous catalyst.)

$$\dot{Q}_{res8} = (iA)^2 \frac{\rho_{res8} t_8}{A_{net}} \quad (\text{the specific resist. } \rho_{res8} \text{ accounts for porosity so } A_{net} \text{ is used})$$

#### Equation 44: Heat generation

$$\dot{n}_{O_2, 9-8} = \dot{n}_{O_2, 8-7}$$

$$\dot{n}_{H_2O, 7-8} = \dot{n}_{H_2O, 8-9}$$

#### Equation 45: Set of molar flows

The overall heat transfer coefficient terms are shown in Equation 46.

$$U_{7-8} = \frac{1}{t_8/2k_8 + t_7/2k_7}$$

$$U_{9-8} = \frac{1}{t_8/2k_8 + 1/h_9}$$

$$U_{9L-8} = \frac{1}{t_8/2k_8 + t_9/2k_9}$$

**Equation 46: Set of overall heat transfer coefficients**

Note: For the convection term,  $1/h_9$ ,  $A_{9\text{void}}$  is used as the area; however, it is assumed that  $h_9A_{9\text{void}}$  is represented by a combined parameter found in the literature (Amphlett et al., 1996) for the heat transfer from the stack to the cathode stream.

The calculation for the vapor and liquid water migration molar flowrates is the same as shown in Layer 3 for the middle section.

The calculation of the thermal mass of the gas/liquid mixture is as follows:

$$\text{thermal mass} = cp_{\text{avg}} (n_{\text{gases}} + n_{\text{liq}})$$

$$n_{\text{gases}} = \frac{PV_{\text{gases}}}{RT_8}$$

$$n_{\text{liq}} = \frac{V_{\text{liq}}\rho_{\text{liq}}}{MW_{\text{H}_2\text{O}}}$$

$$V_{\text{liq}} = V_{8\text{void}} - V_{\text{gases}}$$

$$V_{8\text{void}} = A_{\text{net}8\text{void}}t_8$$

$$V_{\text{gases}} = \varepsilon V_{8\text{void}}$$

LAYER 9: CATHODE GASES FLOWFIELD - The flowfield serves to carry the cathode gases from the entrance point into the fuel cell to the gas exit.

SKETCH:

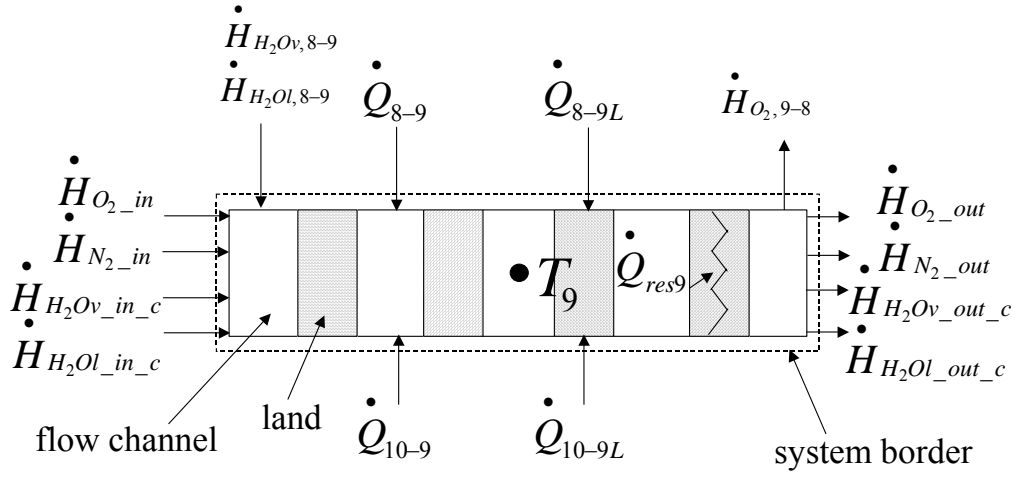


**Figure 48: Cathode channel energy balance**

EQUATIONS:

$$\left( \sum (n_i C p_i)_{gases_9} + \rho_9 (A_{9L} t_9) C p_9 \right) \frac{dT_9}{dt} = \dot{Q}_{8-9} + \dot{Q}_{8-9L} + \dot{Q}_{10-9} + \dot{Q}_{10-9L} + \dot{Q}_{res9} +$$

$$\dot{H}_{O_2, in} + \dot{H}_{N_2, in} + \dot{H}_{H_2Ov, in, c} + \dot{H}_{H_2Ol, in, c} - \dot{H}_{O_2, out} - \dot{H}_{N_2, out} - \dot{H}_{H_2Ov, out, c} - \dot{H}_{H_2Ol, out, c} -$$

$$\dot{H}_{O_2, 9-8} + \dot{H}_{H_2Ov, 8-9} + \dot{H}_{H_2Ol, 8-9}$$

**Equation 47: Energy Balance**

The  $\dot{Q}$  and  $\dot{H}$  expressions in Equation 47 are shown below.

$$\dot{Q}_{8-9} = U_{8-9} A_{9void} (T_8 - T_9)$$

$$\dot{Q}_{8-9L} = U_{8-9L} A_{9L} (T_8 - T_9)$$

$$\dot{Q}_{10-9} = U_{10-9} A_{9void} (T_{10} - T_9)$$

$$\dot{Q}_{10-9L} = U_{10-9L} A_{9L} (T_{10} - T_9)$$

$$\dot{H}_{O_2, in} = \dot{n}_{O_2, in} h_{O_2} (T_{9in})$$

$$\dot{H}_{N_2 in} = \dot{n}_{N_2 in} h_{N_2}(T_{9 in})$$

$$\dot{H}_{H_2Ov in, c} = \dot{n}_{H_2Ov in} h_{H_2Ov}(T_{9 in})$$

$$\dot{H}_{H_2Ol in, c} = \dot{n}_{H_2Ol in} h_{H_2Ol}(T_{9 in})$$

$$\dot{H}_{O_2 out} = \dot{n}_{O_2 out} h_{O_2}(T_{9 out})$$

$$\dot{H}_{N_2 out} = \dot{n}_{N_2 out} h_{N_2}(T_{9 out})$$

$$\dot{H}_{H_2Ov out, c} = \dot{n}_{H_2Ov out} h_{H_2Ov}(T_{9 out})$$

$$\dot{H}_{H_2Ol out, c} = \dot{n}_{H_2Ol out} h_{H_2Ol}(T_{9 out})$$

$$\dot{H}_{O_2 9-8} = \dot{n}_{O_2} h_{O_2}(T_9)$$

$$\dot{H}_{H_2Ov 8-9} = \dot{n}_{H_2Ov 8-9} h_{H_2Ov}(T_8)$$

$$\dot{H}_{H_2Ol 8-9} = \dot{n}_{H_2Ol 8-9} h_{H_2Ol}(T_8)$$

**Equation 48: Set of heat flows**

$$\dot{Q}_{res9} = (iA)^2 \frac{\rho_{res9} t_9}{A_{9L}}$$

**Equation 49: Heat generation**

$$\dot{n}_{O_2 in} - \dot{n}_{O_2 out} = \dot{n}_{O_2 9-8} = \dot{n}_{O_2} = 0.5 \dot{n}_{H_2}$$

$$\dot{n}_{O_2 in} = SR_{air} \dot{n}_{O_2}$$

$$\dot{n}_{H_2O} = \dot{n}_{H_2Ov} + \dot{n}_{H_2Ol}$$

**Equation 50: Set of molar flows**

The overall heat transfer coefficient terms are shown in Equation 51.

$$U_{8-9} = \frac{1}{t_8/2k_8 + 1/h_9}$$

$$U_{8-9L} = \frac{1}{t_8/2k_8 + t_9/2k_9}$$

$$U_{10-9} = \frac{1}{t_{10}/2k_{10} + 1/h_9}$$

$$U_{10-9L} = \frac{1}{t_{10}/2k_{10} + t_9/2k_9}$$

**Equation 51: Set of overall heat transfer coefficients**

Note: For the convection term,  $1/h_9$ ,  $A_{9void}$  is used as the area; however, it is assumed that  $h_9A_{9void}$  is represented by a combined parameter found in the literature (Amphlett et al., 1996) for the heat transfer from the stack to the cathode stream.

The calculation for the vapor and liquid water molar flowrates is similar to what is shown in Layer 3.

The calculation of the thermal mass of the gas/liquid mixture is as follows:

$$thermal\ mass = cp_{avg} (n_{gases} + n_{liq})$$

$$n_{gases} = \frac{PV_{gases}}{RT_9}$$

$$n_{liq} = \frac{V_{liq}\rho_{liq}}{MW_{H_2O}}$$

$$V_{liq} = V_{9void} - V_{gases}$$

$$V_{9void} = A_{9void}t_9$$

$$V_{gases} = \varepsilon V_{9void}$$

LAYER 10: PLATE - On either side of the plate exist channels for the coolant and cathode gases. The plate is solid and non-permeable and serves to completely separate the two flows.

SKETCH:



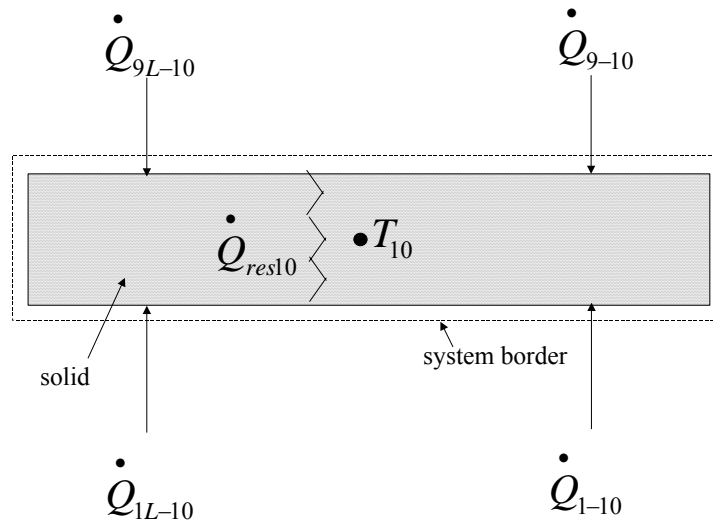


**Figure 49: Plate energy balance**

EQUATIONS:

$$(\rho_{10}V_{10}Cp_{10})\frac{dT_{10}}{dt} = \dot{Q}_{9-10} + \dot{Q}_{9L-10} + \dot{Q}_{1-10} + \dot{Q}_{1L-10} + \dot{Q}_{res10}$$

**Equation 52: Energy Balance**

The  $\dot{Q}$  expressions in Equation 52 are shown below.

$$\dot{Q}_{9-10} = U_{9-10}A_{9void}(T_9 - T_{10})$$

$$\dot{Q}_{9L-10} = U_{9L-10}A_{9L}(T_9 - T_{10})$$

$$\dot{Q}_{1-10} = U_{1-10}A_{1void}(T_1 - T_{10})$$

$$\dot{Q}_{1L-10} = U_{1L-10}A_{1L}(T_1 - T_{10})$$

**Equation 53: Set of heat flows**

$$\dot{Q}_{res10} = (iA)^2 \frac{\rho_{res10}l_{10}}{A_{net}}$$

**Equation 54: Heat generation**

The overall heat transfer coefficient terms are shown in Equation 55.

$$U_{9-10} = \frac{1}{t_{10}/2k_{10} + 1/h_9}$$

$$U_{9L-10} = \frac{1}{t_{10}/2k_{10} + t_9/2k_9}$$

$$U_{1-10} = \frac{1}{t_{10}/2k_{10} + 1/h_1}$$

$$U_{1L-10} = \frac{1}{t_{10}/2k_{10} + t_1/2k_1}$$

**Equation 55: Set of overall heat transfer coefficients**

Notes:

- 1) For the convection term,  $1/h_1$ ,  $A_{1\text{void}}$  is used as the area; however, it is assumed that  $h_1 A_{1\text{void}}$  is represented by a combined parameter found in the literature (Amphlett et al., 1996) for the heat transfer from the stack to the coolant.
- 2) For the convection term,  $1/h_9$ ,  $A_{9\text{void}}$  is used as the area; however, it is assumed that  $h_9 A_{9\text{void}}$  is represented by a combined parameter found in the literature (Amphlett et al., 1996) for the heat transfer from the stack to the cathode stream.

## 7.4 Parameters

### Cell/Endplates

<b>PEM fuel cell stack</b>		
<b>Cell/endplate layers</b>	<b>Value</b>	<b>Source, notes</b>
<b>active area (m<sup>2</sup>)<sup>1</sup></b>	0.03	Sridar et al., 2001
<b>net area (m<sup>2</sup>) approx<sup>1</sup></b>	0.0367	
<b>end plate x 2<sup>2</sup></b>		
Material	Polymer	Argyropoulos et al., 1999
Thickness (m)	0.025	Argyropoulos et al., 1999
k (W/m K)	0.32	Argyropoulos et al., 1999
density (kg/m <sup>3</sup> )	1740	Loctite, 1999
cp (J/kg K)	1464	Tak2000, 2003
specific res (ohm-m)	Insulator	
hA to air (W/K)	17	Amphlett et al., 1996 (represents convective loss from stack)
<b>Bus plate x 2<sup>2</sup></b>		
Material	Copper	Argyropoulos et al., 1999
thickness (m)	0.002	Argyropoulos et al., 1999
k (W/m K)	401	Incropera & DeWitt, 1990
density (kg/m <sup>3</sup> )	8933	Incropera & DeWitt, 1990
cp (J/kg K)	385	Incropera & DeWitt, 1990
specific res (ohm-m)	1.68E-08	Allmeasures.com, 2001
<b>I/F plate x 2<sup>2</sup></b>		
Material	Graphite	Argyropoulos et al., 1999
thickness (m)	0.025	Argyropoulos et al., 1999
k (W/m K)	52	Argyropoulos et al., 1999
density (kg/m <sup>3</sup> )	1400	Incropera & DeWitt, 1990
cp (J/kg K)	935	Incropera & DeWitt, 1990
specific res (ohm-m)	1.67E-04	Berning et al., 2002
<b>Coolant channel x 226<sup>3</sup></b>		
Material	Graphite	Amphlett et al., 1996
thickness (m)	0.002	Maggio et al., 1996
k (W/m K)	30	Maggio et al., 1996
density (kg/m <sup>3</sup> )	1400	Incropera & DeWitt, 1990
cp (J/kg K)	935	Incropera & DeWitt, 1990
specific res (ohm-m)	1.67E-04	Berning et al., 2002

contact area (%)	55%	Mosig, 1998
<b>coolant x 226<sup>3</sup></b>		
Material	50%/50% water/ethylene glycol	The Engineering Toolbox
hA to coolant (W/K)	50	Amphlett et al., 1996
flowrate (kg/s)	0.34 (5 gpm) / 6 (87.5 gpm)	Minimum/maximum pump flowrate available, Gurski, 2000 3 kg/s selected for model and divided among 226 <sup>3</sup> cells
<b>web x 225</b>		
Material	Graphite	Argyropoulos et al., 1999
thickness (m)	0.001	Argyropoulos et al., 1999
k (W/m K)	52	Argyropoulos et al., 1999
density (kg/m <sup>3</sup> )	1400	Incropera & DeWitt, 1990
cp (J/kg K)	935	Incropera & DeWitt, 1990
specific res (ohm-m)	1.67E-04	Berning et al., 2002
<b>anode gas channel x 225</b>		
Material	Graphite	Argyropoulos et al., 1999
thickness (m)	0.001	Mosig, 1998
k (W/m K)	52	Argyropoulos et al., 1999
density (kg/m <sup>3</sup> )	1400	Incropera & DeWitt, 1990
cp (J/kg K)	935	Incropera & DeWitt, 1990
specific res (ohm-m)	1.67E-04	Berning et al., 2002
contact area (%)	55%	Mosig, 1998
<b>anode gas x 225</b>		
Material	H <sub>2</sub> , H <sub>2</sub> O <sup>4</sup>	
hA to anode stream (W/K)	2	Amphlett et al., 1996
density (kg/m <sup>3</sup> )	fn(T)	National Institute of Standards and Technology (NIST), 2003
cp (J/kg K)	fn(T)	NIST, 2003
h (J/mol)	fn(T)	NIST, 2003
H <sub>2</sub> stoich ratio	1.5	Rowe and Li, 2001
pressure (bar)	1	Wöhr, 1998
<b>GDL x 225</b>		
Material	As described in source	Wöhr, 1998

thickness (m)	0.0004	Wöhr, 1998
k (W/m K)	65	Wöhr, 1998
density (kg/m <sup>3</sup> )	2000	Wöhr, 1998
cp (J/kg K)	840	Wöhr, 1998
specific res (ohm-m)	0.000014	Kauranen, 1996 (as cited in Argyropoulos et al., 1999)
contact area (%)	assume properties incl. porosity	
<b>anode catalyst support x 225</b>		
Material	Carbon	Argyropoulos et al., 1999
thickness (m)	0.000065	Argyropoulos et al., 1999
k (W/m K)	0.2	Argyropoulos et al., 1999
density (kg/m <sup>3</sup> )	387	Argyropoulos et al., 1999
cp (J/kg K)	770	NIST, 2003
specific res (ohm-m)	0.000014	Kauranen, 1996 (as cited in Argyropoulos et al., 1999)
contact area (%)	50%	assumption
<b>membrane x 225</b>		
Material	Nafion <sup>®</sup> 117	Argyropoulos et al., 1999; Rowe et al., 2001; Mosig, 1998; Maggio et al., 1996
thickness (m)	0.000183	DuPont, 2000
k (W/m K)	0.21	Maggio et al., 1996
basic wt (kg/m <sup>2</sup> )	0.36	DuPont, 2000
Mass (kg)	13.2E-03	DuPont, 2000 and net area
cp (J/kg K)	1100	PTFE data
specific res (ohm-m)	0.10	Gottesfeld, 1997
<b>cathode catalyst support x 225</b>		
Material	Carbon	Argyropoulos et al., 1999
thickness (m)	0.000065	Argyropoulos et al., 1999
k (W/m K)	0.2	Argyropoulos et al., 1999
density (kg/m <sup>3</sup> )	387	Argyropoulos et al., 1999
cp (J/kg K)	770	NIST, 2003
specific res (ohm-m)	0.000014	Kauranen, 1996 (as cited in Argyropoulos et al., 1999)
contact area (%)	50%	assumption
<b>GDL x 225</b>		
Material	As described in source	Wöhr, 1998

thickness (m)	0.0004	Wöhr, 1998
k (W/m K)	65	Wöhr, 1998
density (kg/m <sup>3</sup> )	2000	Wöhr, 1998
cp (J/kg K)	840	Wöhr, 1998
specific res (ohm-m)	0.000014	Kauranen, 1996 (as cited in Argyropoulos et al., 1999)
contact area (%)	assume properties incl. porosity	
<b>cathode gas channel x 225</b>		
Material	Graphite	Argyropoulos et al., 1999
thickness (m)	0.001	Mosig, 1998
k (W/m K)	52	Argyropoulos et al., 1999
density (kg/m <sup>3</sup> )	1400	Incropera & DeWitt, 1990
cp (J/kg K)	935	Incropera & DeWitt, 1990
specific res (ohm-m)	1.67E-04	Berning et al., 2002
contact area (%)	55%	Mosig, 1998
<b>cathode gas x 225</b>		
Material	O <sub>2</sub> , N <sub>2</sub> , H <sub>2</sub> O <sup>4</sup>	
hA to cathode stream (W/K)	10	Amphlett et al., 1996
density (kg/m <sup>3</sup> )	fn(T)	NIST, 2003
cp (J/kg K)	fn(T)	NIST, 2003
h (J/mol)	fn(T)	NIST, 2003
air stoich ratio	3	Rowe and Li, 2001
pressure (bars)	1	Wöhr, 1998
<b>web x 225</b>		
Material	Graphite	Argyropoulos et al., 1999
thickness (m)	0.001	Argyropoulos et al., 1999
k (W/m K)	52	Argyropoulos et al., 1999
density (kg/m <sup>3</sup> )	1400	Incropera & DeWitt, 1990
cp (J/kg K)	935	Incropera & DeWitt, 1990
specific res (ohm-m)	1.67E-04	Berning et al., 2002

<sup>1</sup>	active area = 300 cm <sup>2</sup> , used for current (Amps) calculations and for energy calculations for channels; % contact as noted net area = 367 cm <sup>2</sup> used for energy calculations for all other layers, is based on approximation of feed holes subtracted from total area; % contact or porosity as noted
<sup>2</sup>	total endplate assembly includes the end plate, bus plate, and interface (I/F) plate
<sup>3</sup>	accounts for extra cooling section in symmetrical stack of arbitrarily selected 225 cells
<sup>4</sup>	inlet relative humidity = 100% (Mosig, 1998; Berning et al., 2002; Rowe and Li, 2001) liquid water in reaction products assumed heat of vaporization taken into account as vapor and liquid enthalpy flows are separated

**Table 7: List of PEM fuel cell stack cell parameters**

<b>System Cooling</b>		
<b>Fuel Cell System Component</b>	<b>mass x specific heat (m x c<sub>p</sub>)</b>	<b>Sources</b>
cells + endplates	62232	see Table 7
startup HX	936	*
humidifier	2808	Arbin (2002)
compressor	29139	Vairex (2003)
fan motor	7368	DC
traction motor	72680	DC
radiator	6615	DC
pump	2500	DC
total component	184278	
stack + manifold coolant	27262	see Table 7
systems piping	9510	assumption
startup HX coolant	1110	Zilka-Marco et al., (1999)
humidifier coolant	6340	assumption
compressor coolant	3170	assumption
fan motor coolant	73	DC
traction motor coolant	5389	DC
radiator coolant	12046	DC

vehicle piping	9510	assumption
pump coolant	634	DC
total coolant	75044	
total component + coolant	259322	
* Zilka-Marco et al., 1999; Matson et al., 1999		

**Table 8: List of  $m \times c_p$  values for system components**